

NUMERICAL INVESTIGATION OF STIFFENED COMPOSITE PANEL INTO
BUCKLING AND POST BUCKLING ANALYSIS UNDER COMBINED
LOADING

A THESIS SUBMITTED TO
THE GRADUATE SCHOOL OF NATURAL AND APPLIED SCIENCES
OF
MIDDLE EAST TECHNICAL UNIVERSITY

BY

ERKAN AKAY

IN PARTIAL FULFILLMENT OF THE REQUIREMENTS
FOR
THE DEGREE OF MASTER OF SCIENCE
IN
AEROSPACE ENGINEERING

SEPTEMBER 2015

Approval of the thesis:

**NUMERICAL INVESTIGATION OF STIFFENED COMPOSITE PANEL
INTO BUCKLING AND POST BUCKLING ANALYSIS UNDER
COMBINED LOADING**

submitted by **ERKAN AKAY** in partial fulfillment of the requirements for the degree of **Master of Science in Aerospace Engineering Department, Middle East Technical University** by,

Prof. Dr. Gülbin Dural Ünver
Dean, Graduate School of **Natural and Applied Sciences**

Prof. Dr. Ozan Tekinalp
Head of Department, **Aerospace Engineering**

Prof. Dr. Yavuz Yaman
Supervisor, **Aerospace Engineering Dept., METU**

Examining Committee Members:

Assoc. Prof. Dr. Melin Şahin
Aerospace Engineering Dept., METU

Prof. Dr. Yavuz Yaman
Aerospace Engineering Dept., METU

Asst. Prof. Dr. Ercan Gürses
Aerospace Engineering Dept., METU

Asst. Prof. Dr. Tuncay Yalçınkaya
Aerospace Engineering Dept., METU

Asst. Prof. Dr. Levent Ünlüsoy
Aeronautical Engineering Dept., UTAA

Date: 04.09.2015

I hereby declare that all information in this document has been obtained and presented in accordance with academic rules and ethical conduct. I also declare that, as required by these rules and conduct, I have fully cited and referenced all material and results that are not original to this work.

Name, Last name : Erkan Akay

Signature :

ABSTRACT

NUMERICAL INVESTIGATION OF STIFFENED COMPOSITE PANEL INTO BUCKLING AND POST BUCKLING UNDER COMBINED LOADING

Akay, Erkan

M.S., Department of Aerospace Engineering

Supervisor: Prof. Dr. Yavuz Yaman

September 2015, 127 pages

This thesis presents the investigation of buckling and post buckling behaviour of stiffened thin walled laminated composite aerospace structures subjected to combined in-plane axial and shear loadings. Due to the fact that the state of stress developing especially in the post-buckling stage is quite complicated under the combined loading, the necessary computational model is usually based on Finite Element Modelling (FEM). In this study, after verifying the FEM methodology and completing the sensitivity studies, the buckling and post buckling phenomenon are examined in order to see the effects of shear loading beside the axial compressive loading on a stiffened composite panel via linear and nonlinear analyses. The results show that under combined in-plane loading of a stiffened panel, additional shear loading beside the axial loading has an influence on the axially critical buckling load capability of the structure depending on the characteristic of the structure like ply orientation.

Keywords: Stiffened Panels, Composites, Buckling, Post-buckling, FEM, Combined Loading

ÖZ

BİRLEŞİK YÜKLEME ALTINDA KİRİŞ DESTEKLİ PLAKALARIN BURKULMA VE BURKULMA SONRASI DAVRANIŞLARININ İNCELENMESİ

Akay, Erkan

Yüksek Lisans, Havacılık ve Uzay Mühendisliği Bölümü

Tez Yöneticisi: Prof. Dr. Yavuz Yaman

Eylül 2015, 127 sayfa

Bu çalışma kesme ve eksenel basma yükü altındaki, kiriş destekli kompozit ince cidarlı bir hava aracı yapısının burkulma öncesi ve sonrası davranışlarının incelenmesini sunmaktadır. Eksenel basma yükü ile birlikte kesme yüküne de maruz kalan kiriş destekli plakalarda, özellikle burkulma sonrası davranışların oldukça karmaşık olmasından dolayı, sonlu elemanlar yöntemi gibi sayısal tabanlı bir çözücü olmadan panel davranışlarını hesaplamak oldukça zordur. Bu çalışmada, sonlu elemanlar modelleme yönteminin doğrulanması ve hassasiyet çalışmalarının ardından, kiriş destekli plakanın burkulma ve burkulma sonrasındaki davranışında eksenel basma yükü ve kesme yükünün etkileri de incelenmiştir. Sonuçlar, eksenel basma yükünün yanında kesme yüküne de maruz kalan plakalarda, yapının tabaka dizim açıları gibi özelliklerine bağlı olarak, kesme yükünün yapının eksenel basma yükü kabiliyetine etkisi olduğunu göstermiştir.

Anahtar Kelimeler: Kiriş Destekli Panel, Kompozit, Burkulma, Burkulma-sonrası, Sonlu Elemanlar Modeli, Birleşik Yükleme

ACKNOWLEDGMENTS

I would like to express sincere appreciation to my supervisor Prof. Dr. Yavuz YAMAN; for his guidance, advice, motivation, continuous support and encouragements throughout this study.

I also wishes to express my gratitude to my wife Emine AKAY; for her understanding and endless love through the duration of my studies. I also thank my wonderful daughters: Ayşe and Zehra, for always making me smile and for understanding on those days when writing this thesis instead of playing games.

Finally, I would like to thank to my family for their patience and moral support throughout the study.

TABLE OF CONTENTS

ABSTRACT	v
ÖZ.....	vi
ACKNOWLEDGMENTS.....	vii
TABLE OF CONTENTS	viii
LIST OF TABLES	xii
LIST OF FIGURES.....	xv
CHAPTERS	
1 INTRODUCTION.....	1
1.1 Motivation of the Study.....	1
1.2 Scope of the Study.....	3
1.3 Limitation of the Study.....	4
1.4 Content of the Study.....	5
1.5 Literature Survey.....	5
2 COMPOSITE STIFFENED PANEL AND BUCKLING PHENOMENON.....	15
2.1 Introduction	15
2.2 Coordinate System for Lamina and Laminates	15
2.3 Selected Laminated Composites	17

2.4	Stiffness Matrices of Thin Laminates	19
2.5	Pre Buckling and Post Buckling of Stiffened Panels	21
2.6	Linear and Nonlinear Buckling Analysis	25
2.7	Conclusion.....	28
3 FINITE ELEMENT MODELLING METHODOLOGY OF THE STIFFENED COMPOSED PANELS		29
3.1	Introduction	29
3.2	Finite Element Modelling of the Laminated Shell Type Composites ..	29
3.3	Stiffened Panel Model Definition	32
3.3.1	Boundary Conditions and Loading	37
3.3.2	Configuration of the Panels.....	40
3.4	Conclusion.....	43
4 SENSITIVITY STUDIES		45
4.1	Introduction	45
4.2	Mesh Refinement	46
4.3	Joint Modelling	51
4.4	Conclusion.....	57
5 VALIDATION STUDIES FOR BUCKLING		59
5.1	Introduction	59
5.2	A Flat Stiffened Panel Under Axial Loading.....	60

5.2.1	Problem Definition for Flat Panel Under Axial Loading	60
5.2.2	Test Set-Up for Flat Panel Under Axial Loading.....	61
5.2.3	Analysis Model for Flat Panel Under Axial Loading.....	62
5.2.4	Solution and Results for Flat Panel Under Axial Loading.....	63
5.3	A Curved Stiffened Panel Under Axial Loading.....	67
5.3.1	Problem Definition for Curved Panel Under Axial Loading	67
5.3.2	Test Set-up for Curved Panel Under Axial Loading.....	69
5.3.3	Analysis Model for Curved Panel Under Axial Loading	70
5.3.4	Solution and Results for Curved Panel Under Axial Loading	71
5.4	A Flat Stiffened Panel Under Shear Loading.....	74
5.4.1	Problem Definition for Flat Panel Under Shear Loading.....	74
5.4.2	Test Setup for Flat Panel Under Shear Loading.....	75
5.4.3	Analysis Model for Flat Panel Under Shear Loading	75
5.4.4	Solution and Results for Flat Panel Under Shear Loading.....	77
5.5	Conclusion.....	78
6	NUMERICAL RESULTS OF LINEAR AND NON-LINEAR BUCKLING ANALYSIS AND DISCUSSION	81
6.1	Introduction	81
6.1.1	Linear Analysis and Results	81
6.1.2	Nonlinear Post Buckling Analysis and Results.....	97

6.2	Conclusion.....	107
7	CONCLUSIONS.....	111
7.1	General Conclusion.....	111
7.2	Future Work Recommendations	113
	REFERENCES.....	115
	APPENDICES	
A.	STIFFNESS MATRICES	121
B.	ANSYS INPUT FILE.....	123

LIST OF TABLES

TABLES

Table 3.1 Material properties for the composite material	32
Table 3.2 Applied Load Ratios.....	40
Table 3.3 Configurations with lay-up sequences for skin, web and flanges	42
Table 3.4 Configuration 13 to 16 with respect to skin lay-up sequences.....	43
Table 4.1 Summarized results table from the output of the mesh sizing parameter	51
Table 4.2 Summarized results table from the output of the sensitivity studies.....	56
Table 5.1 Material properties given for the composite material in [37].....	61
Table 5.2 Material properties given for the composite material in [39].....	69
Table 5.3 Material properties given for the composite material in [40].....	74
Table 6.1 Variation of the shear effect ratio with the different load ratio for P1	83
Table 6.2 Variation of the shear effect ratio with the different load ratio for P2.....	84
Table 6.3 Variation of the shear effect ratio with the different load ratio for P3.....	84
Table 6.4 Variation of the shear effect ratio with the different load ratio for P1_Configuration 13 to 16	85
Table 6.5 Variation of the shear effect ratio with the different load ratio for P2_Configuration 13 to 16	85

Table 6.6 Variation of the shear effect ratio with the different load ratio for P3_Configuration 13 to 16.....	85
Table 6.7 Change on the lay-up of the skin for Configuration 10 to Configuration 12	86
Table 6.8 Variation of the shear effect ratio with the different load ratio for P1_Configuration 10_b to 12_b.....	87
Table 6.9 Variation of the shear effect ratio with the different load ratio for P2_Configuration 10_b to 12_b.....	87
Table 6.10 Variation of the shear effect ratio with the different load ratio for P3_Configuration 10_b to 12_b.....	87
Table 6.11 Comparison study of buckling load calculated with FEM with Equation 6.5 for P1_Configuration 1	89
Table 6.12 Shear Effect Ratio for the low Load Ratio (P_x/P_y) for P1_Configuration 1	90
Table 6.13 Comparison study of buckling load calculated with FEM with Equation 6.5 for P1_Configuration 7	90
Table 6.14 Shear Effect Ratio for the low Load Ratio (P_x/P_y) for P1_Configuration 7	91
Table 6.15 Comparison study of buckling load calculated with FEM with Equation 6.5 for P1_Configuration 10_a.....	91
Table 6.16 Shear Effect Ratio for the low Load Ratio (P_x/P_y) for P1_Configuration 10_a.....	91
Table 6.17 Stress Change on the Path for only axial loading (U_x) and Combined Loading ($U_x/U_y=1$).....	101

Table 6.18 Stress Change on the Path of P2 for pure axial loading (U_x) and Combined Loading ($U_x/U_y=1$)	104
Table 6.19 Stress Change on the Path of P3 for pure axial loading (U_x) and Combined Loading ($U_x/U_y=1$)	107

LIST OF FIGURES

FIGURES

Figure 1.1 Illustration of stiffened composite plate produced for fuselage test [1] ...	1
Figure 1.2 An example of buckling phenomena in aircraft fuselage [2]	2
Figure 1.3 Illustration of shear stretch coupling terms	6
Figure 2.1 Coordinates of Lamina	16
Figure 2.2 Description of the layup in a laminate of unidirectional plies [25]	16
Figure 2.3 Material with three planes of symmetry [25]	17
Figure 2.4 Examples of symmetrical laminates	17
Figure 2.5 Examples of balanced laminates.....	18
Figure 2.6 Cross-Sectional views of various types of angle-ply laminates	18
Figure 2.7 Coordinate notations of individual plies.....	19
Figure 2.8 Illustration of the coupling terms of A_{12} , D_{12} [25].....	21
Figure 2.9 Stiffened panel under compressive load.....	22
Figure 2.10 Definition of first local buckling and global buckling [26].....	23
Figure 2.11 Possible failure modes in the stiffened panels [20]	23
Figure 2.12 Potential failure modes in the stiffened panels [27]	25
Figure 2.13 Sample monitor file to show the buckling detection	27

Figure 3.1 SHELL281 Geometry [36]	31
Figure 3.2 SHELL281 element type options	32
Figure 3.3 One sample of a manufactured T type-stiffener [41].....	33
Figure 3.4 Stiffener geometry and parts	33
Figure 3.5 Shell section definition	34
Figure 3.6 Skin lay-up plot.....	35
Figure 3.7 Simplified FE model of the stringer.....	36
Figure 3.8 Finite element model of P1 and dimensions	37
Figure 3.9 Finite element model of (a) P2 and (b) P3	37
Figure 3.10 Illustrative test set-up (Stiffened aluminum panels subjected to axial) [43]	38
Figure 3.11 Applied boundary conditions and applied constraints	39
Figure 4.1 The FEM of stiffened panel with different element sizing	47
Figure 4.2 The FEM of the stiffened panel with different element sizing-Cont.	48
Figure 4.3 Sensitivity studies of mesh refinement outputs: change of the load vs. end shortening curves according to the baseline model	49
Figure 4.4 First mode shapes of the panels for different mesh sized panels	50
Figure 4.5 Joint Modelling Techniques (a) by using contact elements (b) common elements used model	53
Figure 4.6 Sensitivity study results with respect to mesh size	54
Figure 4.7 First mode shape plotting in accordance with joint modelling type	55

Figure 5.1 The blade-stiffened panel studied by Zhu et al. [37].....	60
Figure 5.2 Cross-sectional view and dimensions of the stiffener [37].....	61
Figure 5.3 (a) Hydraulic compression test machine, (b) Locations of the strain gauges. [37].....	62
Figure 5.4 (a) Boundary Conditions of the stiffened panel, (b) Finite Element Model of the stiffened panel.	63
Figure 5.5 Load with respect to end-shortening curves.	64
Figure 5.6 Numerical vs. experimental results [37]: out-of-plane displacements at buckling region.....	65
Figure 5.7 Numerical vs. experimental results: axial strains on the skin.....	66
Figure 5.8 Numerical vs. experimental results: axial strains on the stringer	67
Figure 5.9 The blade-stiffened test specimen used in [39]	68
Figure 5.10 Dimensions of the Cross-section of the stiffener (mm) [39].....	68
Figure 5.11 Hydraulic compression test machine [39]	69
Figure 5.12 Finite Element Model.	70
Figure 5.13 Boundary Conditions [39]	71
Figure 5.14 The test results of the load-shortening curves of the panels, in conjunction with the measured out-of-plane displacement patterns [39]	72
Figure 5.15 Load-shortening curves of the panels, in conjunction with the measured out-of-plane displacement patterns from FEM results.....	73
Figure 5.16 (a) The blade-stiffened panel, (b) stiffener geometry presented in [40]	74
Figure 5.17 Shear panel test setup [40].....	75

Figure 5.18 FEM model of the flat stiffened panel under shear loading.....	76
Figure 5.19 Boundary Conditions of the flat stiffened panel under shear loading ..	76
Figure 5.20 The out of plane displacement of skin, experimental and numerical results.....	77
Figure 5.21 Mode shape of the panel during the first buckling mode.....	78
Figure 6.1 The percentage of the change in axial critical buckling load with the different load ratio in the panels.....	88
Figure 6.2 Buckling load interaction curves: comparison of Equation 6.3 and FEM results.....	92
Figure 6.3 Post-buckled skin under shear showing post-buckling angle α [27]	93
Figure 6.4 The 1 st mode shape of the Configuration 4 for P1, P2 and P3.....	94
Figure 6.5 The 1 st mode shape of the Configuration 7 for P1, P2 and P3.....	94
Figure 6.6 The 1 st mode shape of the Configuration 13 for P1, P2 and P3.....	95
Figure 6.7 The 1 st mode shape of the Configuration 16 for P1, P2 and P3.....	95
Figure 6.8 The 1 st mode shape of the Configuration 1 for P1, P2 and P3.....	96
Figure 6.9 Stress Path on the panel	97
Figure 6.10 Stress Distribution on the Path for Pre Buckling and Buckling Stage for-P1_Configuration 7 with various loading ratios.....	99
Figure 6.11 Stress Distribution Comparison between the only axial loading (U_x) and combined loading ($U_x/U_y=1$) for P1_Configuration 7	100
Figure 6.12 Stress Distribution on the Path for Pre Buckling and Buckling Stage for P2_Configuration 7 with various loading ratios	102

Figure 6.13 Stress Distribution Comparison between the only axial loading (U_x) and combined loading ($U_x/U_y=1$) for P2_Configuration 7	103
Figure 6.14 Stress Distribution on the Path for Pre Buckling and Buckling Stage for P3_Configuration 7 with various loading ratios	105
Figure 6.15 Stress Distribution Comparison between the only axial loading (U_x) and combined loading ($U_x/U_y=1$) for P3_ Configuration 7	106

LIST OF SYMBOLS AND ABBREVIATIONS

[A]	The extensional stiffness matrix
A_{ij}	Components of the extensional stiffness matrix [A]
A_{16}, A_{26}	Extension-Shear Coupling Terms
[B]	The bending-extension coupling matrix
B_{ij}	Components of the bending-extension coupling matrix [B]
B_{16} ,	Extension-Twist Coupling Term
B_{26}	Bending-Shear Coupling Term
CFRP	Carbon fiber reinforced polymer
[D]	The bending stiffness matrix
D_{ij}	Components of the bending stiffness matrix [D]
D_{16}, D_{26}	Bending-Twisting Coupling Terms
DOF	Degrees of freedom
E_{11}, E_{22}	Longitudinal and transverse modulus
FEM	Finite element modelling
G_{12}	Inplane shear modulus
H_{web}	Height of the web
Th_{flange}	Thickness of the flange

LVDT	Linear variable differential transformer
MPC	Multi point constraints
MxDs	Maximum displacement of the model
M_x, M_y, M_{xy}	Moments per unit length
N_x, N_y, N_{xy}	In-plane forces per unit length
P	Applied compressive load value
P_{cr}	Load value corresponding to first buckling mode
P_x, P_y	Applied load value in X and Y direction
P_{x_cr}, P_{y_cr}	Load value in X and Y direction corresponding to first buckling mode
P_x/P_y	Applied load ratio
RF	Reserve Factor
Th_web	Web thickness
U_x, U_y, U_z	Displacement component in X, Y and Z direction
U_x/U_y	Applied displacement ratio
U	Applied displacement value in compression
U_{cr}	Displacement value corresponding to critical buckling load
$\epsilon_{x0}, \epsilon_{y0}$	In-plane strains
γ_{xy0}	In-plane shear strain
κ_x, κ_y	Bending curvatures

κ_{xy}	Twisting curvatures
θ	The orientations of unidirectional plies
α	The post buckling angle under shear load
ν_{12}	In-plane Poison's ratio

CHAPTER 1

INTRODUCTION

1.1 Motivation of the Study

In the recent decades, new advanced capability materials like fibrous carbon composites have attracted great interest of their use in aerospace structures owing to their favorable properties, just as the high characteristic strength and stiffness. In addition to these properties, weight reduction of fundamental structures in the aircraft is an vital and challenging issue to reduce operating costs. Stiffened panels as shown in Figure 1.1, which are built by thin walled structures supported by stiffeners, are commonly used in the aircraft to get very light structures with highly appreciable bending stiffness and buckling resistance.

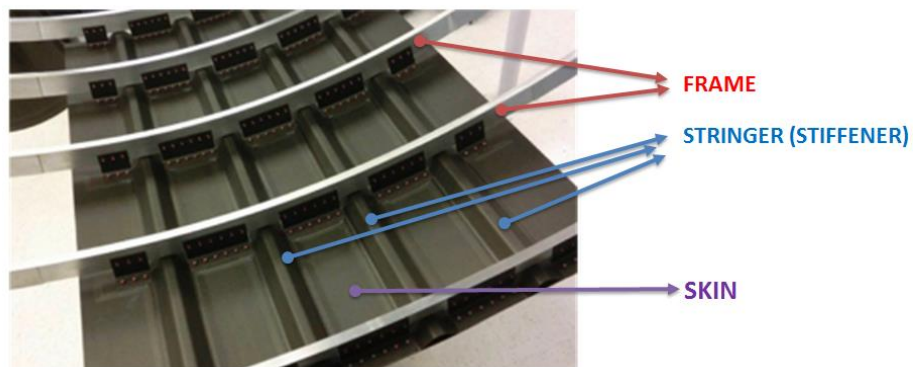


Figure 1.1 Illustration of stiffened composite plate produced for fuselage test [1]

Actually, stiffened shell configuration are dominantly made by aluminium materials. The construction of very effective aluminium based structure is feasible by verified design methods, validated analysis tools with an enormous measure of test outputs, as well in according to strength properties and failure scenarios studied since the end of the eighteenth century. For the last thirty years, through the onset of the new materials, called composites, large amount of studies have been performed to replace the conventional aluminium based shell structure with the composite materials. These structures are generally produced as thin and so tend to buckle as mentioned above.

A skin-stiffener plate, according to its dimension and stiffness properties, can have a variable buckling capabilities. For example, local buckling or skin buckling between stiffeners, is very commonly observed in usual aircraft primary components as illustrated in Figure 1.2.



Figure 1.2 An example of buckling phenomena in aircraft fuselage [2]

After the skin is buckled, the stiffened plate falls into the post-buckling phase and still have an ability to sustain the load with an appropriate re-distribution of the load into the stringers. Especially in aircraft structures, the philosophy of having post-buckling load carrying capability for the structure are frequently used to attain light-weight structures. That is the main reason of being allowed of local skin buckling

allowed at design levels. Therefore, analysis tools for the calculation of the buckling force and of the structure nonlinear behavior in the post-buckling stage have become vital at the initial stages of design.

There are many factors that can influence the buckling and post-buckling of stiffened curved panel like loading condition, the stiffener cross section properties, the shell thickness and the distribution of stiffeners. Although a lot of effort have been put into the buckling and post buckling studies of the aircraft composite parts, the required exact results are yet to be found and research in this area still draws attention from both academia and industry [3]. The key aspect of composite materials, anisotropy is an advantage with regard to structural design, on the other hand, it is also a main reason of complicated structural analysis. Ordinarily, in-house codes have a relative limitation in problem size. To analyze the complex structure with great problem dimensions, commercially developed programs have been commonly preferred [4]. These FEM based programs give correct outputs together with no limitations for boundary conditions, panel shapes with stiffener or ply orientation. It means that analytical approaches are generally limited for only some kind of shape like rectangle or square with definitive boundary conditions. Beside these, due to simplifications achieved, the assumption of orthotropic symmetric laminate are generally preferred in analytical calculations.

1.2 Scope of the Study

Greater part of the research condenses on the buckling behaviour of unstiffened and stiffened panels exposed to in-plane compressive loadings. Some contributions in the form of design charts and guidelines have been developed for unstiffened panels subjected to only in-plane compression or only in-plane shear loadings, but the buckling response of laminated composite stiffened panels subjected to combined (shear and axial) in-plane loading received less attention. Even though it is believed that a lot of similar studies should have been performed in international aircraft

industry; the lack of the results in open literature and national requirements to establish a sound scientific data base on the subject paved way to this study.

In the present study, the main objective is to investigate the shear loading effects on the buckling behaviour of the composite stiffened panels in addition to compressive axial loading. To this end, initially a Finite Element (FE) modelling methodology is developed for a stiffened panel. Later, in order to validate the developed FE modelling methodology, problems whose experimental solutions are available in literature have been selected and solved. After these, a series of different configurations is modelled in order to see the amount of the shear loading effect on the structures over and above the axially compressive loading. In order to accelerate and hence to reduce the computation time, an ANSYS input file is created first for a unique model and then it is modified and extended to make the linear eigenvalue and nonlinear post buckling analysis for different plate configurations.

1.3 Limitation of the Study

The problem considered in this study has the following restrictions:

- The material is taken as orthotropic
- The laminate is mainly chosen as a symmetric balanced laminate composed of 0° , $\pm 45^\circ$, 90° laminas
- Geometric dimension of the stringer and skin is constant apart from the thicknesses and layup sequences
- Only one type of the stringer is used.
- The post-buckling characteristic of the plates in the acceptance of considering only for the geometrical non-linearity, without accounting progressive failure of the composite material and separation issues

1.4 Content of the Study

This thesis is organized as follows:

- In Chapter 2, a brief information about composites terminology used in this study is given. After that, buckling and post buckling phenomena on the composite stiffened panels is explained and the relevant equations for orthotropic layup is given. At the end of the chapter, linear and nonlinear post buckling analysis definitions and procedures are defined.
- In Chapter 3, the finite element modelling methodology of the stiffened panels with their various configurations is presented. These models will be used for the investigation study of the buckling behaviour of the stiffened panels under combined loading.
- In Chapter 4, the performed sensitivity studies with obtained output are shown.
- In Chapter 5, the validation studies of the finite element model of the different stiffened panels under unitary loading conditions are presented with the results of the comparative study.
- In Chapter 6, the results of the analysis are given with necessary explanation.
- In Chapter 7, conclusions drawn according to results obtained in Chapter 6 are provided.

1.5 Literature Survey

Due to fact that many experiments, numerical computations and analytical solutions were carried out to investigate the buckling and post-buckling behaviors of the

stiffened structure over the last two decades, literature on the buckling and post buckling analysis of composite laminates is vast. Therefore, only some of them are presented in this section.

Analytical tools are first hand tool to analyze laminated composite stiffened panels. Finding the smeared stiffness representative of the interested structure as a solution is one of the analytical methods, which is computationally fertile but includes many mistakes especially for the composite stiffened panels subjected to in-plane shear loading [5]. In addition, Stroud et al. [5] stated that the smeared stiffener solution can be used only with caution.

Loughlan [6] investigated the buckling limitation of composite stringer supported shear webs by taking into account stiffener shapes, distance between the stiffeners and the ply layup of the stringers as variables. As a conclusion of this study, for a specific weight, it has been observed that shear buckling allowable of the structure which is a criteria of the structure representing the capability to withstand the shear load can be increased by changing the layup of plies in the stringers.

Loughlan [7] also carried out the effect of couplings on the buckling behaviour of composite stiffened shell type structure exposed to in-plane shear and twisting loading. He revealed that the existence of in-plane shear stretch coupling terms in the stiffness matrices of thin, flat laminates under small deformations has very little influence. These coupling terms provides the structure to be deformed in shear direction under axial forces and inversely to be deformed in axial direction under shear forces as shown in Figure 1.3.

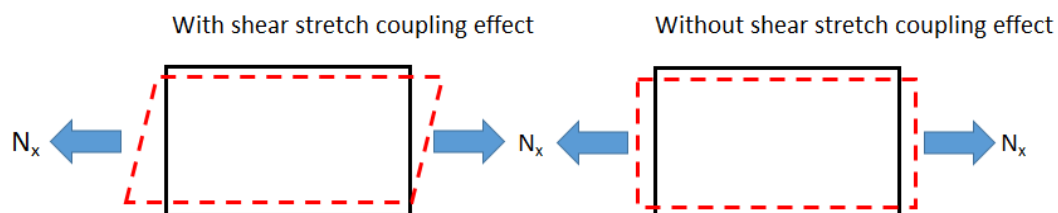


Figure 1.3 Illustration of shear stretch coupling terms

Loughlan [8] studied the effect of axial and bending stiffness coupling on the buckling of different type of layup for anti-symmetric laminates exposed to axial compressive loading in elastic region. Composites made up of various ply orientations were studied to investigate the influence of the axial-bending coupling on the composite structure. Finite strip method has been utilized to calculate the buckling results. The amount of coupling reduced if the number of ply is increased and it showed orthotropic properties for the critical stress levels. Buckling behaviour of anti-symmetric composite plates were sensitively influenced by variation of ply orientations. Results revealed that the optimized ply orientation have less effective in the post-buckling area than post buckled compressive stiffness.

Nemeth [9] has carried out parametric based studies for an orthotropic plate to adapt some common buckling design tables based on applicable non-dimensional constants for unstiffened composite plates exposed to variable loadings. The outcomes demonstrate that the impacts of plate anisotropy are marginally more purported for just simply supported plates than for clamped plates when the plates are subjected to either directly changing edge forces, uniform shear forces, or combined of these heaps. The most imperative finding of the present study is that specially orthotropic and flexural anisotropic plates that are exposed to a tension overwhelmed hub edge load dispersion can bolster shear forces that are bigger in greatness than the shear forces.

A parameter based research study carried out by Chen et al. [10] demonstrated that (1) the stacking arrangements and the lamina thickness influences the post-buckling compressive resistance of composite plates and stiffened panels significantly, and (2) the post-buckling compressive resistance increases fundamentally with the increment of lamina thickness.

Jain et al. [11] investigated the buckling characteristics of the stiffened composite structure with variable stiffener shapes like blade-type, hat-type and T-shape exposed to in-plane shear. Based on the generated database, parameters affecting

the shear buckling behaviour are identified. They have found that high panel orthotropy ratio D_1/D_2 and less pitch length is found better during the numerical studies.

Pevzner et al. [12] analyzed the bending, torsional and combined buckling of curved stiffened structure supported by J-type and T-type stringers. They have written an in-house code that computes buckling forces of composite stiffened curved panels under axial loading. Efficient width calculation method employed during post buckling phase of aluminum stiffened structures has been utilized to composite stiffened curved structures. Different type of strength capability like bending or buckling of the stringers were studied with suggested efficient width calculation principle. Consequences from this calculation principle were compared with test outputs with numerical FEM calculations. Suggested way indicated valid match with tests and numerical results. Moreover, laminated composite stiffened curved panels can be designed and optimized by using the suggested method.

Kassapoglou [13] introduced a new design idea to increase the compression capacity of laminated composite plates. A composite panel with rectangular shape made up of two layups having two common center exposed to axial compressive force is investigated by using Rayleigh-Ritz method. Buckling forces are computed using energy minimization method. The output of FE models and other publicly known FE results are checked and it delivered good outputs apart from the samples which includes twisting-bending coupling because these stiffness's are not taken into account for this method. Based on the outputs, it can be seen that more weight reduction can be achieved by using composite and the presented method.

Kassapoglou [14] studied on a multi-objective optimization of the composite stiffened panels. The aims of the optimization are both to reduce the cost and the weight of the composite stiffened panels. The panel is under the compression load along the two opposite longitudinal edges and shear loads on four edges. The stiffeners can have any different shape and geometry type like L, C, Z, T, J, I and hat. The skin, stiffener thicknesses and the pitch distance between the stringer are

also to be varied. The material failure conditions, manufacturing conditions and buckling loads type are also added as variables. The buckling loads and strength properties are calculated via analytical formulations. The optimization is utilized with a Pareto algorithm by finding Pareto optimum configurations. As a results, it is observed that J shape stringers is the lowest weight configuration among the stringers while T shape stringers is the lowest cost. The optimum configuration taking into account both cost and weight is obtained with T type stringers.

Numerical methods, on the other hand are widely utilized during the analysis of the composite stiffened plates. Thanks to the very fast computers and the efficiency of FE method, various studies have been performed to comprehend the buckling behaviour of laminated composites.

Sarawit et al. [15] analyzed material modelling criteria, elements selection and boundary constraints that are considered in the finite element analysis of thin walled structures. He showed that finite element method with the true modelling suspicions such as elements, boundary conditions, initial conditions, and solution method as defined in the study gives respectable and adequate results.

Guo et al. [16] studied the buckling behavior of laminated panels with a single stiffener exposed to uniaxial compression load with a layer-wise finite element method. They found the influence of the ratio of the plate thickness to length, the variable plate length to width ratios, ply angles, and stiffener height to plate thickness ratios by using parametric studies. It was found that the ‘stiffener depth’ is not an suitable parameter while considering the laminated composites as different stiffness provided by the ply orientation substantially enhances the critical buckling load although the stiffener depth is constant. Also, they revealed that the stiffener has an influence in increasing the buckling load only up to a certain ratio of the stiffener height to the skin thickness.

Bisgani [17] and Bisgani and Lanzi [18] performed the post-buckling analysis of composite panels using dynamical analysis approach. They compared the RIKS

method and explicit method of the ABAQUS and also conducted structural optimization. The results show that the values of the critical buckling loads calculated by the linear eigenvalue numerical analysis, via the non-linear Riks approach and by the dynamic analysis are very close to the analytical outputs. The influence of flaw (imperfection) shape and level of magnitude on buckling loads is additionally examined. The outcomes demonstrate an abatement in the buckling load with an increment in the flaw magnitude, and specifically a higher lessening rate for lesser magnitude flaw. The barrel with lay-up introduction $[45^\circ/-45^\circ]$ s seems less touchy to the geometric flaws than the chamber with lay-up introduction $[0^\circ/45^\circ/-45^\circ/0^\circ]$.

Rahimi et al. [19] studied the influence of the stiffener profile on the buckling of cylindrical shells under axial compression load by FEM. The outcomes (versatile buckling force) for every model were inferred and in light of these outcomes, proportion of buckling qualities to weight parameters were figured for every model and were contrasted with results acquired from different models. The impact of profile of the ribs on the buckling of shells under axial loading can be finished up from the outcomes. Results demonstrated that solidifying the shells expanded the buckling force from 10% in to 36% while diminished the buckling force to weight proportion to 42% up to 52% of an unstiffened shell.

Sudhirsastri et al. [20] performed the analysis to investigate the behavior of the pre and post-buckling analysis of composite stiffened panels with finite element models (ABAQUS). In this study, they performed four examples as follows:

- 1- the four straight stiffeners stiffened composite panel
- 2- the four T stiffeners stiffened composite panel
- 3- the four I stiffeners stiffened composite panel
- 4- the stiffened composite panel by altering the number of stiffeners

In the study, buckling analysis of these four examples composed of the Kevlar/epoxy, woven fabric CFC/epoxy, and E-glass/epoxy composites, stiffened with blade, T and I shaped stiffeners has been performed using the finite element models. Several configurations for the panel and the stiffeners are obtained by combining the materials, layup sequences, the number and shape of the stiffeners in the analysis. They found that, among the configurations considered in the paper, the panel composed of carbon epoxy and four I shaped stiffeners in the ply sequence $(90/0/90/0)_S$ have the maximum buckling load capacity of 122.26 kN.

From the buckling studies, they observed that the buckling load capacity of the composite stiffened panel is reduced by decreasing the number of stiffeners.

Among the panel with three stiffeners, the panel made of I shaped stiffeners has the maximum buckling load capacity. The two I shaped stiffened panel has more buckling load carrying capability than the four straight stiffened panels and the stiffened panel with for T shaped stiffeners.

Some of the studies out of the above ones are carried out by experimental results and if possible comparisons with numerical/analytical modelling for validation purposes.

Bisagni and Cordisco [21] carried out a test to investigate the buckling and post buckling attitude of laminated composite shell type structure. Axial compression and torsional forces were enforced individually and then together with the help of a test equipment which evaluate the geometric defect to investigate the deflection alteration gradually. The influence of layup angles were observed and outputs indicated that there has been no connection between buckling load and load succession, plates can also endure to forces during post buckling era in the absence of any fault.

Falzon and Hitchings [22] performed a test and compare the test results with numerical analyses outputs to learn the post-buckling characteristics of blade type stringer supported composite plate exposed to axial compressive force. A secondary

buckling mode has been monitored in an unpredictable manner after first buckling phase as a dynamically change of mode shape. Arc-length methods has been used to withstand the numerical troubles. However, enhanced explicit dynamic analysis has been used in this investigation due to the encountered troubles in arc-length. An imperfection of a five percentage of highest deformation of initial mode shape has been entered into FE model. Outputs indicated that prediction of the point where mode-switch behaviour occurs has been ensured with a pleasant preciseness utilizing enhanced explicit dynamic analysis.

Hilburger and Starnes Jr. [23] showed the results of a test with an analytical solutions to learn the influence of initial defect on the buckling phase and failure investigation of a cylindrical shell subjected to axial compressive force. Various types of cylinder structure, diameter-to-thickness proportion have been taken into consideration. Effects of conventional and nonconventional initial defect have been considered with numerical analysis. Conventional defect comprises geometrical mid-surface defect and non-conventional defects comprises thickness alteration, separation of the laminae, the geometrically loaded edge defects and non-uniform end loads. Nonlinear static, transient and failure analysis have been used to predict the stable, unstable behaviours and material failures of the structure. Results outlined that a key generally excepted defect influence of a laminated composite thin walled structure can be defined employing the studied defects; more definite calculations can be performed applying the nonlinear analysis that is available in this paper.

Zhu et al. [24] studied the influence of I-shape stiffener with different stiffness values on the buckling and post-buckling behavior of stiffened composite panel exposed to the purely axial compression load. They performed the test on six stiffened composite panel configurations, which were orthogonally designed with two skin configurations and three I-shape stiffener configurations. They have found the following conclusions:

- The buckling capability the stiffened composite panel is found to be sensitive to the stringer design described by its equivalent stiffness in axially compression direction.
- The equivalent stiffness in axially compression direction of the stringer has a little influence on the ultimate failure capability of stiffened composite panels.
- The effect of the skin thickness on buckling load and failure load of the stiffened composite panel is found to be big. On the other hand, the influence of the skin on the buckling load capability is much more than that on the ultimate loads.
- The stiffeners to skin ratio in stiffness point of view should be equalized to obstruct incomplete instability of skin.
- The failure condition of the test specimens were also influenced by the failure of the strengthened ends.

Hence it can be seen that the research mainly focuses on the buckling response of unstiffened and stiffened panels subjected to only in-plane compression or only in-plane shear loading. On the other hand, the buckling reaction of laminated composite stiffened panels subjected to combined (shear and axial) in-plane loading were rather scarce.

Therefore, the main aim of this thesis is also to consider the shear loading effects on the buckling behavior of the composite stiffened panels in addition to the compressive axial loading.

The current study only develops and verifies the numerical models, namely Finite Element Models. It does not attempt nor conduct any experiment. The experimental data necessary for the verification of the numerical models have been used from the open scientific literature.

CHAPTER 2

COMPOSITE STIFFENED PANEL AND BUCKLING PHENOMENON

2.1 Introduction

This chapter intends to give general information about the laminated composite plates and terminologies especially used in this study. This chapter also describe the buckling and post-buckling phenomena of the composite laminated stiffened panels with linear and nonlinear analysis definitions.

2.2 Coordinate System for Lamina and Laminates

A laminate is made up of perfectly bonded layers of lamina with different fiber orientation to represent an integrated structural component. In most practical applications of composite material, the laminates are considered as thin and loaded along the plane of laminates. A thin orthotropic unidirectional lamina as depicted in Figure 2.1 has fiber orientation along the 1-direction and the direction transverse to the fiber along the 2-direction. The x-y coordinates represent the global coordinate system for the lamina.

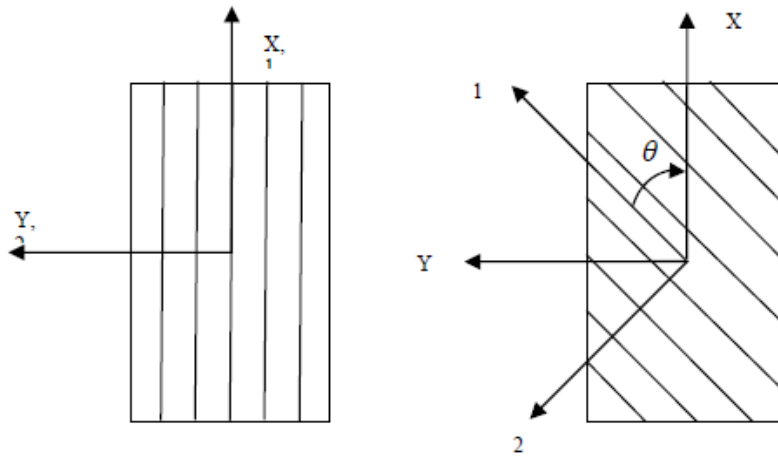


Figure 2.1 Coordinates of Lamina

The orientations of unidirectional plies are defined by the angle θ (in degree) with respect to the x-axis. The angle is positive in the counter clockwise direction. The number of plies in a ply group is described by a numerical subscript. For instance the laminate composed of unidirectional plies and depicted in Figure 2.2 is shown as $[45_3/0_4/90_2/60]$

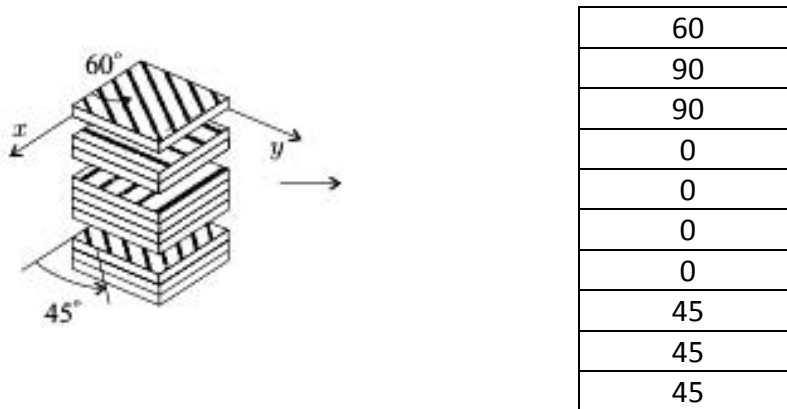


Figure 2.2 Description of the layup in a laminate of unidirectional plies [25]

2.3 Selected Laminated Composites

When there are three mutually perpendicular planes of symmetry with respect to the in line with fibers, the material is called as orthotropic. For an orthotropic material, it is specified the stiffness and compliance matrices in the X_1, X_2 and X_3 coordinate system described in such a way that the axes are perpendicular to the three planes of symmetry as depicted in Figure 2.3.

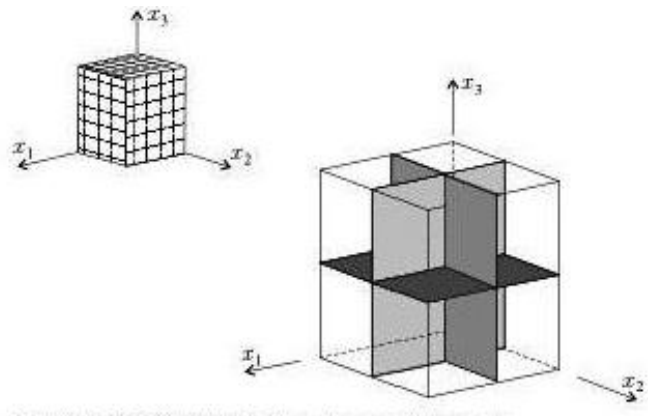


Figure 2.3 Material with three planes of symmetry [25]

When the laminate is symmetrical with respect to the mid-plane it is referred to as a symmetrical laminate. Example of symmetrical laminates are shown in Figure 2.4

-45
-45
0
0
0
0
-45
-45

[-45₂/0₂]_s

45
-45
-45
45
45
-45
-45
45

[45/-45₂/45]_s

Figure 2.4 Examples of symmetrical laminates

In the balanced laminates, for every ply in the $+\theta$ direction there is an identical ply in the $-\theta$ direction. Example of balanced laminates are shown in Figure 2.5.

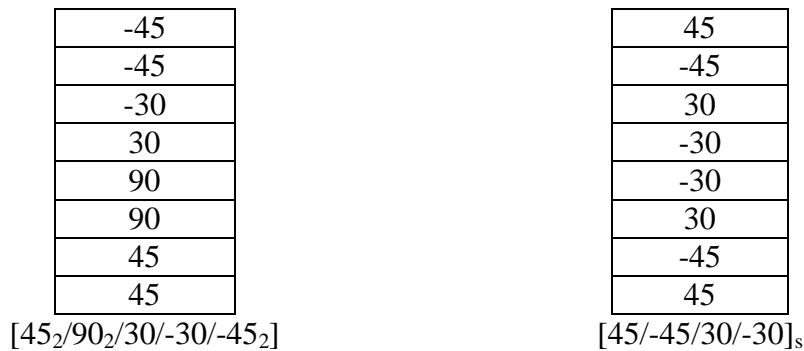


Figure 2.5 Examples of balanced laminates

Under the scope of this study, the laminated composite plates are generally selected as symmetric, balanced and orthotropic. Some combinations of these lay-up definitions are given in Figure 2.6.

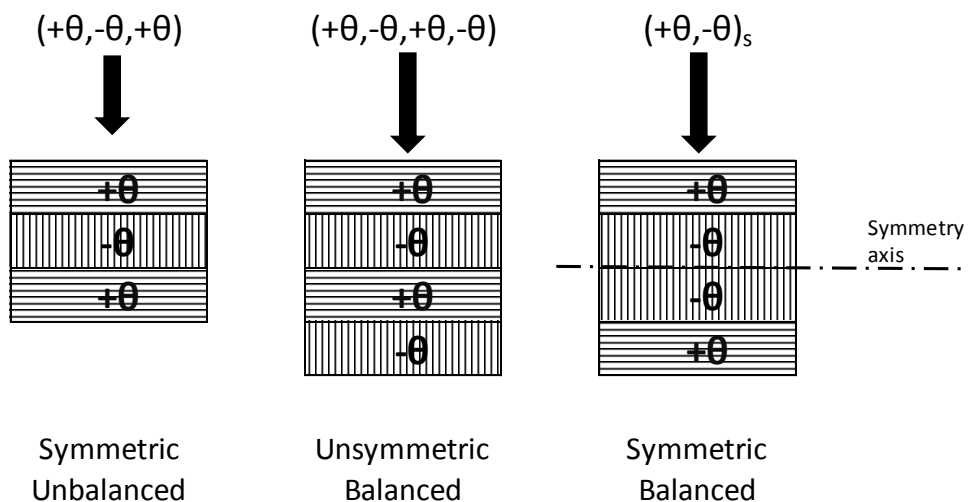


Figure 2.6 Cross-Sectional views of various types of angle-ply laminates

With these selections, the simplification of the stiffness matrix is obtained because for such a laminate, the coupling matrix B is zero due to the fact that the plies at a

distance of +Z and -Z from the reference plane are identical as illustrated in Figure 2.7. h_k and h_{k-1} are the coordinates of the upper and lower surface of the k^{th} lamina.

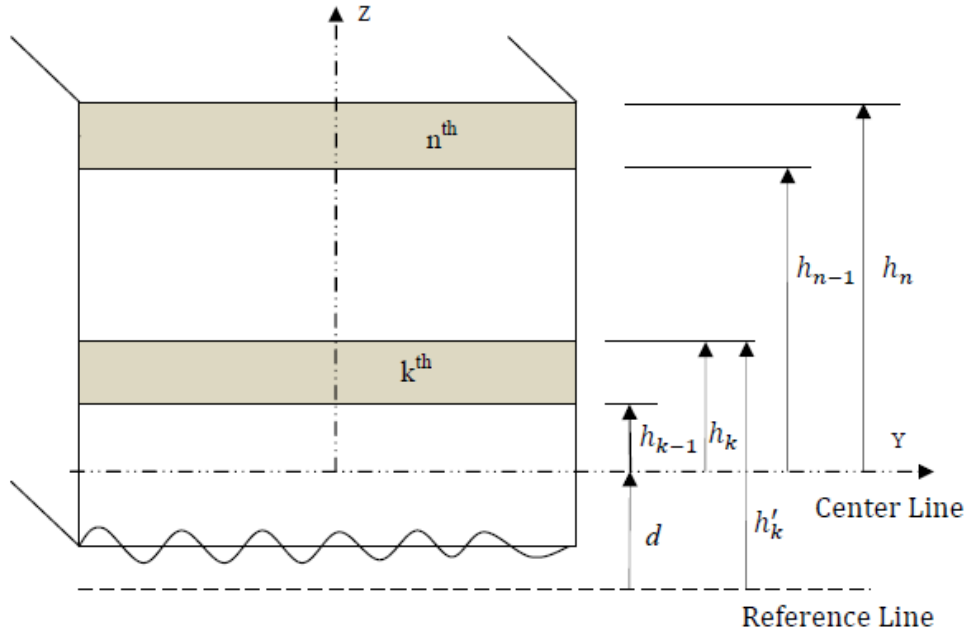


Figure 2.7 Coordinate notations of individual plies

2.4 Stiffness Matrices of Thin Laminates

The laminates are characterized by three stiffness matrices denoted by [A], [B] and [D]. The stiffness matrices in plane forces and moments become :

$$\begin{Bmatrix} N_x \\ N_y \\ N_{xy} \\ M_x \\ M_y \\ M_{xy} \end{Bmatrix} = \begin{bmatrix} A_{11} & A_{12} & A_{16} & B_{11} & B_{12} & B_{16} \\ A_{12} & A_{22} & A_{26} & B_{12} & B_{22} & B_{26} \\ A_{16} & A_{26} & A_{66} & B_{16} & B_{26} & B_{66} \\ B_{11} & B_{12} & B_{16} & D_{11} & D_{12} & D_{16} \\ B_{12} & B_{22} & B_{26} & D_{12} & D_{22} & D_{26} \\ B_{16} & B_{26} & B_{66} & D_{16} & D_{26} & D_{66} \end{bmatrix} \begin{Bmatrix} \varepsilon_{x0} \\ \varepsilon_{y0} \\ \gamma_{xy0} \\ \kappa_x \\ \kappa_y \\ \kappa_{xy} \end{Bmatrix} \quad (2.1)$$

$$\begin{Bmatrix} N \\ M \end{Bmatrix} = \begin{bmatrix} A & B \\ B & D \end{bmatrix} \begin{Bmatrix} \varepsilon_0 \\ \kappa \end{Bmatrix} \quad (2.2)$$

The vectors on the left and right hand side indicate the generalized forces and strains. The [A], [B] and [D] matrices represent the stiffness of a laminate and

indicate the response of the composite structure to in plane forces and moments. A_{ij} are the in plane (axial) stiffness that relate to in plane forces N_x, N_y, N_{xy} to the in plane strains $\varepsilon_{x0}, \varepsilon_{y0}, \gamma_{xy0}$. D_{ij} are the bending stiffness that relate the moments M_x, M_y, M_{xy} to the curvatures $\kappa_x, \kappa_y, \kappa_{xy}$. B_{ij} are the in-plane-out of plane coupling stiffnesses that relate to the in plane forces N_x, N_y, N_{xy} to the curvatures $\kappa_x, \kappa_y, \kappa_{xy}$ and the moments M_x, M_y, M_{xy} to the in-plane strains $\varepsilon_{x0}, \varepsilon_{y0}, \gamma_{xy0}$.

For certain ply arrangements (layups), some of the couplings described do not occur, and the [A], [B] and [D] matrices become simpler.

For balanced laminate, for every unidirectional ply in the $+\theta$ direction there is identical ply in the $-\theta$ direction. Due to this fact, there does not exist any unsymmetrical loading in x-y plane. So extension-shear coupling terms in x and y directions become zero.

$$A_{16}=A_{26}=0 \quad (2.3)$$

For orthotropic laminates, normal forces and bending moments applied in the perpendicular two direction do not cause shear or twist of the laminate. Hence, there are no extension-shear, bending-twist, and extension-twist couplings. It means that, the following elements of the [A], [B] and [D] matrices are zero:

$$A_{16}=A_{26}=0 \quad B_{16}=B_{26}=0 \quad D_{16}=D_{26}=0 \quad (2.4)$$

A laminate is orthotropic when every ply is orthotropic and the orthotropic directions coincide with the x and y directions. As a conclusion, for symmetric, balanced orthotropic laminates, the stiffness matrix take the following form.

$$\begin{array}{ccc}
 [A] & [B] & [D] \\
 \begin{bmatrix} A_{11} & A_{12} & 0 \\ A_{12} & A_{22} & 0 \\ 0 & 0 & A_{66} \end{bmatrix} & \begin{bmatrix} 0 & 0 & 0 \\ 0 & 0 & 0 \\ 0 & 0 & 0 \end{bmatrix} & \begin{bmatrix} D_{11} & D_{12} & 0 \\ D_{12} & D_{22} & 0 \\ 0 & 0 & D_{66} \end{bmatrix} \\
 \end{array} \quad (2.5)$$

So it means that the Equation 2.5 indicates the terms of effecting the buckling phenomenon of the composite. The terms of null do not have any influence during the calculation of the buckling capability of the structure.

The remaining nonzero coupling terms have the visual definition given in Figure 2.8.





Coupling	No Coupling	Element
Extension-extension 		A_{12}
Bending-bending 		D_{12}

Figure 2.8 Illustration of the coupling terms of A_{12} , D_{12} [25]

2.5 Pre Buckling and Post Buckling of Stiffened Panels

Composite plates under compression and/or shear loading are sensitive to buckling failures. For small forces, the panels deform with none of any prominent differences in the shape and load holding capability. At crucial forces, the structure abruptly encounter a big distortion and diminish its load holding capacity, which is described as the pre-buckling phase. Accordingly, the buckling forces or the crucial forces are the forces when a panel goes into unsteady.

Post-buckling is the load regime a panel goes into later than buckling. In a stiffener supported structures, some of the section or the constituents may buckle. Choosing the sequence of which part would be allowed to buckle first is a vital question and needed a detail analysis for creating a lightweight design. For example, for the stiffened panel of Figure 2.9, the subsequent buckling style is able to be observed without material failure :

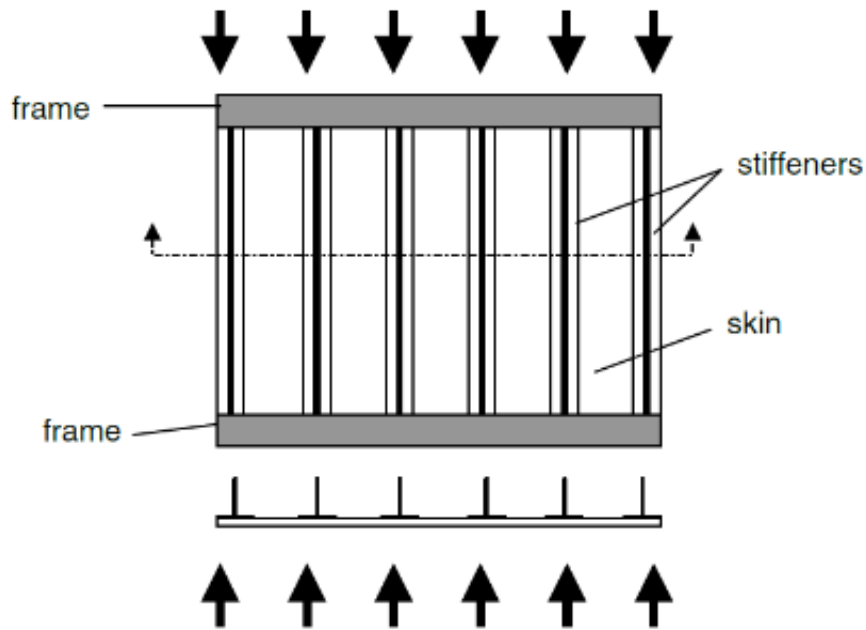


Figure 2.9 Stiffened panel under compressive load

- (a) Local Buckling: skin between stiffeners buckles and stiffeners stay straight, stiffeners continues to hold consequential amount of axial loads;
- (b) Local-Global Buckling: stiffeners buckle as columns
- (c) Global Buckling: panel buckles as a whole, the stiffeners help to principally increase the bending stiffness of the panel;

Figure 2.10 illustrates a realistic (experimentally measured) load-shortening curve of an axially compressed stiffened CFRP panel representing a stringer dominant design.

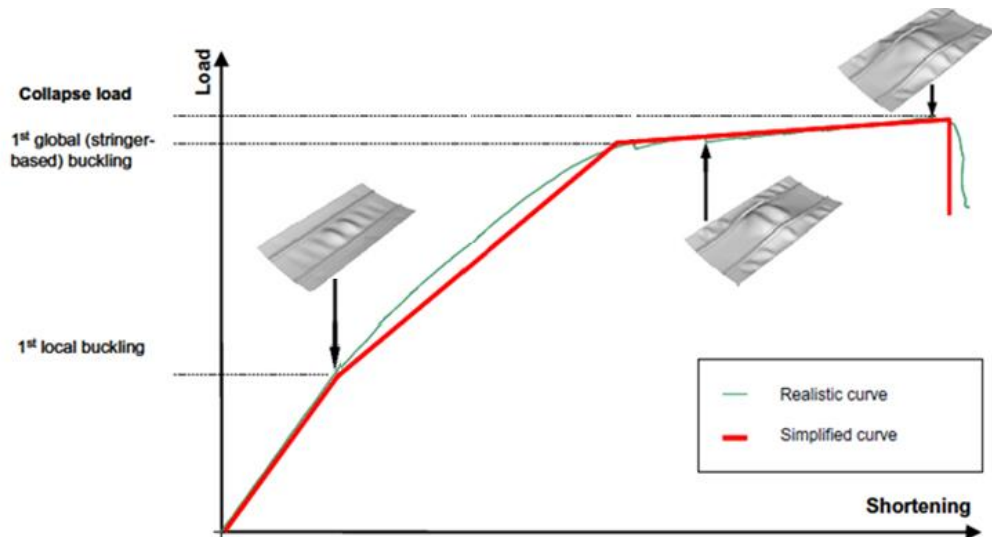


Figure 2.10 Definition of first local buckling and global buckling [26]

It describes the terms of three noticeable force ranks. The minimum one generally stimulates the initial local buckling in which the buckling mode is limited to local skin buckling between the stiffener. The next level creates the first overall buckling which is stiffener based-buckling. The highest load level is arrived at collapse [26].

The above mentioned failure modes are depicted in Figure 2.11. The post-buckling analysis in this study is only dedicated to see the behaviour of the structure after locally skin buckles.

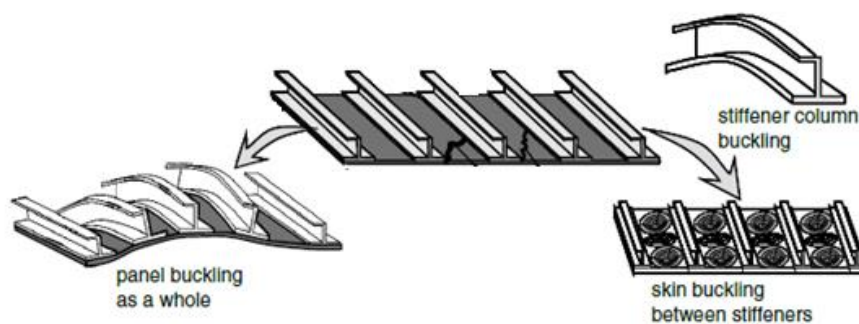


Figure 2.11 Possible failure modes in the stiffened panels [20]

When the stiffeners have adequate bending stiffness to remain without bend and compel the structure to buckle between the stiffener, the stiffener behaves as a boundary condition on the line of the stiffener edge of the panel. Due to the fact that the torsional rigidity of the open cross section stiffeners is very low, they are free to rotate with the skin edge on that portion and the corresponding boundary condition they impose is a simple support (zero deflection but nonzero rotation). That is the one of the reason to select T type (blade) stiffener in panel used in this study. However, the closed-cross-section stiffeners have very high torsional rigidity and they locally force the skin edge to closely fix, it is very close that of a fixed support (zero deformation and incline).

For a panel under compression, the efficient way to design the stiffened panel is to carry the majority of the compressive force by the stiffeners. The required stiffener cross-sectional area is less than the required skin cross-section area in order to sustain the same amount of compressive load. Because of that, after the critical buckling load is encountered, the stiffeners still remain without bending (no column buckling and no crippling) and the panel is not allowed to buckle as a whole.

Hence, generally, the buckling sequences for a post-buckled shell type structure supported with stiffener exposed to compression claims that buckling of the skin between stiffeners occurs at the beginning. The same principal is also valid for a panel buckling under shear load, enforcing the skin between stiffeners to buckle at the beginning is also preferable.

When combined loading of shear and an axial load (tension or compression) applied on a structure as the main subject of this study, the condition of stress improving in the post-buckling skin is extremely complicated and very difficult to acquire without a pleasurable computational model, usually based on finite elements as mentioned in chapter 1.

A stringer supported laminated plates exposed to both shear and compression is illustrated in Figure 2.12

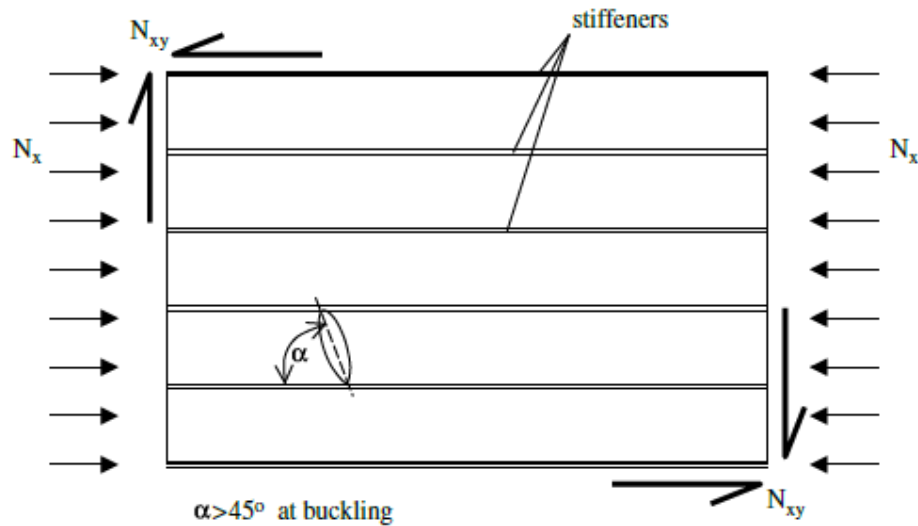


Figure 2.12 Potential failure modes in the stiffened panels [27]

A standard half-wave of the buckled panel is also shown in the figure. Figure out that, dissimilar to the pure shear situation in which the post-buckling angle α begins at 45° at buckling and reduces moderately with growing load, the attendance of a compressive load holds the half wave closer to the 90° orientation, i.e. the post-buckling angle α starts higher than 45° at buckling [27].

2.6 Linear and Nonlinear Buckling Analysis

The linear buckling (eigenvalue) analysis calculates the hypothetical buckling capability of an perfectly linear elastic system. In more explicitly, the linear eigenvalue buckling analysis of a structure yields the results by using classical Euler method. It gives a good indication of the critical buckling load within the elastic limit of the material. Moreover, the nonlinear buckling analysis uses a non-linear static analysis with progressively growing loads to investigate the load level where the stiffened plate turns into an unstable one. Hence, non-linear buckling analysis is more precise method and is suggested for the design or interpretation of real structures. An analysis of geometrical non-linearity is also carried out, with the purpose of detail study of the pre and post-buckling events. The computation time

required for the nonlinear analysis is an order of magnitude greater than that for the linear analysis, indicating significant nonlinearity with response (near the buckling load).

In order to run the linear buckling analysis in ANSYS, a static solution with pre-stress effects must be obtained, which must be followed by the eigenvalue buckling solution using the Block Lanczos method and mode expansion.

If a structure is perfectly symmetric (that is, its geometry including the mesh patterns and loading are both symmetric), the non-symmetrical buckling does not occur numerically, and a nonlinear buckling analysis fails because of non-symmetrical buckling responses cannot be triggered. In order to overcome this problem, some small geometric imperfections (similar to those caused by manufacturing of a real structure) must be introduced for triggering the nonlinear buckling responses.

From the beginning of 1900, several theoretical and experimental studies involving metallic thin-walled structures and, in the last decade, also involving composite structures have been devoted to the investigation of the influences of the initial geometrical flaws on the buckling load [28], [29] and [30]. The impact of the flaw on the buckling events including unsupported thin shells is widely known and comprehensively acknowledged as one of the principal sources of inadequate test-FEA interrelation. According to the theory that the impact of the initial flaw can mainly adapt the buckling behaviour of thin-walled structures under axial compression, it has been made a decision to measure the shape of the panel skin [31].

In this study, an initial imperfection is defined as a maximum displacement of 5% of the skin thickness with respect to the first two buckling modes of the stiffened panel. The similar definitions for an imperfection on the composite panel can also be found in [32], [33] and [34].

The nonlinear buckling analysis becomes a static analysis and performed after adding imperfections with large deflection activation in ANSYS solver. In order to perform the analysis, the load must be allowed to increase by using very small time increments so that the expected critical buckling load can be predicted accurately.

Buckling initiation is difficult to detect by visual inspection but can be observed by plotting a load-displacement curve or by a monitor file inspection. To detect the moment of buckling initiation, one should carefully study the monitor file created during run. During the initial buckling the sign of the MxDs change as shown in Figure 2.13.

SOLUTION HISTORY INFORMATION FOR JOB: shell1_LC_onlyaxial.mntr
ANSYS RELEASE 16.0 09:00:44 06/19/2015

LOAD STEP	SUB-STEP	NO. ATMP	NO. ITER	TOTL ITER	INCREMENT TIME/LFACT	TOTAL TIME/LFACT	VARIAB 1 MONITOR CPU	VARIAB 2 MONITOR MXDS	VARIAB 3 MONITOR MxP1
1	1	1	3	3	0.10000E-01	0.10000E-01	132.94	-0.20000E-01	0.78886E-30
1	2	1	1	4	0.10000E-01	0.20000E-01	204.64	-0.40000E-01	0.78886E-30
1	3	1	1	5	0.15000E-01	0.35000E-01	264.67	-0.70000E-01	0.78886E-30
1	4	1	1	6	0.22500E-01	0.57500E-01	333.06	-0.11500	0.78886E-30
1	5	1	1	7	0.33750E-01	0.91250E-01	395.60	-0.18250	0.78886E-30
1	6	1	2	9	0.50625E-01	0.14188	493.54	-0.28375	0.78886E-30
1	7	1	3	12	0.75938E-01	0.21781	616.58	-0.43563	0.78886E-30
1	8	2	3	30	0.35000E-01	0.25281	1404.1	-0.50563	0.78886E-30
1	9	1	18	48	0.35000E-01	0.28781	1949.8	-0.58664	0.78886E-30
1	10	1	4	52	0.35000E-01	0.32281	2135.3	1.5719	0.78886E-30
1	11	1	3	57	0.32300E-01	0.37331	2300.9	2.3470	0.78886E-30
1	12	1	3	60	0.78750E-01	0.45406	2411.5	3.0010	0.78886E-30
1	13	1	2	62	0.10000	0.55406	2493.5	3.5	86E-30

The sign is changed

Figure 2.13 Sample monitor file to show the buckling detection

If the convergence difficulty is observed due to buckling of the structure during the run, it indicates the onset of a post-buckling analysis. Due to the fact that the post-buckling state is unstable, specific methods are necessary to compensate. In a static analysis, nonlinear stabilization is the best option. When the structure goes into post buckling stage during the running, the analysis can be terminated and stabilization option in the program would be activated from the sub-step in which the change in time (or load) increment or displacement value is distinctive and sign is reversed as shown in Figure 2.13.

2.7 Conclusion

In this chapter, a brief information about the composite structures is given together with the introduction of their terminologies. In addition to these, the buckling and post-buckling phenomena of the stiffened panels are defined.

CHAPTER 3

FINITE ELEMENT MODELLING METHODOLOGY OF THE STIFFENED COMPOSED PANELS

3.1 Introduction

To perform the numerical analysis on the purpose of this study, the geometry and material properties of the stiffened panels would be defined first. Then, the boundary conditions and load application criteria should be described. In accordance with this, the geometrical and material information including dimension of the each member (skin, stringer), lamina properties with ply orientations, selection criteria for stiffener shape and boundary condition with load application techniques will be presented in this chapter.

After physical definition of the problems, the finite element modelling methodology of the stiffened composite panels will be introduced. Three different panels will be created basically by altering the number of stiffener on the panels and denoted as P1, P2 and P3. For all the three panels are rectangular flat panel with the size of 600 mmX800 mm. Several configurations for each panel are generated by changing the layup sequence of the skin and stiffener with different thickness.

3.2 Finite Element Modelling of the Laminated Shell Type Composites

The strength and deformation analyses of laminates can be performed in different levels depending on the detailed necessity which is determined by the degree of

desired post-processing. When a detailed stress level is necessary, the strength analyses are computed at the composing level which is fibre and matrix level. In this case, it is necessary to input the micro-structure information including the fibre model with geometrical distribution, and the mechanical properties of the materials. If a less detailed approach is required like buckling analysis on laminate level or stress analysis in lamina level, the composite material can be described by using an orthotropic material properties [35].

For the buckling analysis at the laminate level, the properties of each lamina like the orientation of each lamina with respect to the x-axis of the laminate, the thickness, and the elastic material properties have to be known prior to the analysis. Then, the software computes the matrices [A], [B] and [D] as defined in Chapter 2.4 internally. In this way, the software can compute the eigenvalues with corresponding eigenvectors (mode shapes) in laminate level.

Choosing the correct element type based on the problem characteristics and desired results is very important when using the FEM to analyze composites. The main non-layered and layered shell elements types used in ANSYS allow one to model thin to moderately thick shells, up to an edge-to-thickness ratio of 10. Some of them have 4 nodes and others have 8 nodes using interpolation functions of higher degree. These shell elements are defined in 3D space and have six degrees of freedom (DOF) at each node (translations in the nodal x, y, and z directions and rotations about the nodal x, y, and z axes). The 6th DOF (rotation about the z axis) is included in the shell formulation to allow modelling of folded plates, but it would not be necessary if the shell surface is smooth.

SHELL281 is chosen in this investigation thanks to the advanced nonlinear skills. It is appropriate for slender to deliberately-thick shell structures. The element consists of eight nodes with six DOF at each node: translations in the x, y, and z axes, and rotations about the x, y, and z-axes. (If it is preferred to use the membrane alternative, the element possesses translational DOF only.) SHELL281 is

appropriate for linear, big rotation, and/or large strain nonlinear implementation. Alter in shell thickness is regarded for in nonlinear analyses. The element has a capability for follower (load stiffness) influence of distributed pressures. SHELL281 can also be preferred for layered implementations for designing composite shells or sandwich construction. The element framing is established on logarithmic strain and true stress measures. The element kinematics enable for pieced membrane strains (elongated). However, the curvature alters in the frame of a time augmentation are supposed to be small. Figure 3.1 shows the shape, node positions, and the element coordinate system for this element. The element is described by shell partition information and by eight nodes (I, J, K, L, M, N, O and P) [28].

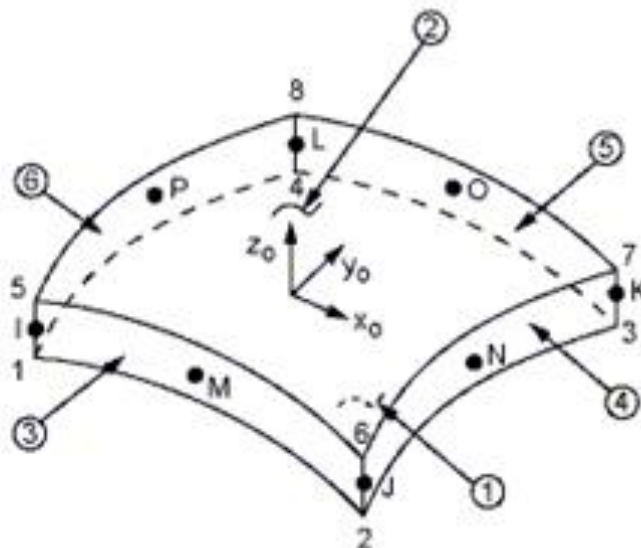


Figure 3.1 SHELL281 Geometry [36]

where x_0 = Element x-axis if element orientation (ESYS) is not provided.

x = Element x-axis if element orientation is provided.

Shell281 element type options are selected as given in Figure 3.2.

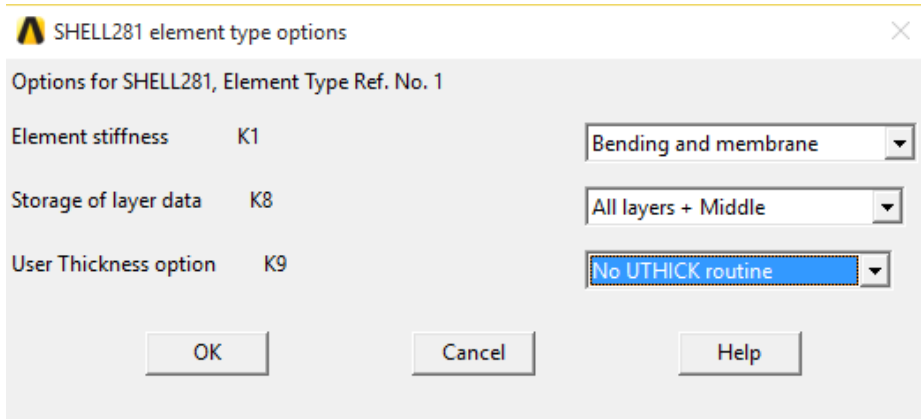


Figure 3.2 SHELL281 element type options

3.3 Stiffened Panel Model Definition

For the stiffened panels under consideration, the structure is modelled as flat. Normally, in aircrafts, the structure is slightly curved to make a closed cylindrical or elliptic section. However, most of the structures in the literature are modelled as flat panels as presented in Chapter 1. Also, since these structures have a big radius of curvature when compared to the stiffener and panel dimensions, it is assumed that modelling the structure as flat will not affect the buckling performance much.

The panel and stiffener dimensions are extracted from the test specimen [3] to simulate as much as close a real structure dimensions. Carbon/epoxy AS4/3501-6 pre-preg plies, with thickness of 0.117 mm [41] are used as the matrix material. The mechanical properties of the structure composed of variable laminas are recorded in Table 3.1. The material is defined in Ansys as linear-elastic orthotropic material model.

Table 3.1 Material properties for the composite material

E_{11}	E_{22}	G_{12}	ν_{12}
147 GPa	9 GPa	5 GPa	0.3

The principal purpose of stringers is to enhance the buckling strength of plates without enlarging the plate thickness. For the same amount of cross-sectional area,

the T type supporters owns a larger value of second moment of area when comparing with the rectangular shape stiffener. On top of that, they have more strength against beam-column buckling [42] and [14]. Thus, for three examples P1, P2 and P3 are stiffened with constant dimension T type stiffeners, capital located upside down, as shown in Figure 3.4.

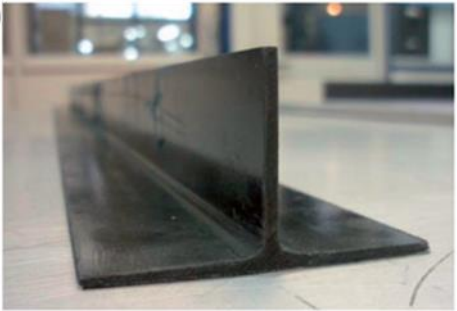


Figure 3.3 One sample of a manufactured T type-stiffener [41]

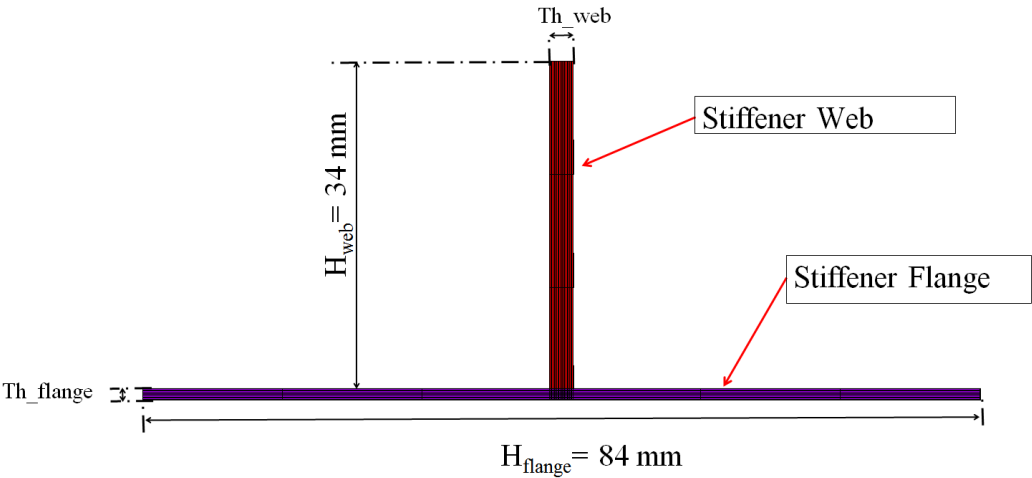


Figure 3.4 Stiffener geometry and parts

For a cross section depicted in Figure 3.3, the structure needs to be modelled with shell elements. Since shell elements are two dimensional, the three dimensional walls of the stiffener must be replaced with a reference surface. The thickness

effects should also be transferred to the FE analysis program as shell element property.

After creation of the solid model by using mid-surface of the each part (skin, web, flange) in ANSYS, three different shell lay-up properties for skin, web and flange have been defined by entering orientation, thickness and material information for each ply that constitutes the laminate by using Shell Section module in Ansys. In Figure 3.5, the input window for the "skin" lay-up section is illustrated as an example. For the other two components named web and flange, the section lay-up properties are defined in similar way.

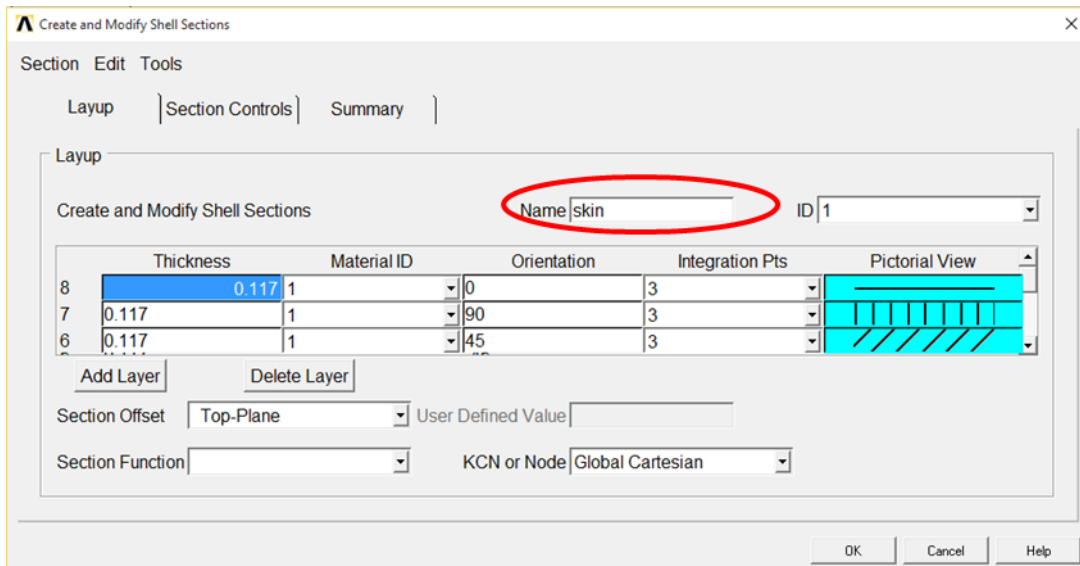


Figure 3.5 Shell section definition

The plotted skin lay-up as an example is also shown in Figure 3.6.

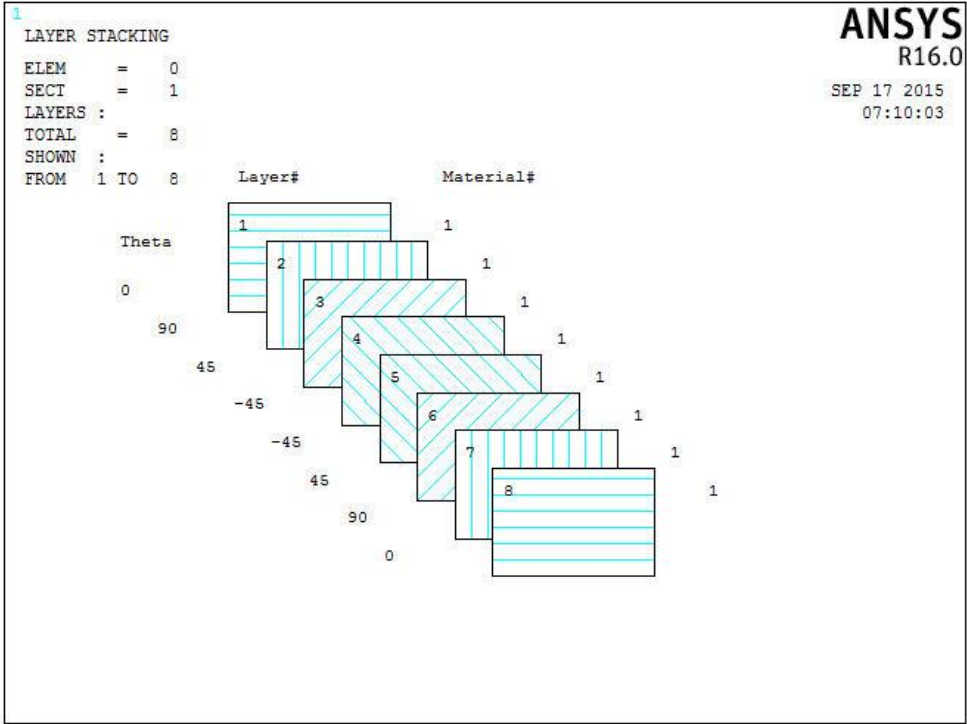


Figure 3.6 Skin lay-up plot

As seen in Figure 3.7, the blade vertical surface is represented by a surface located at the mid-plane. Also, the flange of the stiffener is modelled with a surface at the bottom, the thickness offset of the defined shell elements are out of this surface. An offset of the thickness is defined to the stringer and skin in order to take into account its certain bending stiffness. In Figure 3.7, the thicknesses are represented with an exaggerated drawing, but the surface dimensions of vertical section is so wide that the shell representation of the flanges does not change the surface dimensions of this middle vertical section.

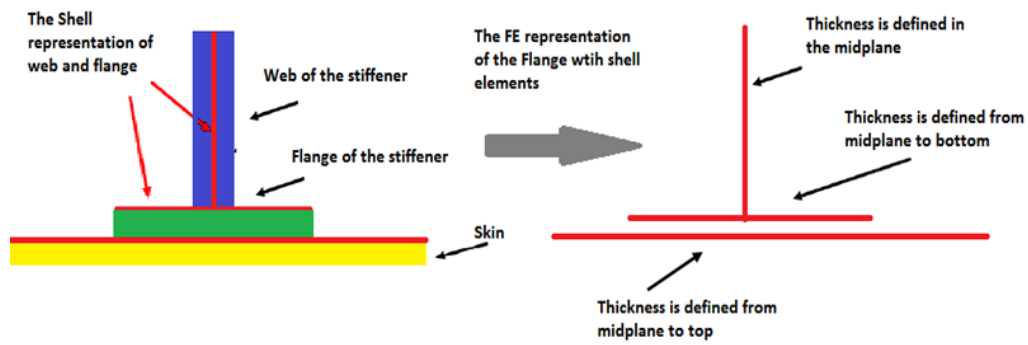


Figure 3.7 Simplified FE model of the stringer

Skin to stiffener connection in ANSYS is modelled by using contact elements. The assembling parts with contact elements is modelled and meshed independently, and then by assigning convenient contact algorithms at interval of the meshes of the skin and stiffener flange. Detail information about the contact is given in Chapter 4.1.2. The

Figure 3.8 and Figure 3.9 show the finite element model of P1, P2 and P3 panels with mesh size of 15 mm.

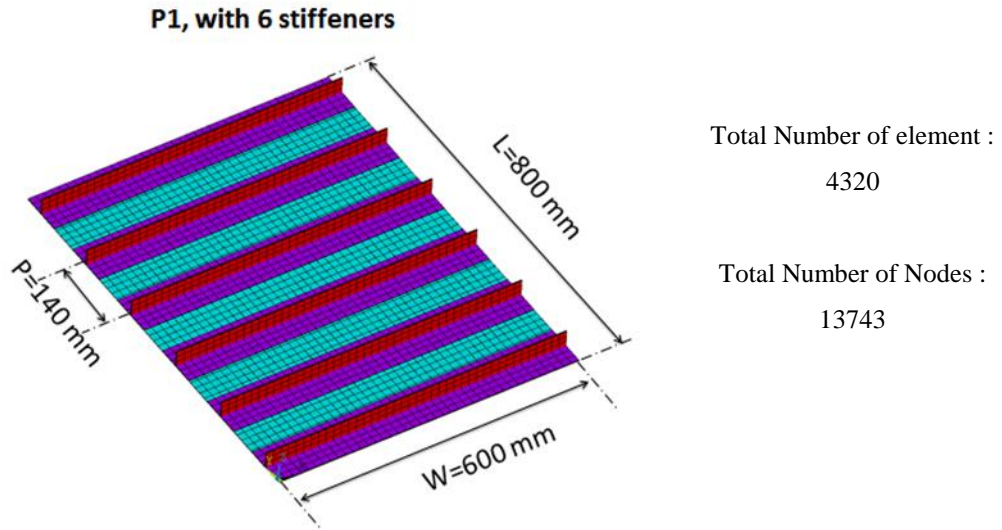


Figure 3.8 Finite element model of P1 and dimensions

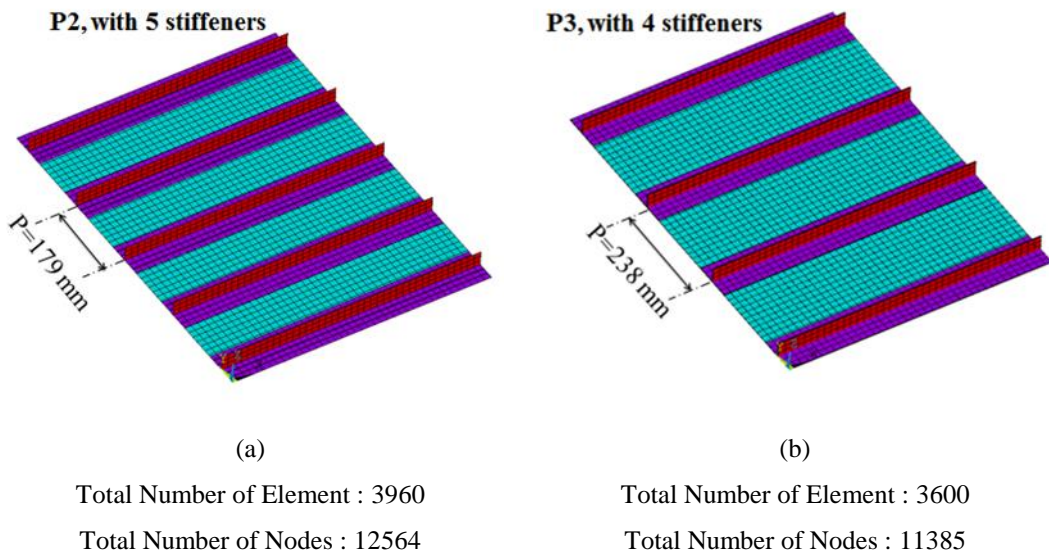


Figure 3.9 Finite element model of (a) P2 and (b) P3

3.3.1 Boundary Conditions and Loading

The boundary conditions for this structure are such that it can represent the test conditions performed in [36]. For the buckling analysis in this study, the fixed

bottom edge of the panel is simply restrained in the longitudinal, lateral and vertical direction. The line of rotation of the specimen end coincides with the center of the cylindrical roller, indicated by point c in Figure 3.10, ensuring that the axial load is always directed through this line. Also, the longitudinal edges of the panel are restrained in the lateral direction due to allow movement of the specimen in y direction. In the test condition this restriction is provided by Teflon plates as shown in illustrative Figure 3.10 . Lateral supports hold the specimen constant along the z direction [43]

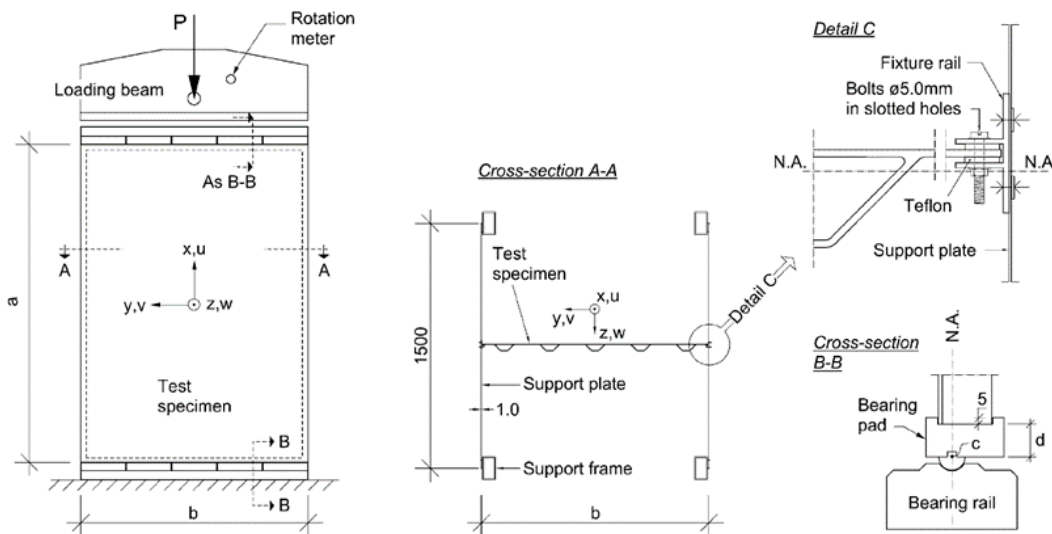


Figure 3.10 Illustrative test set-up (Stiffened aluminum panels subjected to axial) [43]

Under the above mentioned information, the boundary conditions for the structure are depicted in Figure 3.11. The lower edge is fixed in the longitudinal, lateral and vertical direction. Four edges of the panel are also restrained in the lateral direction. The load is applied through the whole cross section of the upper edge of the structure by giving displacement value in x and y direction.

The axial load is applied to the structure as a constant value of 2 mm displacement in x direction (U_x) as shown in Figure 3.11 for all of the analyses carried out. On the

other hand, due to the fact that the aim of this study is to investigate the shear load effect on the structure buckling capability beside the axial loading, the shear load will be applied on the structure in y direction as a variable values of displacement (U_y) as indicated in Table 3.2

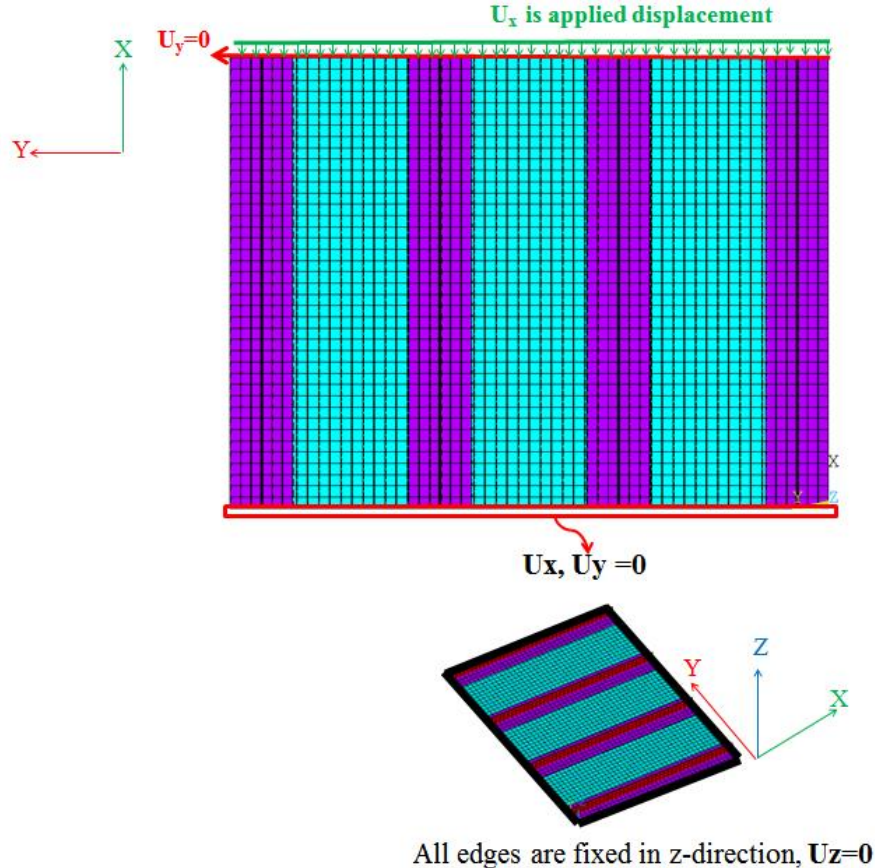


Figure 3.11 Applied boundary conditions and applied constraints

Table 3.2 Applied Load Ratios

Load Case Definition (LC)	Applied Load as displacement	
	Ux	Uy
	mm	mm
LC1	2	0
LC2	2	0.125
LC3	2	0.25
LC4	2	0.5
LC5	2	1
LC6	2	1.5
LC7	2	1.75
LC8	2	2

In this study, the results will be evaluated mainly based on the ratio of applied axial load to applied shear load ratio. These loads are obtained by reading the reaction force on the nodes of the upper transverse edge of the panel which are depicted on Figure 3.11.

3.3.2 Configuration of the Panels

The skin and stringer ply angles are variable to see the effect of the layup. The ply angles of the skin and stringer should be selected among -45° , 0° , 45° , 90° because of the manufacturing constraints as in the other studied models in this thesis. The layup of the skin are generally symmetric and balanced to reduce bending extension and shear extension coupling effects except for one skin layup to observe the unbalanced layup skin effect. The plates analyzed are thin, and the transverse shear strains are regarded as ineffective. They are made up of laminates with an uncontrolled number of layers, according to the supposition, of symmetric lay-up, i.e. $B_{ik} = 0$, and null membrane anisotropy, i.e. $A_{16} = A_{26} = 0$. Moreover, the bending-twisting coupling terms D_{16} and D_{26} are not disregard, hence the formulation can be put into practice to the investigation of plates composed of symmetric and balanced laminates as mentioned in Chapter 2 in detail.

For each of the panels P1, P2 and P3, there are 12 different configurations (as defined Configuration) as given in the Table 3.3. All the skins are symmetric and balanced orthotropic plates except for skin 4. Skin 4 is symmetric but not balanced orthotropic plates as mentioned above, so the effect of such kind of panel is also investigated.

In Appendix A, calculated A, B and D values are given for each configurations.

Table 3.3 Configurations with lay-up sequences for skin, web and flanges

Configuration Number	Type of element	Lay-up sequence	Number of Layer	Thickness (mm)
Conf.1	skin_1	(0 90 45 -45) _s	8	0.936
	flange_1	(0 90 45 0 -45) _s	10	1.17
	web_1	(0 90 45 0 -45 45 0 -45 90 0) _s	20	2.34
Conf.2	skin_1	(0 90 45 -45) _s	8	0.936
	flange_1	(0 90 45 0 -45) _s	10	1.17
	web_2	(45 0 -45 45 0 -45 90 0) _s	16	1.872
Conf.3	skin_1	(0 90 45 -45) _s	8	0.936
	flange_1	(0 90 45 0 -45) _s	10	1.17
	web_3	(0 -45 0 45 90) _s	10	1.17
Conf.4	skin_2	(0 45 0 -45 45 -45) _s	12	1.404
	flange_2	(0 0 90 0 45 -45) _s	12	1.404
	web_1	(0 90 45 0 -45 45 0 -45 90 0) _s	20	2.34
Conf.5	skin_2	(0 45 0 -45 45 -45) _s	12	1.404
	flange_2	(0 0 90 0 45 -45) _s	12	1.404
	web_2	(45 0 -45 45 0 -45 90 0) _s	16	1.872
Conf.6	skin_2	(0 45 0 -45 45 -45) _s	12	1.404
	flange_2	(0 0 90 0 45 -45) _s	12	1.404
	web_3	(0 -45 0 45 90) _s	10	1.17
Conf.7	skin_3	(0 90 45 -45 0 45 -45) _s	14	1.638
	flange_3	(0 90 0 0 45 0 -45) _s	14	1.638
	web_1	(0 90 45 0 -45 45 0 -45 90 0) _s	20	2.34
Conf.8	skin_3	(0 90 45 -45 0 45 -45) _s	14	1.638
	flange_3	(0 90 0 0 45 0 -45) _s	14	1.638
	web_2	(45 0 -45 45 0 -45 90 0) _s	16	1.872
Conf.9	skin_3	(0 90 45 -45 0 45 -45) _s	14	1.638
	flange_3	(0 90 0 0 45 0 -45) _s	14	1.638
	web_3	(0 -45 0 45 90) _s	10	1.17
Conf.10	skin_4	(0 0 90 0 -45 45 0 -45 90 0 0) _s	22	2.574
	flange_4	(0 90 0 0 0 90 0 45 0 -45 0) _s	22	2.574
	web_1	(0 90 45 0 -45 45 0 -45 90 0) _s	20	2.34
Conf.11	skin_4	(0 0 90 0 -45 45 0 -45 90 0 0) _s	22	2.574
	flange_4	(0 90 0 0 0 90 0 45 0 -45 0) _s	22	2.574
	web_4	(0 90 0 0 45 0 -45 -45 0 45 90 0) _s	24	2.808
Conf.12	skin_4	(0 0 90 0 -45 45 0 -45 90 0 0) _s	22	2.574
	flange_4	(0 90 0 0 0 90 0 45 0 -45 0) _s	22	2.574
	web_5	(0 90 0 0 0 90 0 0 0 -45 0 45 90 0) _s	28	3.276

Also apart from these 12 configurations, 4 additional configuration are created to just observe the skin lay-up effect being formed full 0 degrees lay-up to nearly full 45 degrees lay-up as shown in Table 3.4.

Table 3.4 Configuration 13 to 16 with respect to skin lay-up sequences

Configuration Number	Type of element	Lay-up sequence	Number of Layer	Thickness (mm)
Conf.13	skin_5	(0 45 -45 45 -45 45 -45) _s	14	1.638
	flange_3	(0 90 0 0 45 0 -45) _s	14	1.638
	web_1	(0 90 45 0 -45 45 0 -45 90 0) _s	20	2.34
Conf.14	skin_6	(0 0 0 45 -45 45 -45) _s	14	1.638
	flange_3	(0 90 0 0 45 0 -45) _s	14	1.638
	web_1	(0 90 45 0 -45 45 0 -45 90 0) _s	20	2.34
Conf.15	skin_7	(0 0 0 0 0 45 -45) _s	14	1.638
	flange_3	(0 90 0 0 45 0 -45) _s	14	1.638
	web_1	(0 90 45 0 -45 45 0 -45 90 0) _s	20	2.34
Conf.16	skin_8	(0 0 0 0 0 0 0) _s	14	1.638
	flange_3	(0 90 0 0 45 0 -45) _s	14	1.638
	web_1	(0 90 45 0 -45 45 0 -45 90 0) _s	20	2.34

3.4 Conclusion

In this chapter, the physical properties of the problems was defined first. After this definition, the baselines of finite element modelling were established and FE models were created with application of the boundary condition successfully. In Appendix B, the created ANSYS input file is presented. Also configurations of the panels were tabulated and presented. To verify the baseline characteristics of the FE model of these three panels like mesh size, joint modelling, contact algorithms, the sensitivity and validations studies will be performed in Chapter 4 and Chapter 5 respectively

CHAPTER 4

SENSITIVITY STUDIES

4.1 Introduction

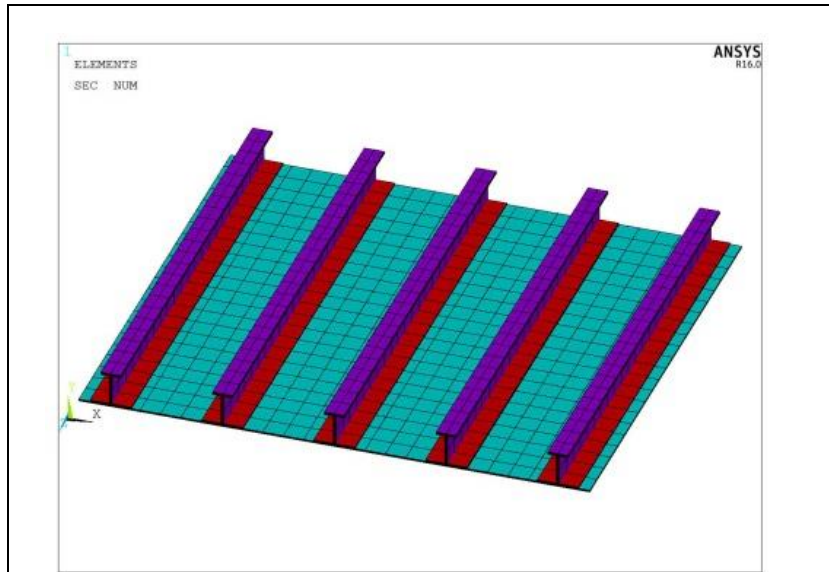
The purpose of the sensitivity studies is to verify the baseline FEM characteristics of the stiffened panels defined in Chapter 3. Under this purpose, the results of the baseline FEM characteristics are compared with the results obtained by the variability parameters on the model. The baseline FEM characteristics of the stiffened panels defined in Chapter 3 are :

- 1- The size of 15 mm elements are used to create the mesh.
- 2- Stiffener to skin connection was modelled by Contact element (Bonded-always)
- 3- Shell281 element type is used.

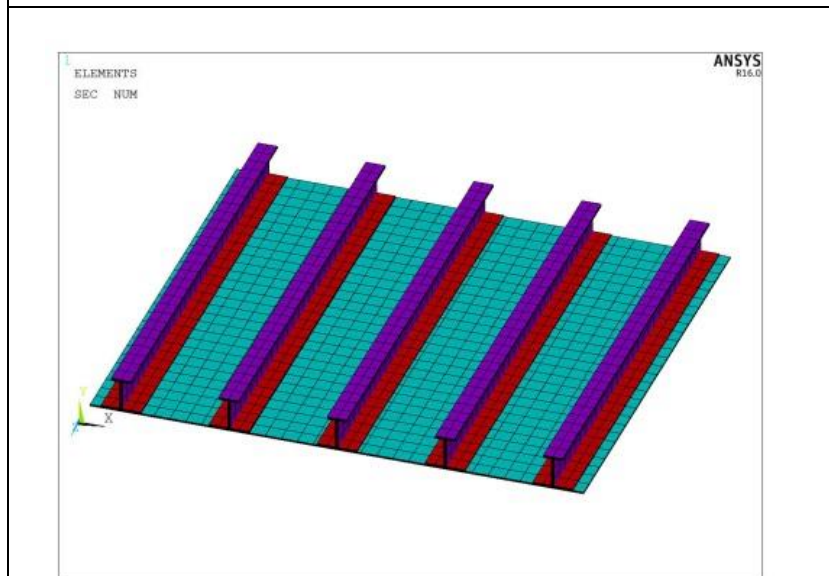
The variability parameters used during the sensitivity studies are the element sizing, joint modelling and the contact modelling technique. The comparison of the parameters are summarized in tables in terms of qualitative and quantitative assessment according to the baseline model results at the end of the each parameter. The related computation times necessary to fulfil the analysis are also given in these tables.

4.2 Mesh Refinement

The first parameter used in the sensitivity study is the mesh size of the models. The mesh refinement of sensitivity study started with a baseline model with a fully integrated shell elements with 15 mm element size. Three additional variants are created by altering the element size, namely: two coarse element size, owing an element size of 20 mm and 25 mm, and a fine element size with a 10 mm. The finite element models with different element sizes are depicted in Figure 4.1.

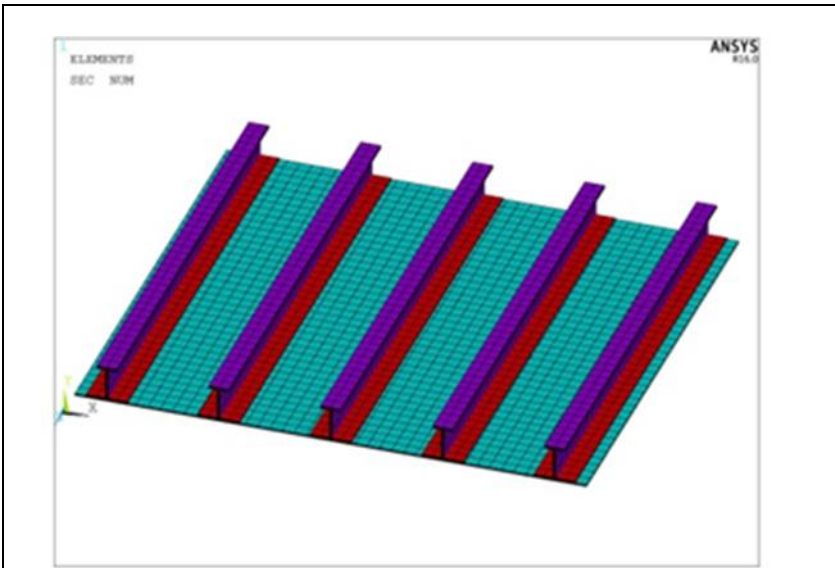


a) Coarse Mesh: Element Size : 25 mm
 Total Number of Element : 1210
 Total Number of Nodes : 4010



b) Baseline Mesh : Element Size : 20 mm
 Total Number of Element : 2128
 Total Number of Nodes : 6878

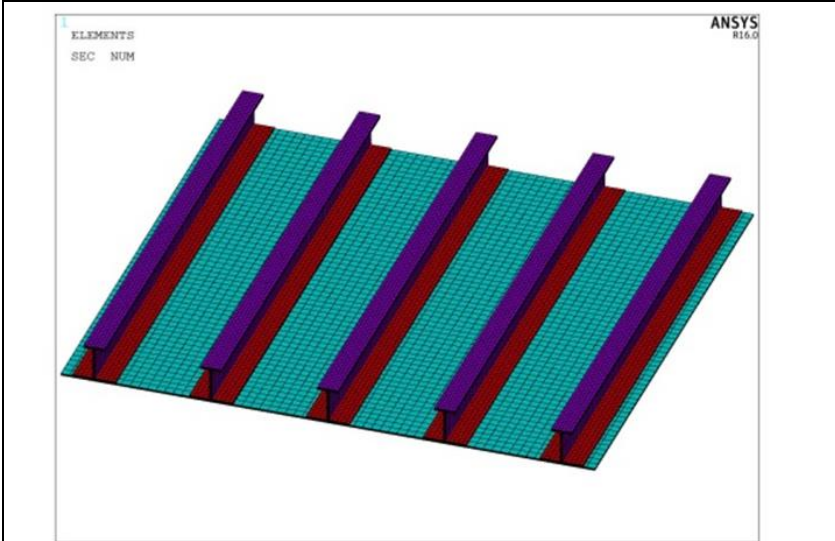
Figure 4.1 The FEM of stiffened panel with different element sizing



c) Baseline Mesh : Element Size : 15 mm

Total Number of Element : 3264

Total Number of Nodes : 10428



d) Fine Mesh: Element Size : 10 mm

Total Number of Element : 17160

Total Number of Nodes : 53070

Figure 4.2 The FEM of the stiffened panel with different element sizing-Cont.

A comparison of the meshes with three different sizes is carried out on the basis of load vs end shortening curves. Differences with respect to the baseline model are shown in Figure 4.3. This figure is created from the load vs end shortening curves of each meshed sized model without considering critical buckling point of the panel. The results show that there is a maximum $\pm 1.5\%$ differences of the 10 mm, 20 mm and 25 mm mesh sized model in reference to baseline model. It indicates that the slope of the each load vs end-shortening curves are very close to each other. On the other hand, the drawback of mesh sized 20 mm has an convergence difficulty after $U/U_{cr}=1.3$. The computation time is a disadvantage of the mesh sized 10 mm. It is 2 times higher than baseline model as seen in Table 4.1.

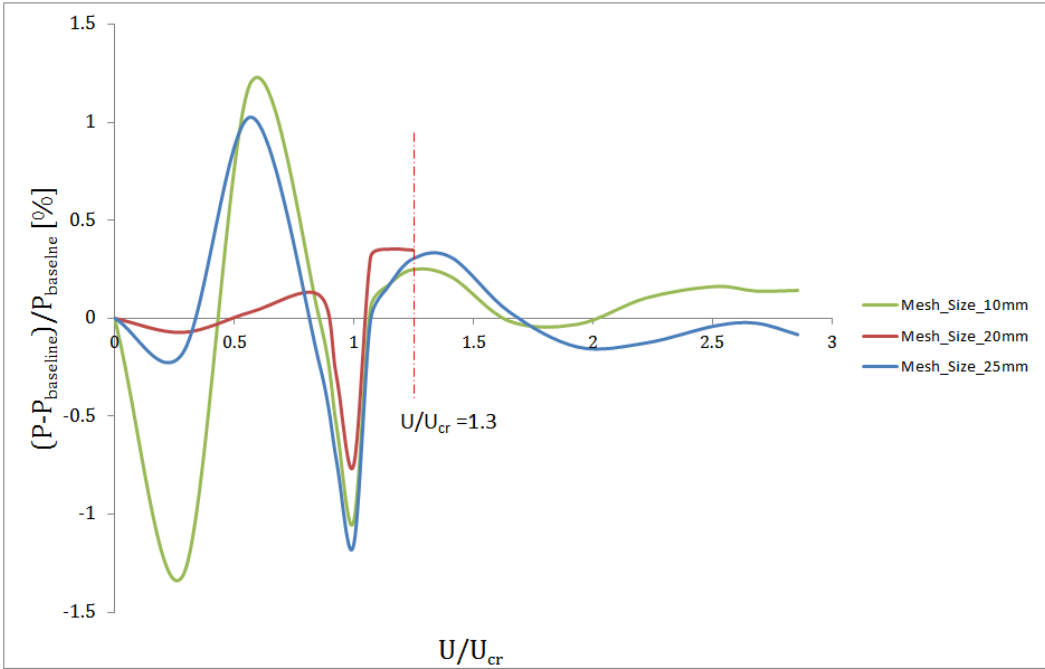


Figure 4.3 Sensitivity studies of mesh refinement outputs: change of the load vs. end shortening curves according to the baseline model

The mode shapes of the panel during the first buckling mode is also investigated. The first buckling mode shape for this case is expected to be four half waves in the last bay between two adjacent stringers which is based on the experimental results [37]. In Figure 4.4, the first mode shape of the each model with different element

sizing is depicted. It can be seen that 2nd model have 5 half waves, so it is eliminated. On the other hand, among the 1st, 3rd and 4th models, the most sound deflected shape is that of the 1st model.

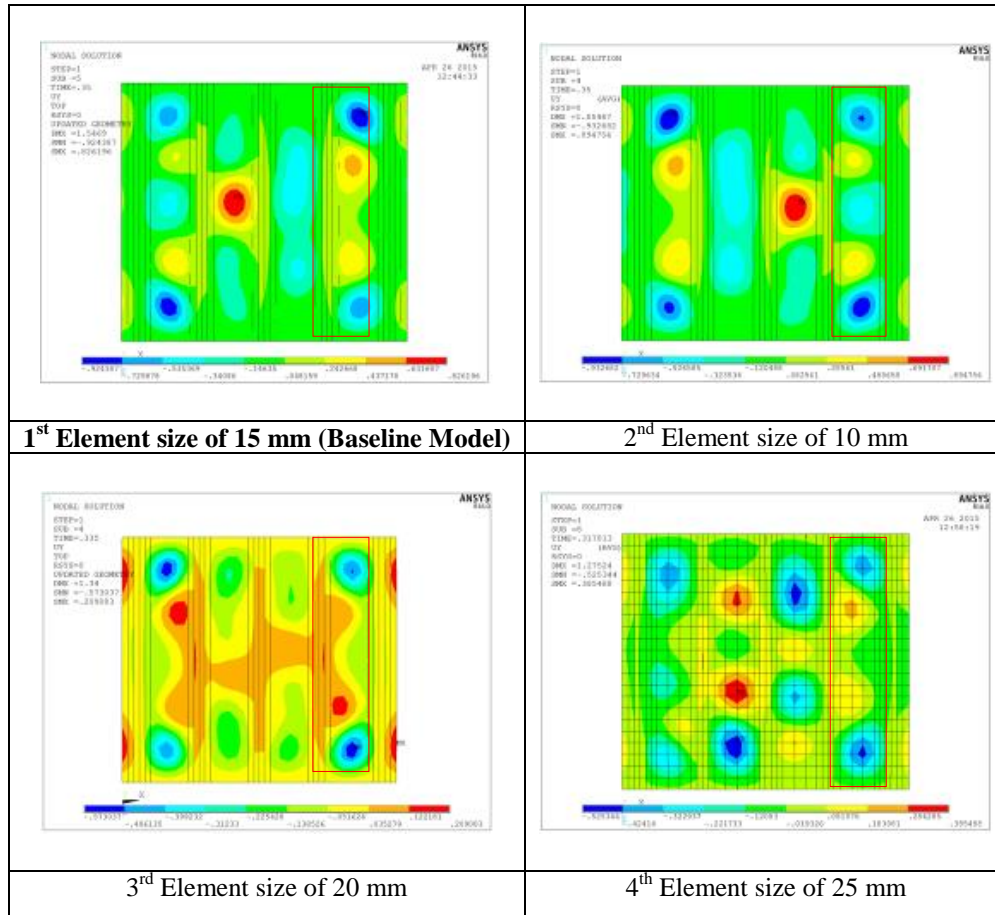


Figure 4.4 First mode shapes of the panels for different mesh sized panels

The outputs of the mesh size sensitivity studies are tabulated in Table 4.1. It can be seen that the baseline model give better results when compared with the others.

Table 4.1 Summarized results table from the output of the mesh sizing parameter

	Refinement	Joint Modelling	First Buckling Load	CPU Time	1 st Mode Shape Similarity to the test result
Bonded (Always) contact	Base_15mm	Bonded (Always) contact	517 KN	1526	Good
	Fine_10mm	Bonded (Always) contact	517 KN	7846	Good
	Coarse_20mm	Bonded (Always) contact	495 KN	1737	Satisfactory
	Coarse_25mm	Bonded (Always) contact	511 KN	618	Satisfactory

4.3 Joint Modelling

The second parameter investigated under the sensitivity studies is the joint modelling technique with and without contact elements between stiffener and skin.

Skin to stiffener connection in ANSYS can be modelled by using contact elements or using common elements at the interface area. The FE code presents a kind of contact element options as point-to-surface or surface-to-surface with high-order or low-order elements. In ANSYS, there are several contact algorithm like rough, separable, bonded that can use either of MPC (Multi Point Constraints), Augmented Lagrange and Penalty methods for connecting different meshes so that they can move together. In this thesis, a MPC based bonded contact algorithm is used for connecting the nodes of the panel and the stiffeners. This contact algorithm is very

easy to build in ANSYS. The assembling parts (skin or stiffener) with contact elements are created and meshed individually, and then by assigning convenient contact algorithms in the middle of the meshes of the skin and stiffener flange. After the definition of the contact between the parts, they are able to move together under deformation of the assembly. An ideal contact after sensitivity studies was decided to be bonded (always) with type nodes-to-surface. The detailed information about the contact types in ANSYS can be found in [36].

The other way to join the skin to stiffener bottom flange is to use the same/common elements in interface region. In Figure 4.5, the above mentioned two joint modelling techniques are plotted from the cross-section view of the skin-stiffener interface.

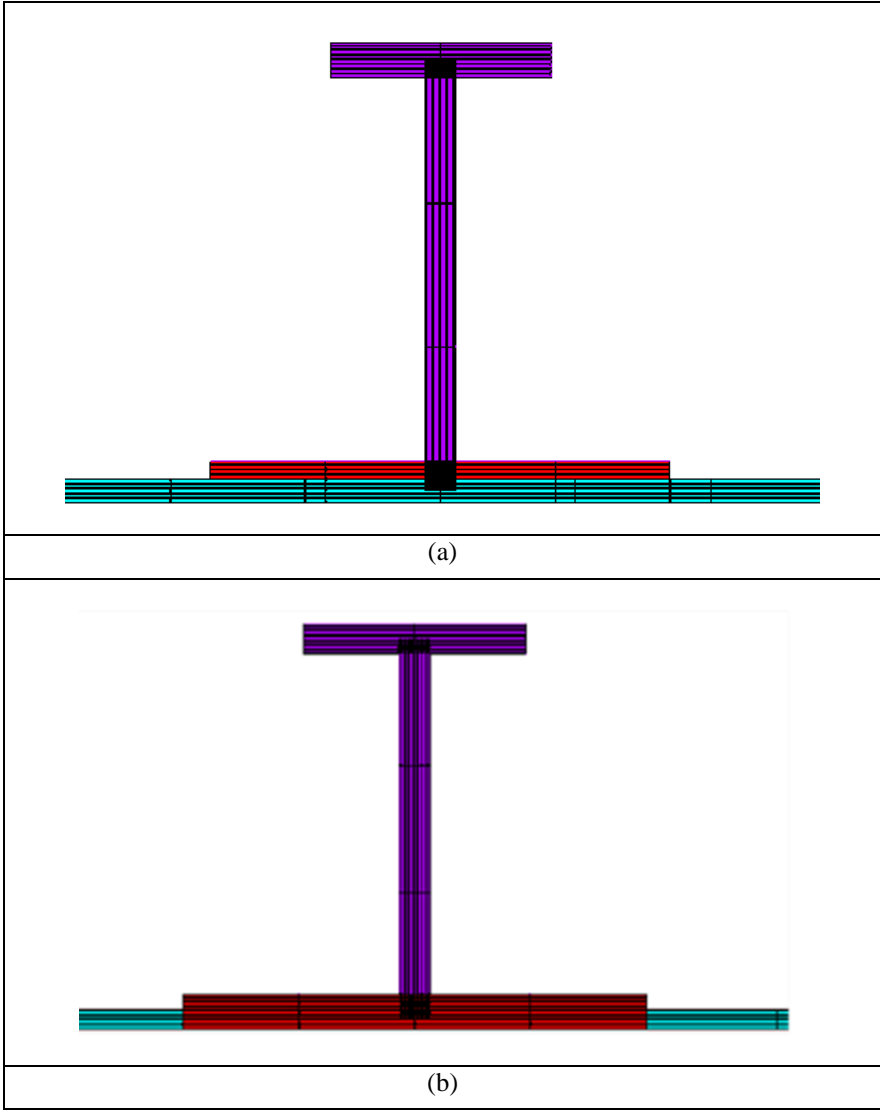


Figure 4.5 Joint Modelling Techniques (a) by using contact elements (b) common elements used model

In assembling the parts without contact elements, the joint between the skin and stiffener is obtained by using common elements at the interface location and

jointed basically using the same nodes. Two kind of mesh size (10 mm and 15 mm) for this joint modelling are compared with baseline model.

The third parameter selected to compare is the different contact algorithms defined in the ANSYS. The baseline model is created with bonded (always) contact type between the stringer and skin. This model is compared with other two contact types in ANSYS which are the “no separation” contact and “bonded” contact.

The results of those joint related parameters are shown in Figure 4.6 in terms of applied force with respect to end-shortening diagrams with the differences according to the base-line model. Although it can be observed from the figure that the bonded contact results are very close to the base model, it can be seen in Table 4.2 that the first buckling load is very earlier developed with poor mode shape. The other joint type has a divergence more than 15 % according to the baseline model loading at the same displacement ratio.

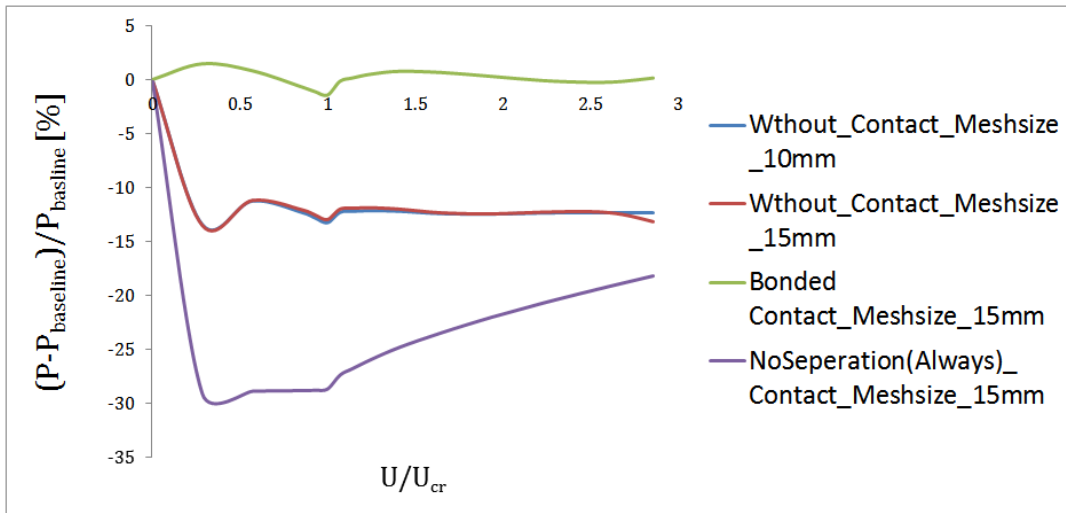


Figure 4.6 Sensitivity study results with respect to mesh size

In Figure 4.7, the primary mode state of the every FE model with joint modelling types is depicted. According to this figure, 3th and 4th ones are close to the baseline model.

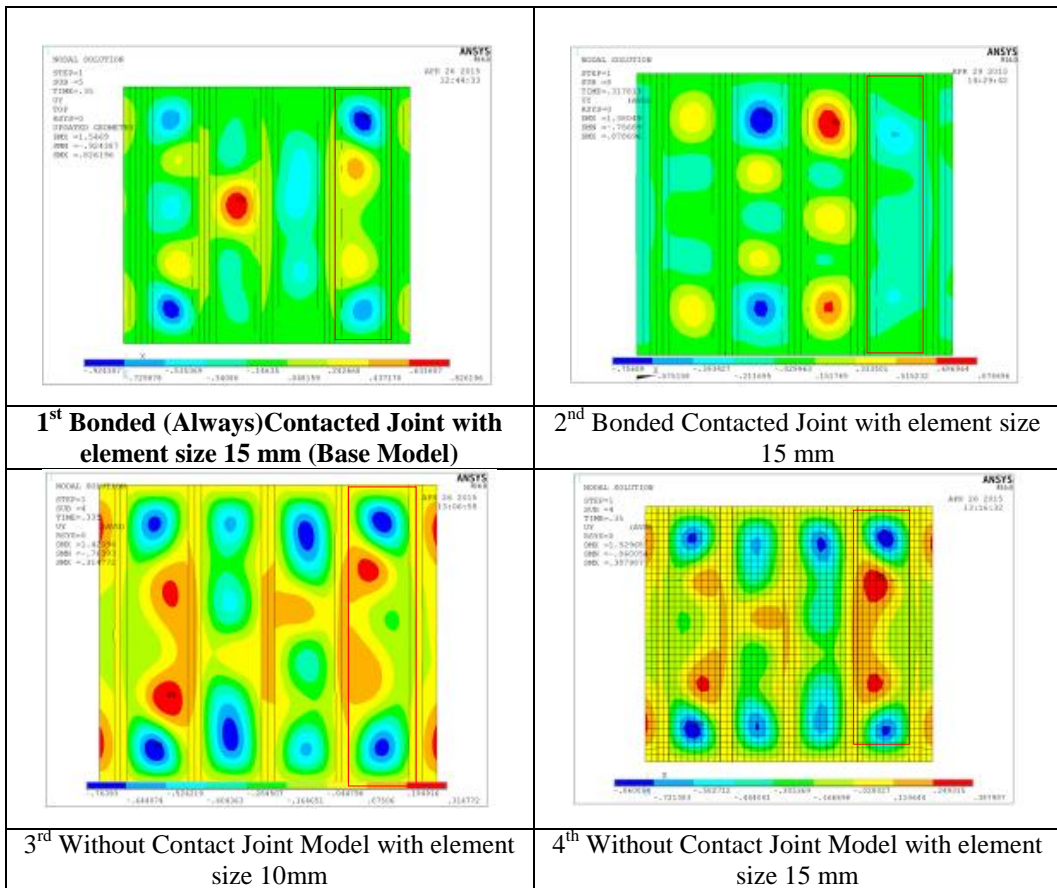


Figure 4.7 First mode shape plotting in accordance with joint modelling type

The outputs of the mesh size sensitivity studies are tabulated in Table 4.2. And it can be inferred that baseline model results are better than the others.

Table 4.2 Summarized results table from the output of the sensitivity studies.

	Refinement	Joint Modelling	First Buckling Load	CPU Time	1st Mode Shape Similarity to the test result
	Base_15mm	Bonded (Always) contact	517 KN	1526	Good
Integrated Node Joints	Fine_10mm	Integrated Node Joints	434 KN	3040	Good
	Mesh size 15mm	Integrated Node Joints	453 KN	641	Good
Different Contact Modelling	Mesh size 15mm	Bonded Contact Mesh_Size_15mm	469 KN	2308	Poor
	Mesh size 15mm	No Separation Contact Mesh_Size_15	No Buckling observed.	2021	Poor

4.4 Conclusion

The results from the sensitivity studies indicate that the base model selected due to best matching with test outputs [37] represents a good compatible results among the efficiency of the numerical outputs and run time when checking against with the other parameters.

CHAPTER 5

VALIDATION STUDIES FOR BUCKLING

5.1 Introduction

In this chapter, the results of the various validation studies for different type of stiffened panels having different loading conditions will be given. Due to the fact that the validation of the numerical buckling analysis results is very crucial, the outputs of the numerical analysis are correlated with the test outcomes. Under the scope of this study , no experimental studies have been performed. Therefore, the test results which are available in literature have been used in order to verify the developed numerical model. Three models with their experimental results have been selected from the literature. These are :

1. A Flat Stiffened Panel Under Axial Loading performed by Zhu et al. [37]
2. A Curved Stiffened Panel Under Axial Loading done by Zimmermann et al. [39]
3. A Flat Stiffened Panel Under Shear Loading performed by Taki et al. [40]

In this chapter, beside the results of the comparison studies between the numerical and test outputs from the literature, the information about the geometry and test set-up of the specimens provided by related papers is also given.

5.2 A Flat Stiffened Panel Under Axial Loading

5.2.1 Problem Definition for Flat Panel Under Axial Loading

In [37], I shape stiffened panel is produced and tested to investigate the buckling behavior of the stiffened panels. The shape of the panel is flat and five stiffeners are attached to it as shown in Figure 5.1. The panel has the dimensions of 617 mm width and 630 mm length and the stiffeners have dimensions of 50 mm height. The shape of stiffeners is shown in Figure 5.2. A compression load is applied in the longitudinal direction of the panel and its buckling characteristics are investigated.

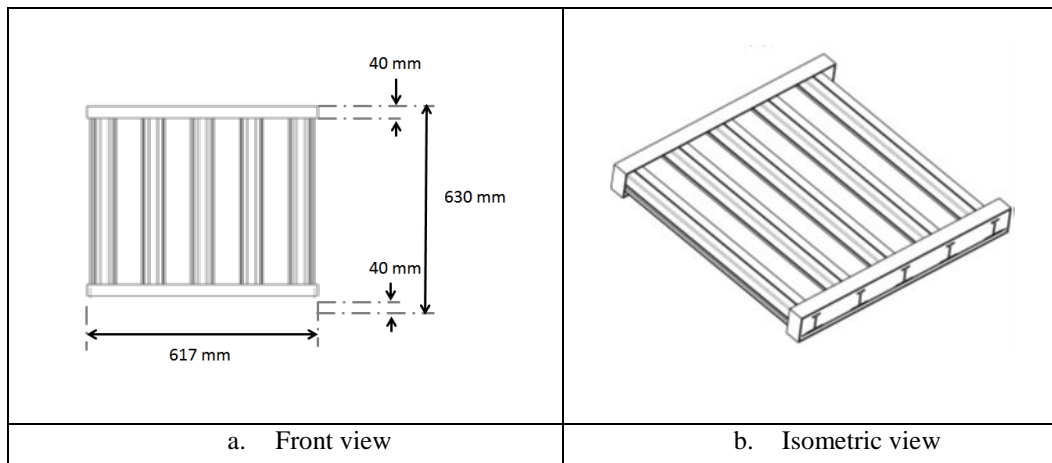


Figure 5.1 The blade-stiffened panel studied by Zhu et al. [37]

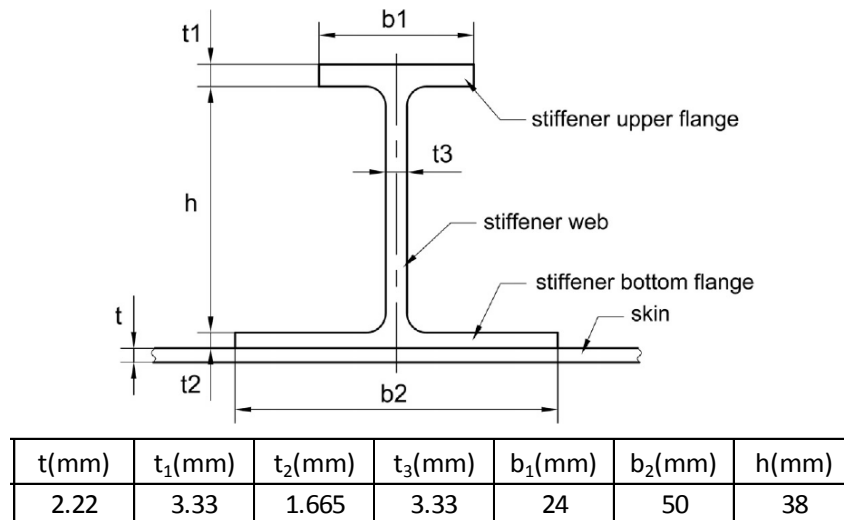


Figure 5.2 Cross-sectional view and dimensions of the stiffener [37]

The skin and the stiffeners are both made of composite material CYCOM 977-2, the material properties are also given in Table 5.1. The lay-up of the plate is [45/-45/0/90/-45/45]_s. The lay-up of the supporter outer flange and the stiffener web is [45/0/0/-45/90/-45/0/0/45]_s. The lay-up of the supporter bottom flange is [45/0/0/-45/90/-45/0/0/45]. The thickness of each layer is 0.185 mm.

Table 5.1 Material properties given for the composite material in [37]

E_{11}	E_{22}	G_{12}	ν_{12}
140.5 GPa	8.54 GPa	4.37	0.3

5.2.2 Test Set-Up for Flat Panel Under Axial Loading

The uni-axial compression tests of the panels have been performed using a hydraulic test machine with a max. capability of 5000 KN [37] as shown in Figure 5.3 (a). The strain gauges were located as shown in Figure 5.3 (b).

A hydraulic actuator in vertical movement capability is placed in the below of the specimen, on the other hand, the upper part is fixed during the tests. The other two lateral sides of the specimen were free.

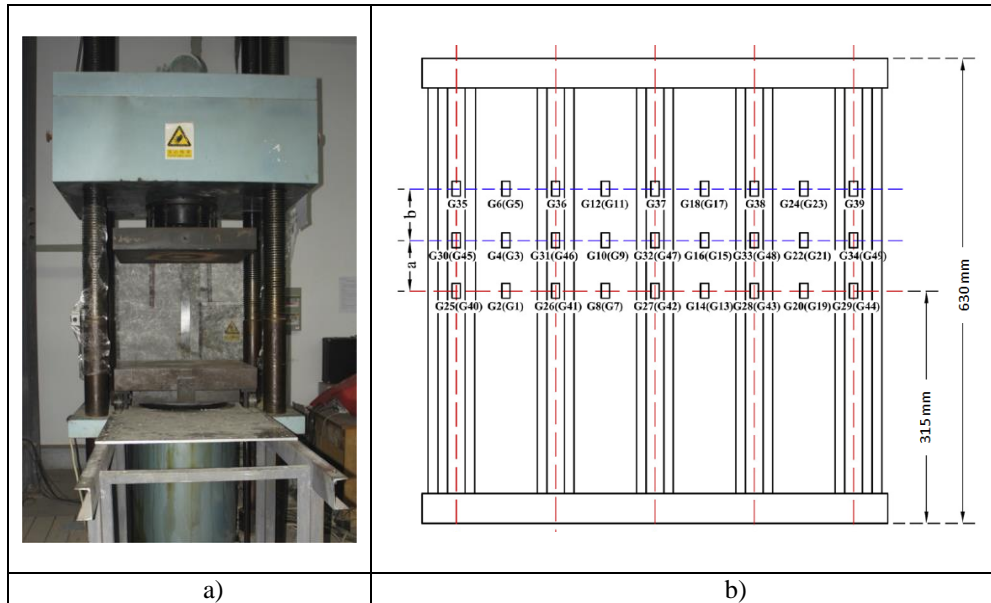


Figure 5.3 (a) Hydraulic compression test machine, (b) Locations of the strain gauges. [37]

5.2.3 Analysis Model for Flat Panel Under Axial Loading

The structure is modelled in ANSYS. The blade type stiffeners are simply composed with flanges and web. Blade-stiffeners are modelled as shell elements with their bottom surfaces in the flanges and mid-planes in the blade. The FEM definition is exactly complied with rules of the baseline model. Shell 281 element is used with 15 mm element size. Bonded (always) contact algorithm is described between the stiffener and skin. The meshed model is depicted in Figure 5.4 (b). The panel is fixed from lower side in all direction while the load is introduced as a uniform displacement on the complete upper edge, see Figure 5.4 (a), as a static load since it was a static buckling test. The lateral two side is free in all directions.

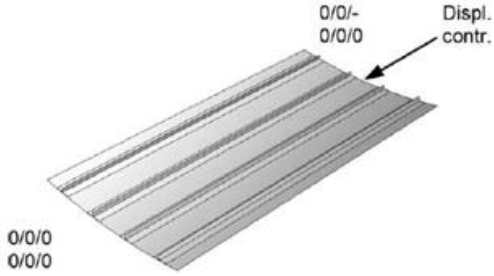
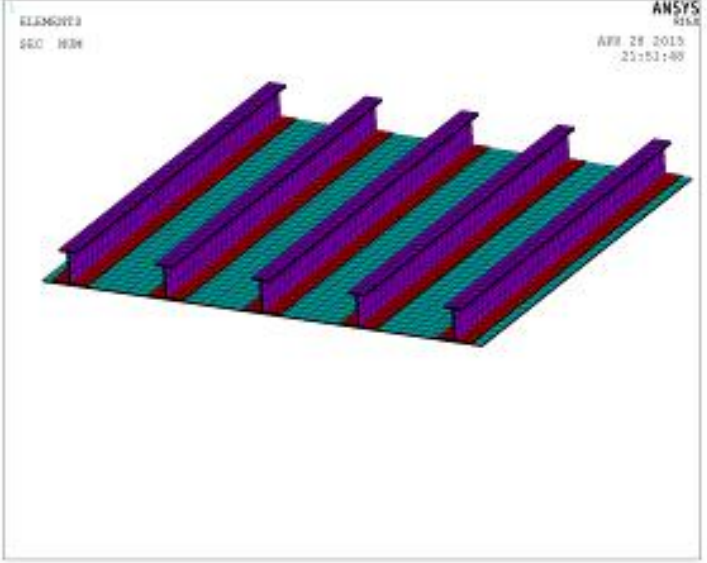
	<p>a) Boundary Conditions of the Stiffened Panels</p>
	<p>b) Finite Element Model of Stiffened Panel</p> <p>Total Number of Element : 3264</p> <p>Total Number of Nodes : 10428</p>

Figure 5.4 (a) Boundary Conditions of the stiffened panel, (b) Finite Element Model of the stiffened panel.

5.2.4 Solution and Results for Flat Panel Under Axial Loading

The numerical and experimental results of a flat panel under axial loading in according to the applied force with respect to end-shortening of the panel are shown in Figure 5.5. From Figure 5.5, it can be seen that the numerical curve is in good agreement with test results up to nearly 2.1 mm deflection of the panel. This point is also determined as the indication of the first buckling mode of the test panel. After this point, the differences between the compared two curves start to diverge slightly

and break off at nearly 3.5 mm deformation of the panel. The probable reasons for this bifurcation are due to one or the combination of the following failure mode on the panel:

- local buckling on the flange or the web of the stiffener
- stringer-skin de-bonding (peeling) in the tested panels
- local material failure on the panel

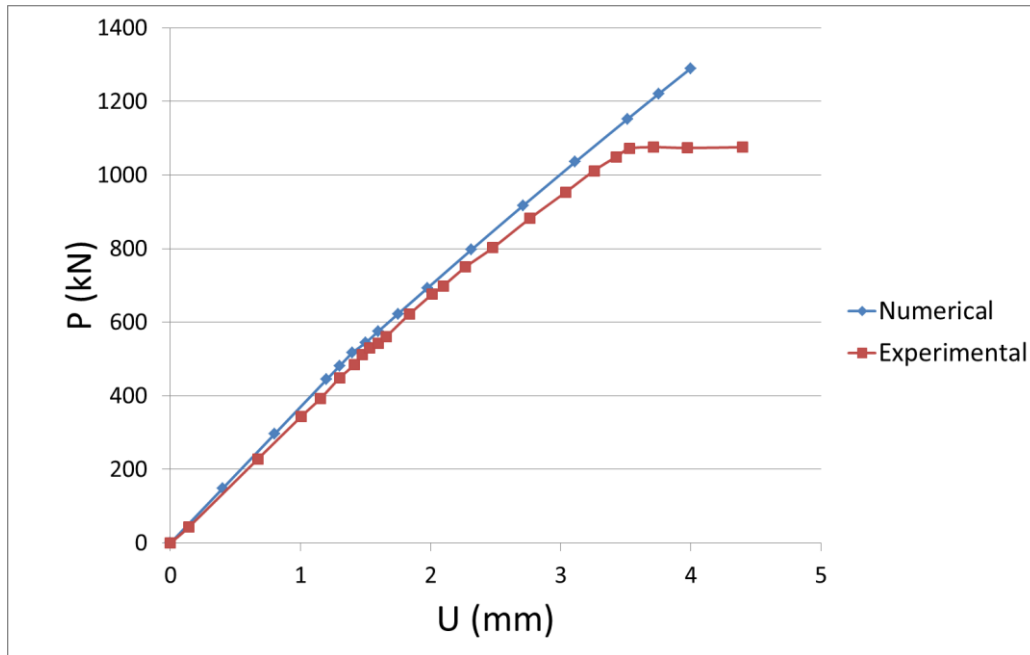
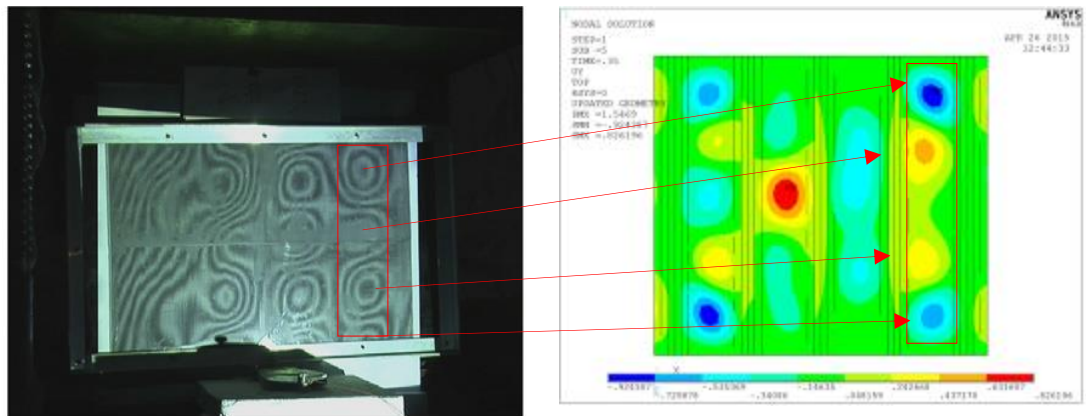


Figure 5.5 Load with respect to end-shortening curves.

In order to verify the assessment of the buckling mode shape, the out of plane displacements obtained by the Moirè fringes and those interpreted by means of FEM are compared in Figure 5.6 at the first buckling phase (P_{cr}). As a result of this buckling mode shape comparison, the consistency between numerical and test outputs is qualitatively adequate.



a) Moiré patterns of the test specimen for the first buckling mode starting region [37]

b) Model out of displacement at the first buckling load in FEM

Figure 5.6 Numerical vs. experimental results [37]: out-of-plane displacements at buckling region

In addition to the load vs. end-shortening comparisons, the load vs. strain comparison studies have been performed. The axial strain tensor obtained by FEM is checked against the strain gauges data at the same location on the test specimens. For this study, specimen 2 is selected from the paper [37], since the necessary data needed to validate the numerical model is given for this specimen. There are two location selected to compare the strain data. In the skin side, back to back strain gauge in the mid-section of the panel labelled as G14/G13 as shown in Figure 5.3-b have been chosen. In the stiffener side, the strain gauge in the mid-section of the panel located on the inner flange of the middle stringer labelled as G27 as shown in Figure 5.3-b has been selected.

In Figure 5.7 and Figure 5.8, the FEM and test outputs are compared in according to strain data in the axial direction. When the skin is considered, before the buckling, FEM and test deliveries are very close to the each other, which shows the correct recalculation of the certain stiffness. A sufficient result is also an acceptable level in the value of the critical load, the differences is about the magnitude of about 6 % assessed at the bifurcation of strain location. In the post buckling area, the

numerical model is described by a long way off development of the data at middle of the bay, as a consequence of a buckling composition, which is somehow distinctive in figure as regards to the test one.

Although the stiffness of the FE model are well estimated to the test specimen, the critical buckling load (bifurcation point) determined at FE model is lower than the value of experimental result. This is possibly caused by the finite element model which is more ideal with respect to the experimental specimen which contains inevitable imperfection. Hence the geometric imperfection has to be introduced into the FE model by some variables like selected mode shape obtained by eigenvalue buckling analysis and scaling factor. The percentage errors between the numerical and experimental values of the buckling load (imperfection point) is 6%, and this value is in acceptable level [38].

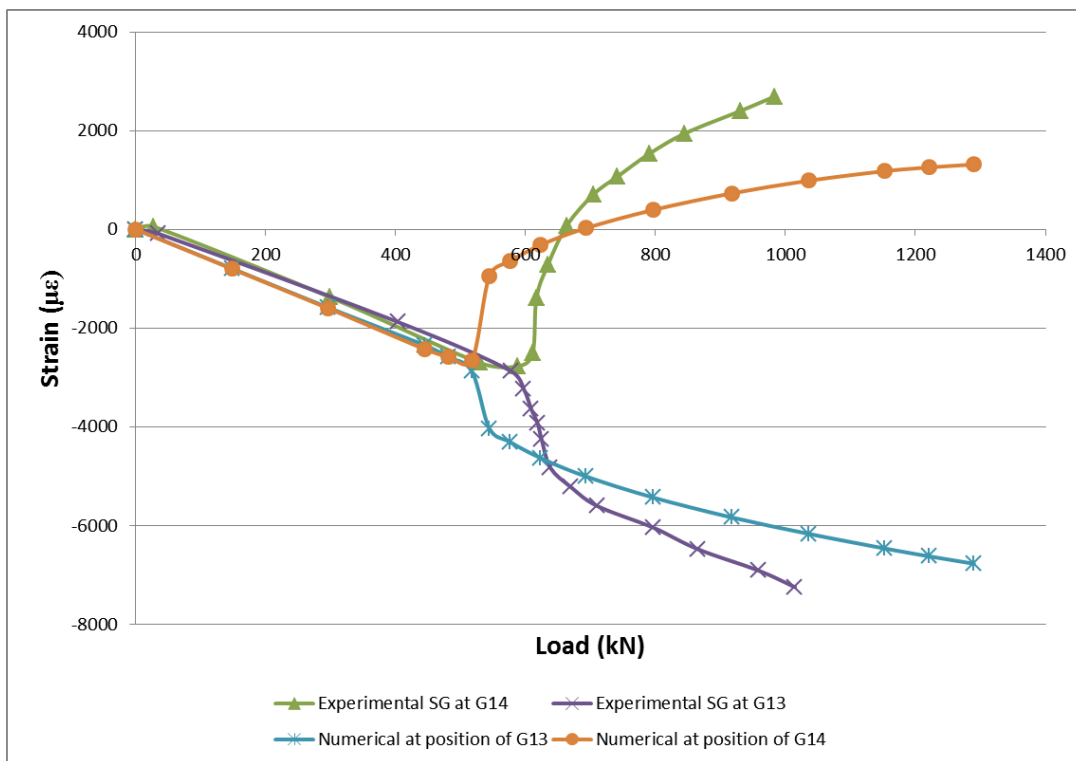


Figure 5.7 Numerical vs. experimental results: axial strains on the skin

In the stiffener, the strains calculated numerically are insignificantly difference than the ones attained via test for the same load. This limited distinction is assumed to be sufficient because they do not effect FEM behavior of the structure.

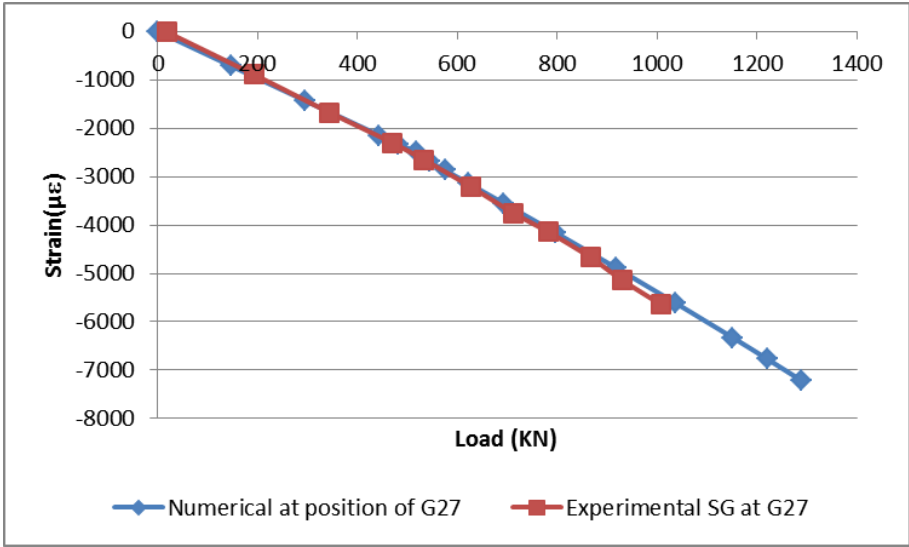


Figure 5.8 Numerical vs. experimental results: axial strains on the stringer

5.3 A Curved Stiffened Panel Under Axial Loading

5.3.1 Problem Definition for Curved Panel Under Axial Loading

In [39], a T shape stiffened panel is manufactured and tested. The shape of the panel is a curved 1000 mm radius and four stiffeners are attached to it as seen in Figure 5.9. The panel has dimensions of 419 mm width and 780 mm length and the stiffeners have dimensions of 140 mm height and 37.9 mm flange length. The shape of stiffeners are as shown in Figure 5.10. A compression load is applied in the longitudinal direction of the panel and its buckling characteristics are investigated.

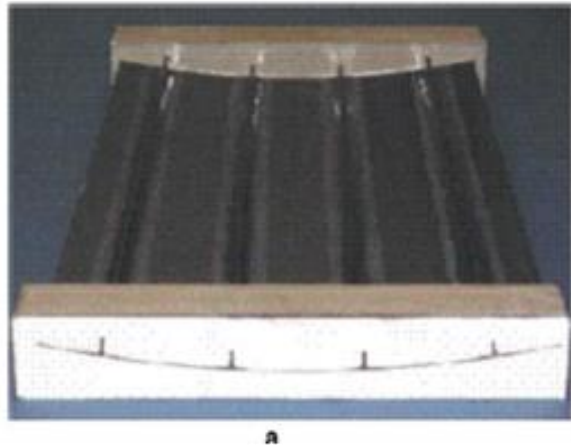


Figure 5.9 The blade-stiffened test specimen used in [39]

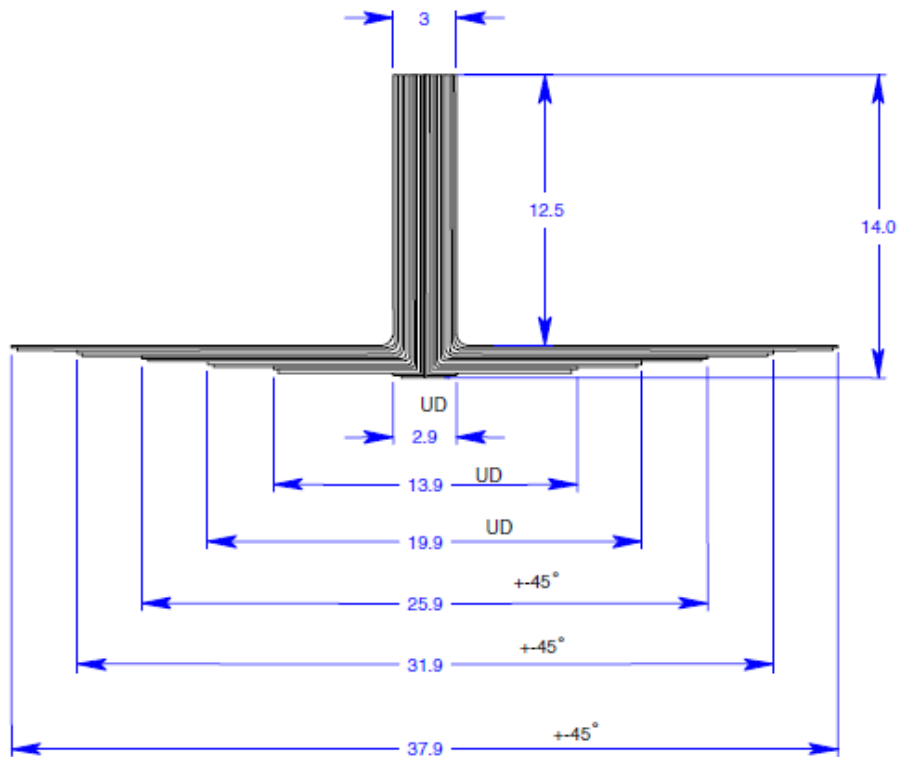


Figure 5.10 Dimensions of the Cross-section of the stiffener (mm) [39]

The skin and the stiffeners are both made of the prepreg material IM7/8552, the material properties are also given in Table 5.2. The stacking sequence of the skins are $[90/45/-45/0]_s$. The stacking sequence of the stiffener web is $[(+45/-45)_3/0_6]_s$. The stacking sequence of the stiffener blade is shown in Figure 5.9. The thickness of each layer is 0.125 mm.

Table 5.2 Material properties given for the composite material in [39]

E_{11}	E_{22}	G_{12}	ν_{12}
146.535 GPa	9.720 GPa	6.054	0.34

5.3.2 Test Set-up for Curved Panel Under Axial Loading

The test sample is placed between an axially supporting top plate and a lower drive plate. The prepared test rig is shown in Figure 5.11.



Figure 5.11 Hydraulic compression test machine [39]

5.3.3 Analysis Model for Curved Panel Under Axial Loading

The structure is modelled in ANSYS. The blade type stiffeners are simply composed with flange and web. Blade-stiffeners are modelled as shell elements with their bottom surfaces mid-planes in the blade and web. The FEM definition is exactly complied with rules of the baseline model. Shell 281 element is used with 15 mm element size. Bonded (always) contact algorithm is described between the stiffener and skin. The meshed model is depicted in Figure 5.12. The FE model consists of 15325 elements and 49040 nodes.

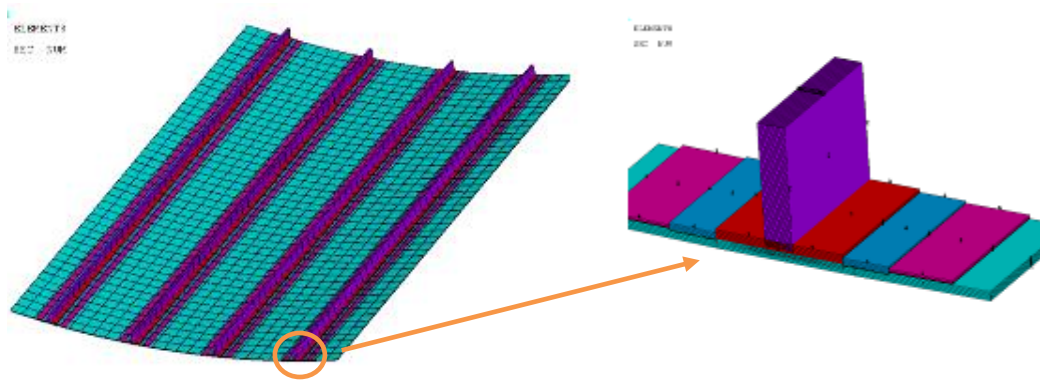


Figure 5.12 Finite Element Model.

The constraints of the panel can be depicted in Figure 5.13; the first row define the constraints of the edges in translator directions of X, Y and Z directions, the second row describe the rotatory directions of Rx, Ry an Rz directions. “0” means the related directions is fixed, on the other hand “-” means that the related direction is not fixed. The load is applied to the structure as a displacement on the upper edge of the panel in axial direction.

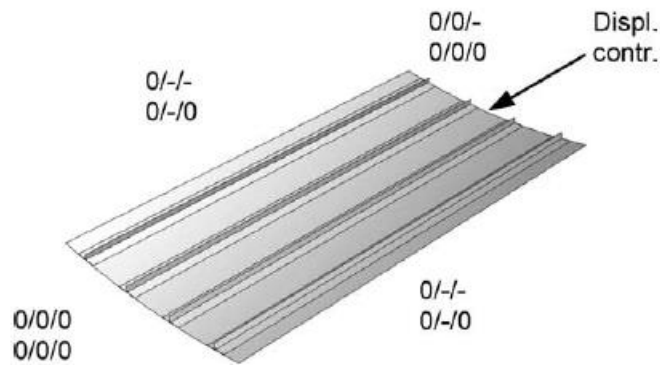


Figure 5.13 Boundary Conditions [39]

5.3.4 Solution and Results for Curved Panel Under Axial Loading

Figure 5.14 shows the test results of the applied force- end-shortening diagrams of the panels, with the obtained out-of-plane deformation shape owing to some important points observed during the test.

The curves can be separated principally by three sections, the first one is the large linear partition of the curves and then a transition phase between them, which include a small part of applied force reduce between 1.3 and 1.6 mm shortening. The initial observed local buckling is occurred in the position of 0.7 mm shortening. After that a combined overall buckling happens in the middle of the right side of the panel at 1.54 mm shortening. From there, the overall buckle increase .

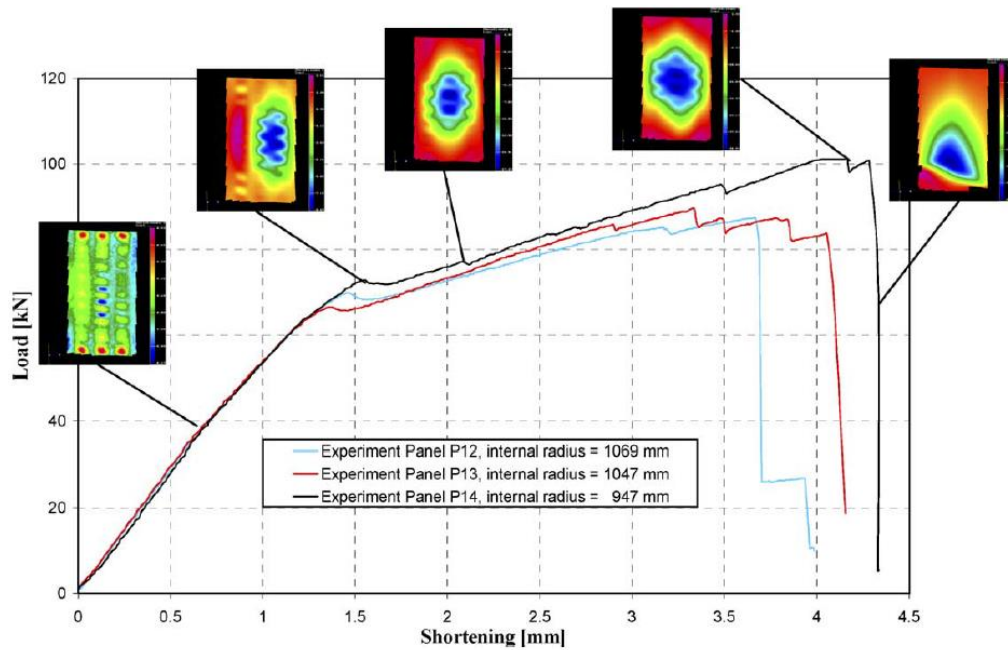


Figure 5.14 The test results of the load-shortening curves of the panels, in conjunction with the measured out-of-plane displacement patterns [39]

The following load-shortening curves are computed with the curved panel. It is shown in Figure 5.15 together with the respective experimental ones. Buckling stage observed in the experimental results is very similar to the computational results as shown in Figure 5.14. The local buckling starts at shortening of 0.7 mm and the global buckling mode start at 1.5 mm. Figure 5.15. shows the comparison results of load vs. end-shortening diagrams with mode shapes. The numerical results is plotted up to 2.0 mm due to convergence difficulties.

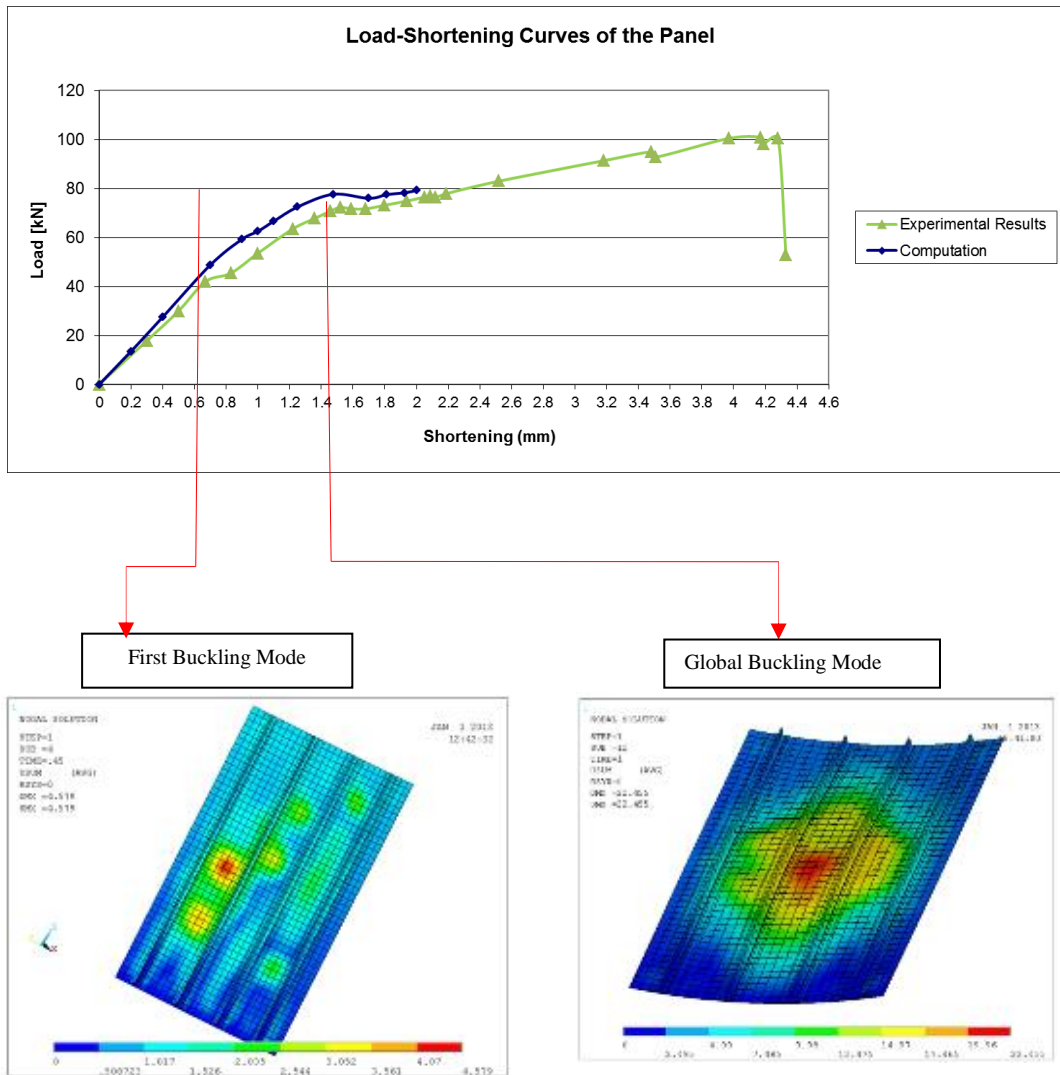


Figure 5.15 Load-shortening curves of the panels, in conjunction with the measured out-of-plane displacement patterns from FEM results

As a result, the matching is good far from the beginning, including the first part of the transition stage of the post buckling area. From there, the numerical simulations of the panels are too stiff.

5.4 A Flat Stiffened Panel Under Shear Loading

5.4.1 Problem Definition for Flat Panel Under Shear Loading

In [40], a I shape stiffened panel is manufactured and tested. The shape of the panel is flat and four stiffeners are attached to it as seen in Figure 5.16 (a). The panel has dimensions of 600 mm width and 300 mm length and the stiffeners have dimensions of 50 mm flange width. The shape of stiffeners are as shown in Figure 5.16 (b). A compression load is applied in the diagonal direction of the panel and its buckling characteristics are investigated.

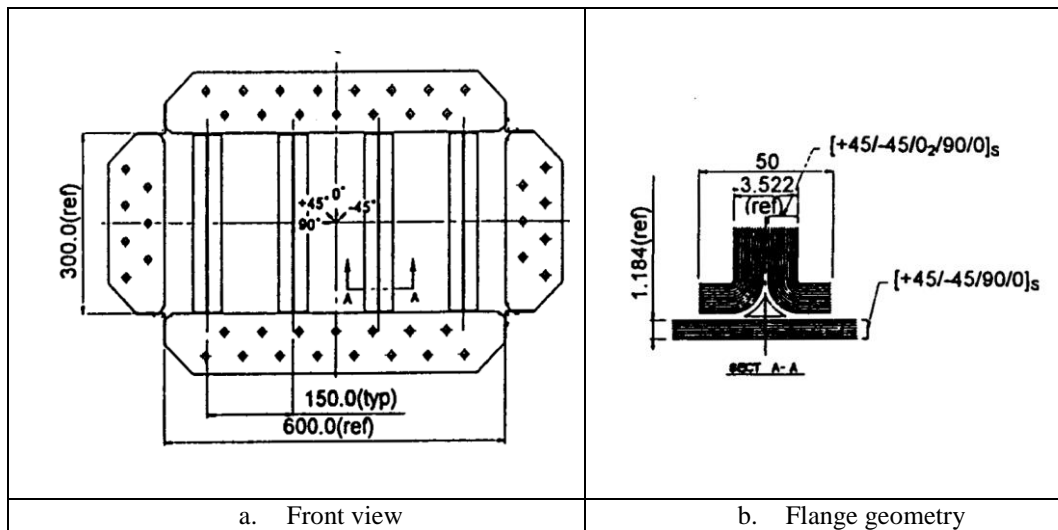


Figure 5.16 (a) The blade-stiffened panel, (b) stiffener geometry presented in [40]

The skin and the stiffeners are both made of composite material Graphite/Epoxy, the material properties are also given in Table 5.3. The stacking sequence of the skin are $[0/90/-45/45]_s$. The stacking sequence of the stiffener pad-up is $[0/90/-45_2/45/-45]_s$. The thickness of each layer is 0.148 mm.

Table 5.3 Material properties given for the composite material in [40]

E_{11}	E_{22}	G_{12}	ν_{12}
162 GPa	8.8 GPa	4.5	0.35

5.4.2 Test Setup for Flat Panel Under Shear Loading

The setup of the panel shear test is shown in Figure 5.17. A “picture frame” test rig is utilized to establish pure shear load to a test specimen. The angle of the plate is cautiously formed to yield pure shear force situation.

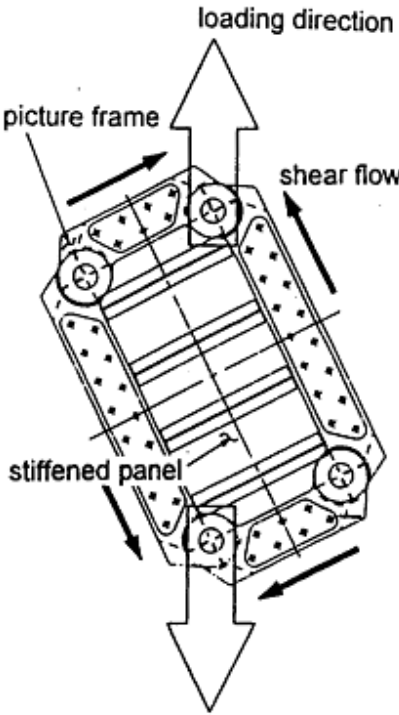


Figure 5.17 Shear panel test setup [40]

5.4.3 Analysis Model for Flat Panel Under Shear Loading

The finite element model was developed by considering the same methodology described during the creation of the baseline model defined in Chapter 3. The finite element model of the structure is shown in Figure 5.18. The model is composed of 1440 elements and 4669 nodes.

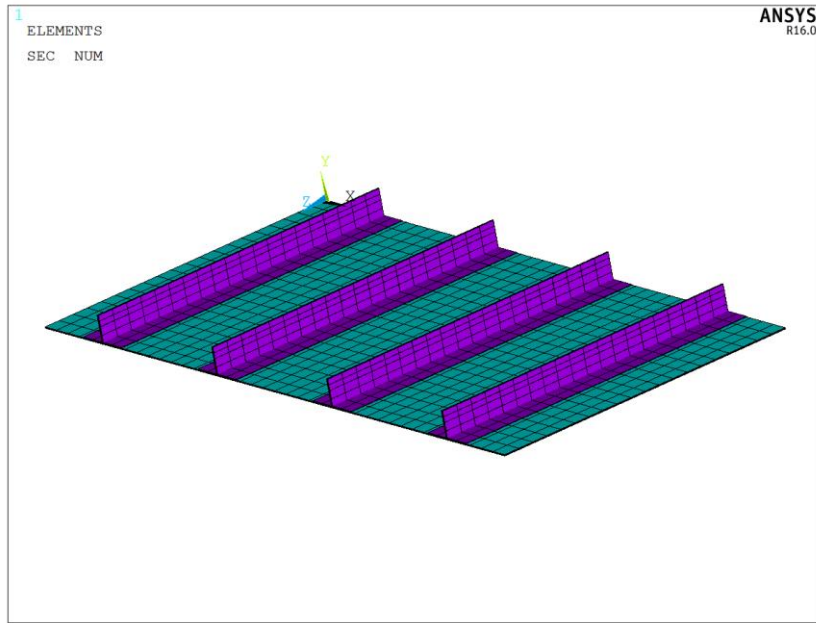


Figure 5.18 FEM model of the flat stiffened panel under shear loading

The standard boundary conditions can be seen from Figure 5.19, “0” means constrained in defined direction and rotation. The load is applied as a prescribed axial displacement along the whole circumferential edge (skin as well as stringer) of the panel.

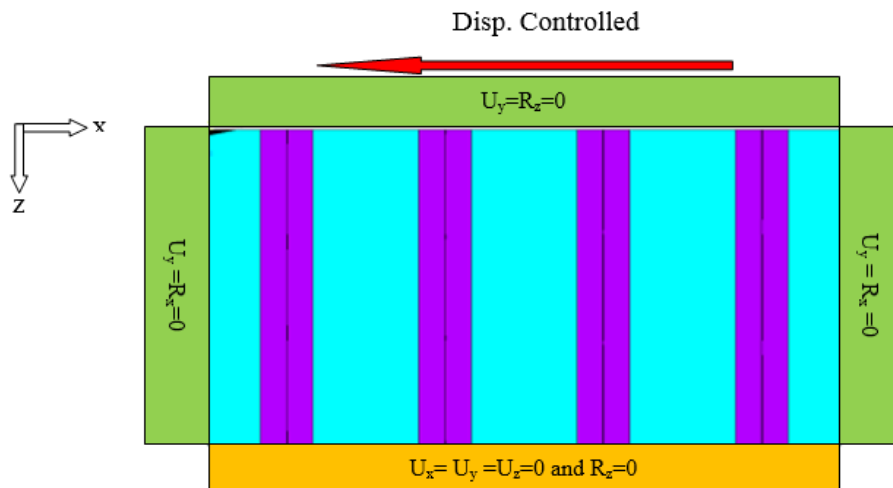


Figure 5.19 Boundary Conditions of the flat stiffened panel under shear loading

5.4.4 Solution and Results for Flat Panel Under Shear Loading

The experimental and numerical out-of-plane displacements comparison are shown in Figure 5.20. The diagram check the output obtained by the LVDT at middle of the two adjacent stiffener against the related out-of-plane deformations obtained by the FE model.

In the region of the first buckling shear load , numerical and test outputs are very close to each other, which shows the correct representation of the actual stiffness. In the post-buckling field, the FE model is characterized by a quite different evolution of the deflection at buckled region, which is mainly due to local failure of the test panel.

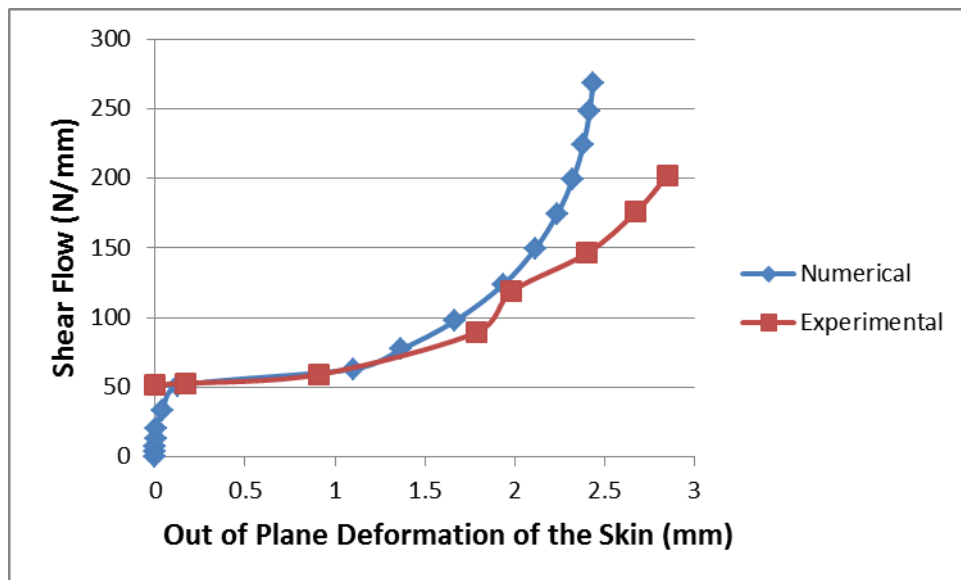


Figure 5.20 The out of plane displacement of skin, experimental and numerical results

First buckling mode shape obtained by numerical analysis is shown in Figure 5.21.

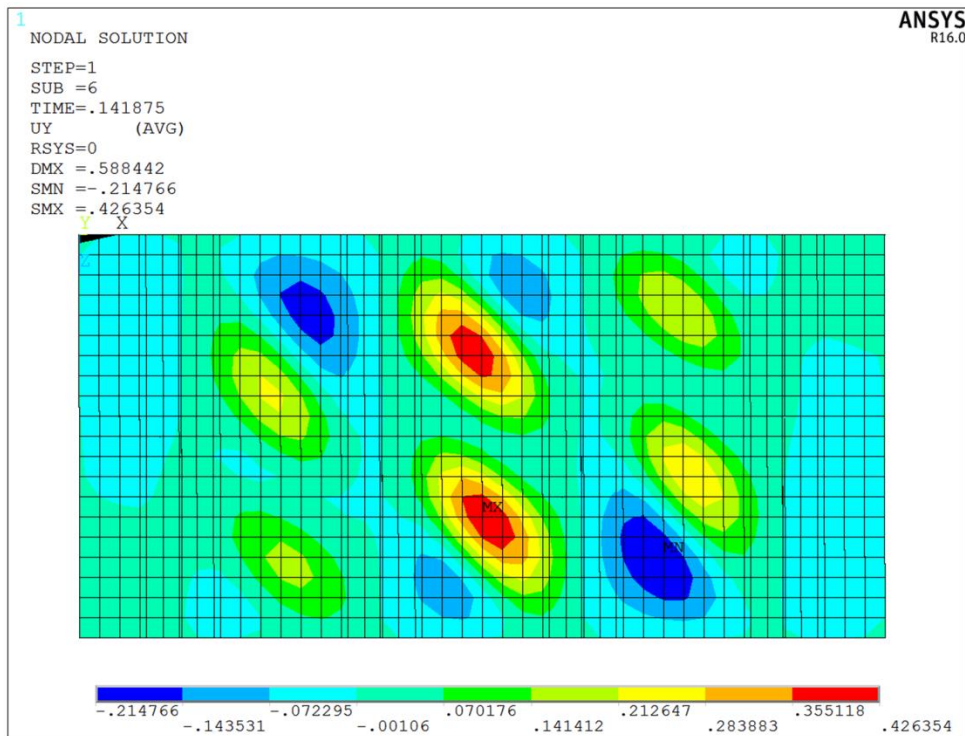


Figure 5.21 Mode shape of the panel during the first buckling mode

5.5 Conclusion

This section compares the numerical analyses considering the post-buckling behaviour of composite stiffened panels with the results of the experimental studies in the literature. Three different full non-linear finite element analyses were carried out in order to predict the post-buckling behaviour of the panels given in the literature as the result of the experimental studies. The results of the numerical analyses, performed with considering an initial geometrical imperfection, are close to and in good agreement with the experimental test results in terms of the pre-buckling and the post-buckling stiffness as well as in terms of the buckling loads.

A good correlation is also obtained considering the out-of-plane deformations and the buckling patterns; hills and valleys identified for the tested panels deformations are well predicted by the numerical analyses.

Comparison between the load end shortening curves obtained by the experimental tests and determined by the numerical analyses results in the percentage errors of 6-7 %.

Since the numerical values are determined to be in good agreement for the compared experimental values; the developed model and methodology are believed to be satisfactory and hence will be used in analyzing the different panels.

CHAPTER 6

NUMERICAL RESULTS OF LINEAR AND NON-LINEAR BUCKLING ANALYSIS AND DISCUSSION

6.1 Introduction

Under the scope of this thesis, the linear and the non-linear buckling analysis have been performed respectively. The eigenvalue buckling analysis calculate the theoretically buckling capability of an perfect linear elastic structure. That is to say, the linear buckling analysis produces the classical Euler solution, which is not a conservative solution taking into account the flaws on the structure and non-linearity. On the contrary, the nonlinear buckling analysis uses a non-linear static analysis with progressively growing forces to find out the critical force value which turns the structures into unsteady situation. Hence, non-linear buckling analysis is more precise way and is suggested for the design or assessment of substantial structures.

Under the scope of this work, it is firstly performed linear eigenvalue analysis for all of the configurations because of low computation time but sufficiently reliable results. On the other hand, the nonlinear analyses are carried out only for one configurations due to high computation time.

6.1.1 Linear Analysis and Results

The fundamental consequences of concern in the buckling analysis are to calculate eigenvalues and corresponding the buckling modes shapes. The buckling forces for

each mode are assumed by multiplying the eigenvalue with the nominal force value utilized in the analysis. In other words,

$$\text{Critical Buckling load} = \text{Eigenvalue} \times \text{Axial load} \quad (6.1)$$

For each configuration, the analyses are performed with respect to variable ratio of applied axial displacement to applied shear displacement (U_x/U_y) as defined in Table 3.2. The applied load ratio (P_x/P_y) is obtained by dividing the total reaction forces in X direction to the total reaction forces in Y direction getting from the nodes of the upper edge of the panel which are given the displacement constraints in x and y direction as indicated in Table 3.2. In that way, the results are tabulated or depicted to see the shear load effect on the axial buckling load capability of the structure for each load ratio (P_x/P_y). The shear effect on the structure buckling capability is investigated in two ways. The first way is to see the change on the critical axial buckling load due to shear load application, the second way to observe the mode shape change on the first eigenvalue frequency.

6.1.1.1 Shear Effect Ratio Investigation

The percentage change ratio of the axial critical buckling load due to combined loading (shear and axial) to the critical axial buckling load due to only axial loading is called “Shear Effect Ratio”.

$$\text{Shear Effect Ratio} = \frac{P_{x_critical_pure_axial} - P_{x_critical_combined}}{P_{x_critical_pure_axial}} \times 100 \quad (6.2)$$

The Calculated Shear Effect results are presented in two manners. If the shear load has small effect on the structure, the results for these configurations are shown by tables. The Table 6.1, Table 6.2 and Table 6.3 show the effect of the shear load on the structure with variable load ratio for P1, P2 and P3 with related configurations respectively.

Table 6.1 Variation of the shear effect ratio with the different load ratio for P1

	P1_Configuration 4			P1_Configuration 5			P1_Configuration 6		
	P_x/P_y	P_{cr}	Shear Effect Ratio %	P_x/P_y	P_{cr}	Shear Effect Ratio %	P_x/P_y	P_{cr}	Shear Effect Ratio %
LC1		45508	-		41837	-		38191	-
LC2	71.43	45491	0.04	67.77	41853	-0.04	66.00	38203	-0.03
LC3	35.72	45521	-0.03	33.88	41862	-0.06	33.00	38209	-0.05
LC4	17.86	45530	-0.05	16.94	41862	-0.06	16.50	38203	-0.03
LC5	8.93	45474	0.08	8.47	41792	0.11	8.25	38118	0.19
LC6	5.95	45326	0.40	5.65	41629	0.50	5.50	37939	0.66
LC7	5.10	45222	0.63	4.84	41515	0.77	4.71	37815	0.98
LC8	4.46	45097	0.90	4.24	41381	1.09	4.12	37669	1.37

	P1_Configuration 10			P1_Configuration 11			P1_Configuration 12		
	P_x/P_y	P_{cr}	Shear Effect Ratio %	P_x/P_y	P_{cr}	Shear Effect Ratio %	P_x/P_y	P_{cr}	Shear Effect Ratio %
LC1		380843	-		384959	-		38191	-
LC2	148.65	382113	-0.33	149.33	386243	-0.33	151.96	38203	-0.33
LC3	74.32	383251	-0.63	74.66	387395	-0.63	75.98	38209	-0.63
LC4	37.16	385130	-1.13	37.33	389292	-1.13	37.99	38203	-1.13
LC5	18.58	387208	-1.67	18.67	391438	-1.68	19.00	38118	-1.70
LC6	12.39	387051	-1.63	12.44	391347	-1.66	12.66	37939	-1.70
LC7	10.62	386169	-1.40	10.67	390493	-1.44	10.85	37815	-1.50
LC8	9.29	384767	-1.03	9.33	389135	-1.08	9.50	37669	-1.17

Table 6.2 Variation of the shear effect ratio with the different load ratio for P2

	P2_Configuration 4			P2_Configuration 5			P2_Configuration 6		
	P_x/P_y	P_{cr}	Shear Effect Ratio %	P_x/P_y	P_{cr}	Shear Effect Ratio %	P_x/P_y	P_{cr}	Shear Effect Ratio %
LC1		22372			20776			18804	
LC2	74.22	22408	-0.16	70.66	20808	-0.15	68.93	18832	-0.15
LC3	37.11	22439	-0.30	35.33	20835	-0.28	34.47	18857	-0.28
LC4	18.56	22487	-0.51	17.66	20877	-0.49	17.23	18894	-0.48
LC5	9.28	22527	-0.69	8.83	20910	-0.65	8.62	18926	-0.65
LC6	6.19	22496	-0.55	5.89	20881	-0.50	5.74	18902	-0.52
LC7	5.30	22455	-0.37	5.05	20843	-0.32	4.92	18870	-0.35
LC8	4.64	22397	-0.11	4.42	20790	-0.07	4.31	18825	-0.11

	P2_Configuration 10			P2_Configuration 11			P2_Configuration 12		
	P_x/P_y	P_{cr}	Shear Effect Ratio %	P_x/P_y	P_{cr}	Shear Effect Ratio %	P_x/P_y	P_{cr}	Shear Effect Ratio %
LC1		181910			183924			186261	
LC2	156.02	182407	-0.27	156.68	184423	-0.27	159.18	186769	-0.27
LC3	78.01	182850	-0.52	78.34	184875	-0.52	79.59	187222	-0.52
LC4	39.01	183614	-0.94	39.17	185643	-0.93	39.79	187995	-0.93
LC5	19.50	184562	-1.46	19.59	186603	-1.46	19.90	188971	-1.46
LC6	13.00	184745	-1.56	13.06	186795	-1.56	13.26	189174	-1.56
LC7	11.14	184554	-1.45	11.19	186603	-1.46	11.37	188995	-1.47
LC8	9.75	184187	-1.25	9.79	186234	-1.26	9.95	188628	-1.27

Table 6.3 Variation of the shear effect ratio with the different load ratio for P3

	P3_Configuration 4			P3_Configuration 5			P3_Configuration 6		
	P_x/P_y	P_{cr}	Shear Effect Ratio %	P_x/P_y	P_{cr}	Shear Effect Ratio %	P_x/P_y	P_{cr}	Shear Effect Ratio %
LC1		15687			14749			13685	
LC2	65.60	15730	-0.27	63.03	14788	-0.26	61.78	13718	-0.24
LC3	32.80	15766	-0.51	31.51	14820	-0.48	30.89	13746	-0.44
LC4	16.40	15820	-0.85	15.76	14868	-0.80	15.45	13787	-0.74
LC5	8.20	15853	-1.06	7.88	14898	-1.01	7.72	13814	-0.94
LC6	5.47	15793	-0.68	5.25	14844	-0.64	5.15	13770	-0.62
LC7	4.69	15730	-0.27	4.50	14788	-0.26	4.41	13722	-0.27
LC8	4.10	15644	0.27	3.94	14711	0.26	3.86	13659	0.20

	P3_Configuration 10			P3_Configuration 11			P3_Configuration 12		
	P_x/P_y	P_{cr}	Shear Effect Ratio %	P_x/P_y	P_{cr}	Shear Effect Ratio %	P_x/P_y	P_{cr}	Shear Effect Ratio %
LC1		114739			115723			117147	
LC2	143.06	115113	-0.33	143.58	116100	-0.33	145.49	117522	-0.32
LC3	71.53	115439	-0.61	71.79	116426	-0.61	72.75	117854	-0.60
LC4	35.76	115948	-1.05	35.90	116945	-1.06	36.37	118387	-1.06
LC5	17.88	116421	-1.47	17.95	117427	-1.47	18.19	118906	-1.50
LC6	11.92	116174	-1.25	11.97	117186	-1.26	12.12	118718	-1.34
LC7	10.22	115792	-0.92	10.26	116817	-0.94	10.39	118372	-1.05
LC8	8.94	115269	-0.46	8.97	116291	-0.49	9.09	117875	-0.62

For the configuration from 13 to 16 , the result are also tabulated in tables Table 6.4 to Table 6.6 for P1, P2 and P3 panels.

Table 6.4 Variation of the shear effect ratio with the different load ratio for
P1_Configuration 13 to 16

	P1_Configuration 13			P1_Configuration 14			P1_Configuration 15			P1_Configuration 16		
	P_x/P_y	P_{cr}	Shear Effect Ratio %	P_x/P_y	P_{cr}	Shear Effect Ratio %	P_x/P_y	P_{cr}	Shear Effect Ratio %	P_x/P_y	P_{cr}	Shear Effect Ratio %
LC1		55967	-		60303			73254			90522	
LC2	50.01	55975	-0.01	82.38	60313	-0.02	143.35	73254	0.00	335.17	90522	0.00
LC3	25.00	55971	-0.01	41.19	60319	-0.03	71.67	73254	0.00	167.58	90506	0.02
LC4	12.50	55932	0.06	20.60	60303	0.00	35.84	73228	0.04	83.79	90445	0.08
LC5	6.25	55730	0.42	10.30	60182	0.20	17.92	73085	0.23	41.90	90230	0.32
LC6	4.17	55369	1.07	6.87	59946	0.59	11.95	72817	0.60	27.93	89870	0.72
LC7	3.57	55129	1.50	5.88	59783	0.86	10.24	72634	0.85	23.94	89647	0.97
LC8	3.13	54857	1.98	5.15	59589	1.18	8.96	72426	1.13	20.95	89387	1.25

Table 6.5 Variation of the shear effect ratio with the different load ratio for
P2_Configuration 13 to 16

	P2_Configuration 13			P2_Configuration 14			P2_Configuration 15			P2_Configuration 16		
	P_x/P_y	P_{cr}	Shear Effect Ratio %	P_x/P_y	P_{cr}	Shear Effect Ratio %	P_x/P_y	P_{cr}	Shear Effect Ratio %	P_x/P_y	P_{cr}	Shear Effect Ratio %
LC1		28803			29043			32463			37644	
LC2	50.30	28820	-0.06	86.05	29062	-0.07	157.26	32472	-0.03	410.28	37643	0.00
LC3	25.15	28832	-0.10	43.03	29076	-0.11	78.63	32474	-0.04	205.14	37640	0.01
LC4	12.58	28839	-0.12	21.51	29087	-0.15	39.31	32461	0.01	102.57	37629	0.04
LC5	6.29	28794	0.03	10.76	29046	-0.01	19.66	32358	0.32	51.29	37583	0.16
LC6	4.19	28675	0.45	7.17	28919	0.43	13.10	32154	0.95	34.19	37509	0.36
LC7	3.59	28586	0.76	6.15	28823	0.76	11.23	32014	1.38	29.31	37462	0.48
LC8	3.14	28476	1.14	5.38	28704	1.17	9.83	31850	1.89	25.64	37408	0.63

Table 6.6 Variation of the shear effect ratio with the different load ratio for
P3_Configuration 13 to 16

	P3_Configuration 13			P3_Configuration 14			P3_Configuration 15			P3_Configuration 16		
	P_x/P_y	P_{cr}	Shear Effect Ratio %	P_x/P_y	P_{cr}	Shear Effect Ratio %	P_x/P_y	P_{cr}	Shear Effect Ratio %	P_x/P_y	P_{cr}	Shear Effect Ratio %
LC1		20855			20603			21787			24921	
LC2	44.47	20877	-0.11	77.11	20625	-0.11	139.92	21796	-0.04	355.78	24920	0.00
LC3	22.24	20892	-0.18	38.55	20641	-0.19	69.96	21798	-0.05	177.89	24918	0.01
LC4	11.12	20901	-0.22	19.28	20650	-0.23	34.98	21783	0.02	88.95	24908	0.05
LC5	5.56	20837	0.09	9.64	20582	0.10	17.49	21675	0.51	44.47	24871	0.20
LC6	3.71	20663	0.92	6.43	20401	0.98	11.66	21467	1.47	29.65	24807	0.45
LC7	3.18	20536	1.53	5.51	20270	1.62	9.99	21328	2.10	25.41	24766	0.62
LC8	2.78	20383	2.26	4.82	20111	2.39	8.74	21168	2.84	22.24	24720	0.81

The observation into Table 6.1 to Table 6.6 yields some negative Shear Effect Ratios in different level of load ratios. This means that the axial buckling capability of the structure is increased with the application of the shear load on the structure. This case is applicable generally for the higher load ratio relatively.

From the tables above, it is also observed that the stiffener thickness, layup configurations slightly influence the Shear Effect Ratio. In other words, the change occurred on critical axial buckling load due to shear load do not rely on the bending and axial stiffness of the stiffener

The last commonly observed thing for the configurations listed from Table 6.1 to Table 6.6 is that they do not include any ply in orientation of 90^0 . This rule is just broken for the Configuration 10 to Configuration 12 which are symmetric but not balanced layup sequences of the plies. The strong dependence of the results on 90^0 oriented ply of the laminates led to additional investigations.

To see the effect of the perpendicular oriented ply (90^0) to applied axial loading direction in the laminated composite, ply layup of the skin Configuration 10 to Configuration 12 are changed for three panels P1, P2 and P3 as illustrated in Table 6.7.

Table 6.7 Change on the lay-up of the skin for Configuration 10 to Configuration 12

Skin Layup	Definition	Configuration Name
(0 0 90 0 -45 45 0 -45 90 0 0),	Symmetric but not balanced	Configuration 10 to Configuration 12
(0 0 90 0 -45 45 0 -45 \downarrow 45 0 0),	Symmetric and balanced with 90^0	Configuration 10a to Configuration 12a
(0 0 \downarrow 0 0 -45 45 0 -45 45 0 0),	Symmetric but not balanced without 90^0	Configuration 10b to Configuration 12b

The results are obtained as expected that the shear effect ratio are small for the Configuration 10_b to 12_b for three panels as shown in Table 6.8 due to missing 90^0 ply oriented in perpendicular to the axial loading direction. For Configuration 10_a to 12_a, the shear effect ratio are higher value bigger than 5.

Table 6.8 Variation of the shear effect ratio with the different load ratio for
P1_Configuration 10_b to 12_b

	P1_Configuration 10_b			P1_Configuration 11_b			P1_Configuration 12_b		
	P_x/P_y	P_{cr}	Shear Effect Ratio %	P_x/P_y	P_{cr}	Shear Effect Ratio %	P_x/P_y	P_{cr}	Shear Effect Ratio %
LC1		226825	-		229412	-		232813	-
LC2	126.37	226775	0.02	126.80	229354	0.03	128.20	232763	0.02
LC3	63.19	226668	0.07	63.40	229255	0.07	64.10	232654	0.07
LC4	31.59	226313	0.23	31.70	228907	0.22	32.05	232302	0.22
LC5	15.80	225001	0.80	15.85	227623	0.78	16.02	231019	0.77
LC6	10.53	222929	1.72	10.57	225594	1.66	10.68	228990	1.64
LC7	9.03	221625	2.29	9.06	224319	2.22	9.16	227708	2.19
LC8	7.90	220156	2.94	7.93	222877	2.85	8.01	226274	2.81

Table 6.9 Variation of the shear effect ratio with the different load ratio for
P2_Configuration 10_b to 12_b

	P2_Configuration 10_b			P2_Configuration 11_b			P2_Configuration 12_b		
	P_x/P_y	P_{cr}	Shear Effect Ratio %	P_x/P_y	P_{cr}	Shear Effect Ratio %	P_x/P_y	P_{cr}	Shear Effect Ratio %
LC1		113006			114114			114862	
LC2	122.88	112963	0.04	123.14	114064	0.04	123.79	114811	0.04
LC3	61.44	112899	0.10	61.57	113999	0.10	61.90	114739	0.11
LC4	30.72	112705	0.27	30.78	113806	0.27	30.95	114537	0.28
LC5	15.36	112075	0.82	15.39	113167	0.83	15.47	113872	0.86
LC6	10.24	111115	1.67	10.26	112190	1.69	10.32	112853	1.75
LC7	8.78	110506	2.21	8.80	111573	2.23	8.84	112210	2.31
LC8	7.68	109811	2.83	7.70	110862	2.85	7.74	111480	2.94

Table 6.10 Variation of the shear effect ratio with the different load ratio for
P3_Configuration 10_b to 12_b

	P3_Configuration 10_b			P3_Configuration 11_b			P3_Configuration 12_b		
	P_x/P_y	P_{cr}	Shear Effect Ratio %	P_x/P_y	P_{cr}	Shear Effect Ratio %	P_x/P_y	P_{cr}	Shear Effect Ratio %
LC1		74471			75073			75622	
LC2	116.48	74429	0.06	116.73	75031	0.06	117.35	75579	0.06
LC3	58.24	74366	0.14	58.37	74968	0.14	58.67	75515	0.14
LC4	29.12	74205	0.36	29.18	74799	0.36	29.34	75332	0.38
LC5	14.56	73679	1.06	14.59	74258	1.09	14.67	74773	1.12
LC6	9.71	72901	2.11	9.73	73464	2.14	9.78	73945	2.22
LC7	8.32	72424	2.75	8.34	72973	2.80	8.38	73429	2.90
LC8	7.28	71877	3.48	7.30	72418	3.54	7.33	72856	3.66

For the Higher Shear Effect ratio more than 5 % are shown by diagrams to visualize the results explicitly.

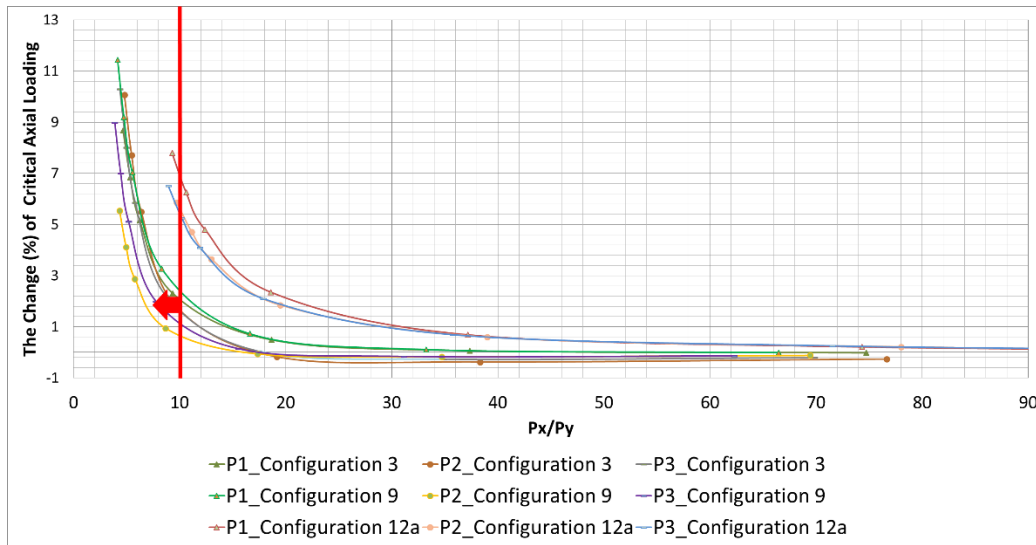


Figure 6.1 The percentage of the change in axial critical buckling load with the different load ratio in the panels

From the Figure 6.1, it is clearly seen that the effect of the shear load on the axial critical buckling capability of the structure is increased very fast for the value of P_x/P_y lower than nearly 10. Therefore, the stiffened panel design exposed to the low P_x/P_y ratio should be given more attention than high P_x/P_y ratio due to high gradient of degradation on the axial buckling capability of the structure. To endorse this claimed argument about the ratio effect, additional analyses have been performed. Due to the fact that linear eigenvalue analyses carried out for this study are limited to the value of $P_x/P_y = 4$, for the values lower than $P_x/P_y = 4$, an interaction equation of the form [14] is used to calculate the Shear Effect Ratio for some sample configurations with low Load Ratio lower than 4.

$$R_c + R_s^2 = 1 \quad (6.3)$$

$$R_c = \frac{P_x}{P_{x_{cr}}} \quad R_s = \frac{P_y}{P_{y_{cr}}} \quad (6.4)$$

R_c and R_s are the proportional relation of the implemented compression and shear loads to the corresponding buckling loads when the loads are implemented separately. The separate compression and shear buckling forces for the panels are determined via FEM. For compression alone, the panel as a whole buckles when the applied load P_x , equals to P_{x_cr} . For shear alone, the panel as a whole buckles when the applied load P_y , equals to P_{y_cr} . The reserve factor (RF) meaning the ratio of applied load to critical buckling load for combined load case (shear versus axial force). It is calculated [44] as follow:

$$RF = \frac{2}{(R_c + \sqrt{R_c^2 + 4R_s^2})} \quad (6.5)$$

Before proceeding, it will be initially verified the accuracy of this kind of calculation method. For this purpose, the eigenvalues calculated by linear eigenvalue buckling analysis are compared with the RFs for the combined loading cases of P1 with Configuration 1 and results are tabulated in Table 6.11. It is seen that the differences are in the acceptable level. So, it can be used RF value calculated via interaction equation 6.5 instead of eigenvalue calculated via FEM for lower P_x/P_y .

Table 6.11 Comparison study of buckling load calculated with FEM with Equation 6.5 for P1_Configuration 1

P_x (N)	P_y (N)	P_{x_cr} (N)	P_{y_cr} (N)	R_x	R_y	RF	Eigenvalue_FEM	%Difference
313360	3738	43416	23566	7.218	0.159	0.138	0.139	0.063
313360	7477	43416	23566	7.218	0.317	0.138	0.138	0.135
313360	14953	43416	23566	7.218	0.635	0.137	0.138	0.315
313360	29906	43416	23566	7.218	1.269	0.135	0.136	0.736
313360	44859	43416	23566	7.218	1.904	0.130	0.132	1.202
313360	52336	43416	23566	7.218	2.221	0.127	0.129	1.446
313360	59812	43416	23566	7.218	2.538	0.125	0.127	1.690

The Shear Effect Ratio results obtained from the calculation of RFs are shown in Table 6.12. It is seen that the values for $P_x/P_y=2.62$, the critical axial buckling force is decreased 26 %, and for $P_x/P_y =1.30$, the critical axial buckling force is decreased nearly 50 % in agreed with the assertion mentioned above.

Table 6.12 Shear Effect Ratio for the low Load Ratio (P_x/P_y) for P1_Configuration1

P_x (N)	P_y (N)	P_{x_cr} (N)	P_{y_cr} (N)	R_x	R_y	RF	P_{x_cr} combined (N)	Shear Effect Ratio %	P_x/P_y
313360	119624	43416	23566	7.218	5.076	0.102	31855	26.628	2.62
313360	239248	43417	23566	7.217	10.152	0.070	21786	49.821	1.31

For P1 with configuration 7, the verification study results are shown in Table 6.13. .For this case, the differences are also in the acceptable level.

Table 6.13 Comparison study of buckling load calculated with FEM with Equation 6.5 for P1_Configuration 7

P_x (N)	P_y (N)	P_{x_cr} (N)	P_{y_cr} (N)	R_x	R_y	RF	Eigenvalue_FEM	%Difference
449920	6272	121150	83908	3.714	0.075	0.269	0.269	0.055
449920	12543	121150	83908	3.714	0.149	0.269	0.269	0.095
449920	25086	121150	83908	3.714	0.299	0.268	0.268	0.120
449920	50172	121150	83908	3.714	0.598	0.263	0.263	-0.015
449920	75258	121150	83908	3.714	0.897	0.255	0.254	-0.293
449920	87801	121150	83908	3.714	1.046	0.251	0.250	-0.450
449920	100344	121150	83908	3.714	1.196	0.246	0.244	-0.610

The calculated Shear Effect Ratio results also indicate the same inference that the buckling capability of the structure is getting worse with low load ratios as shown in Table 6.14. For $P_x/P_y=2.24$, the critical axial buckling force is decreased 23 %. For $P_x/P_y =1.12$, the critical axial buckling force is decreased nearly 46 %.

Table 6.14 Shear Effect Ratio for the low Load Ratio (P_x/P_y) for P1_Configuration7

P_x (N)	P_y (N)	P_{x_cr} (N)	P_{y_cr} (N)	R_x	R_y	RF	P_{x_cr} combined (N)	Shear Effect Ratio %	P_x/P_y
449920	200688	121150	83908	3.714	2.392	0.205	92105	23.974	2.24
449920	401376	121150	83908	3.714	4.784	0.143	64383	46.857	1.12

In order to show the criticality of the lower P_x/P_y ratio on the structure, the third sample is chosen as P1 with Configuration 10_a. The verification study results as depicted in Table 6.15 and the Shear Load Effect Ratio calculated via Interaction Equation formula as shown in Table 6.16 indicate the similar conclusions with the before mentioned 2 sample cases.

Table 6.15 Comparison study of buckling load calculated with FEM with Equation 6.5 for P1_Configuration 10_a

P_x (N)	P_y (N)	P_{x_cr} (N)	P_{y_cr} (N)	R_x	R_y	RF	Eigenvalue_FEM	%Difference
752165	6515	327221	173040	2.299	0.038	0.435	0.435	-0.049
752165	11092	327221	173040	2.299	0.064	0.435	0.434	-0.150
752165	22184	327221	173040	2.299	0.128	0.434	0.432	-0.439
752165	44368	327221	173040	2.299	0.256	0.430	0.424	-1.384
752165	66552	327221	173040	2.299	0.385	0.423	0.412	-2.703
752165	77644	327221	173040	2.299	0.449	0.420	0.406	-3.451
752165	88736	327221	173040	2.299	0.513	0.415	0.398	-4.228

Table 6.16 Shear Effect Ratio for the low Load Ratio (P_x/P_y) for P1_Configuration 10_a

P_x (N)	P_y (N)	P_{x_cr} (N)	P_{y_cr} (N)	R_x	R_y	RF	P_{x_cr} combined (N)	Shear Effect Ratio %	P_x/P_y
752165	177472	327221	173040	2.299	1.026	0.372	279644	14.540	4.24
752165	354944	327221	173040	2.299	2.051	0.286	214868	34.336	2.12

Being supplementary to the results above, interaction curves obtained via FEM and equations 6.3 to 6.5 is compared to see the similarity of the results in a visual way. Figure 6.2 shows the output of this comparison. The study is just performed for one

sample case (P1_Configuration 1) but it can be extended for remaining configuration if needed. This figure can be also regarded as a verification of linear eigenvalue FEM analysis with interaction equation .

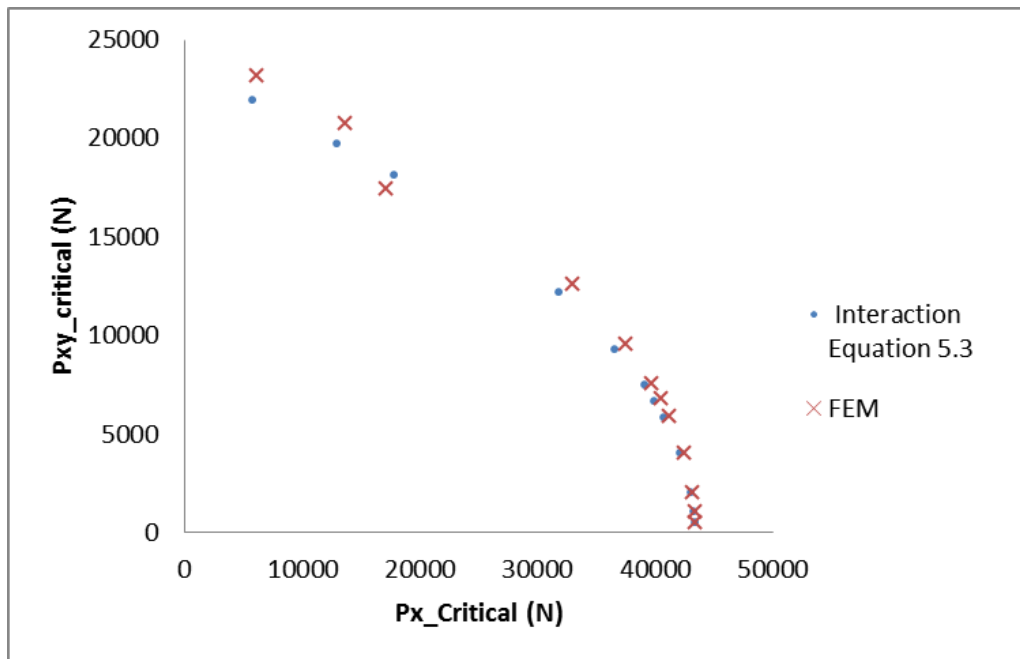


Figure 6.2 Buckling load interaction curves: comparison of Equation 6.3 and FEM results

At the end of this chapter, it summarized that the results show the correctness of the assertion drawn with respect to Figure 6.1 in which the curve behaves like asymptotic for the ratio of P_x/P_y , lower than 10 and the shear effect on the structure is getting higher for even small gradient change on the ratio of the forces in this range.

6.1.1.2 Mode Shape Investigation

Further investigations are dedicated to see the shear load effect on the results of the shape. The eigen modes can be viewed by post-processing the results in the visualization module in ANSYS.

The buckling pattern consists of half-waves confined between the stiffeners. These half-waves make an angle α with the stiffener axis as shown in Figure 6.3.

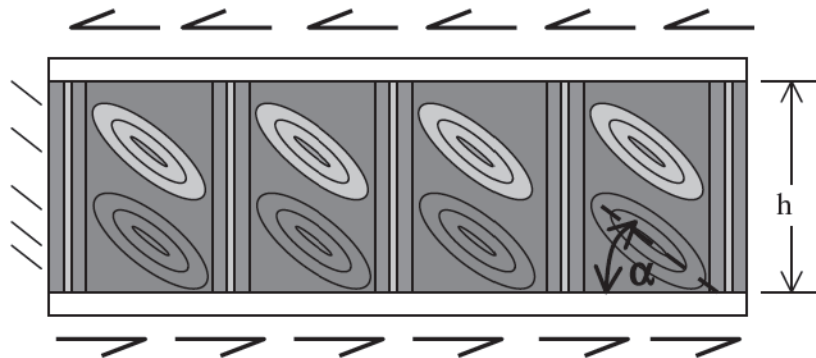


Figure 6.3 Post-buckled skin under shear showing post-buckling angle α [27]

The investigations on the mode shape is first to see the change on this α due to shear load application in addition to axial loading.

From Figure 6.4 to Figure 6.8 , the 1st mode shapes obtained via linear eigenvalue analysis are illustrated for different sample configuration for each P1, P2 and P3 panels.

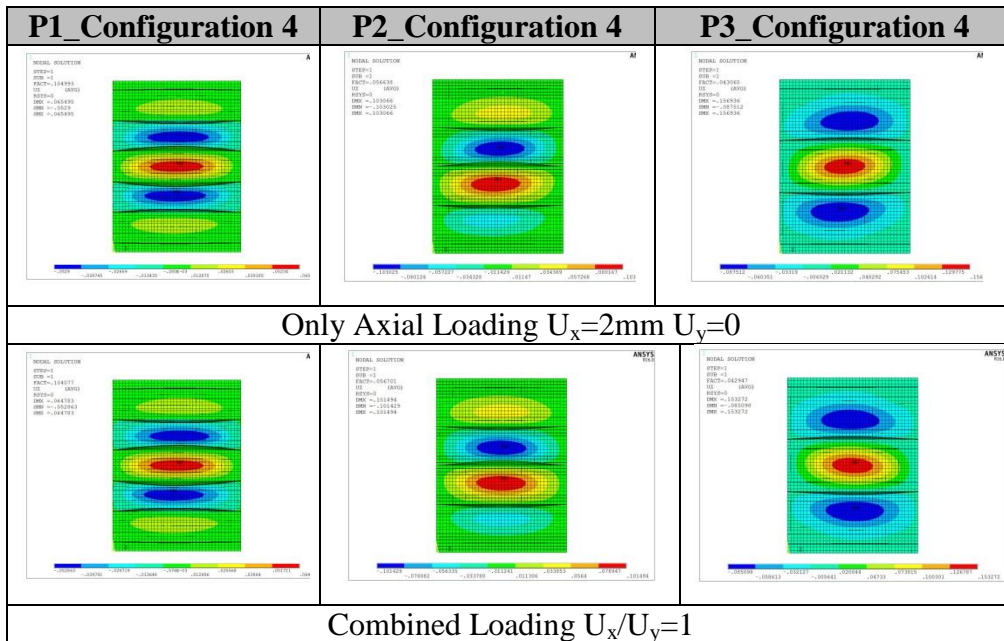


Figure 6.4 The 1st mode shape of the Configuration 4 for P1, P2 and P3

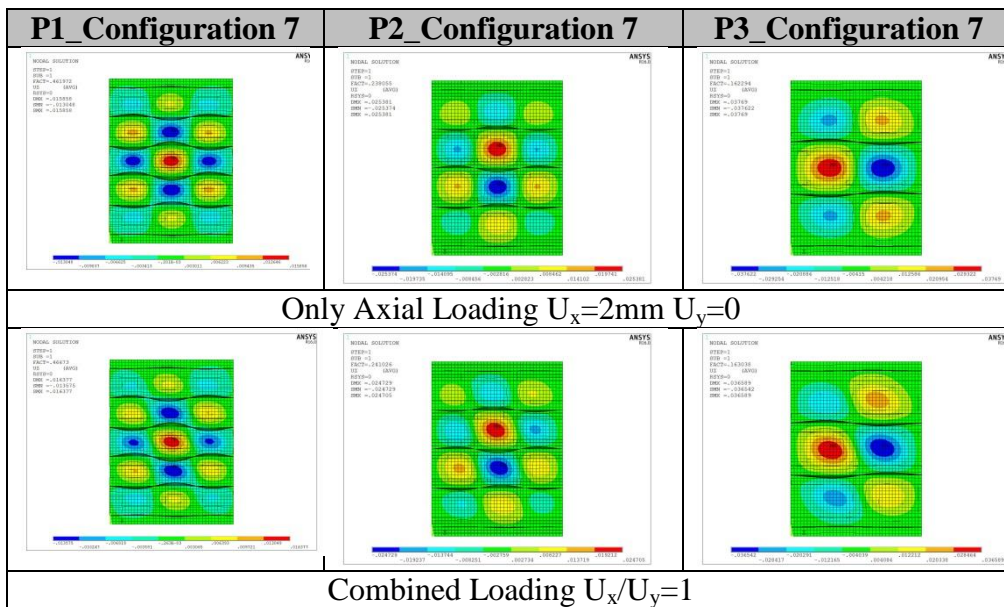


Figure 6.5 The 1st mode shape of the Configuration 7 for P1, P2 and P3

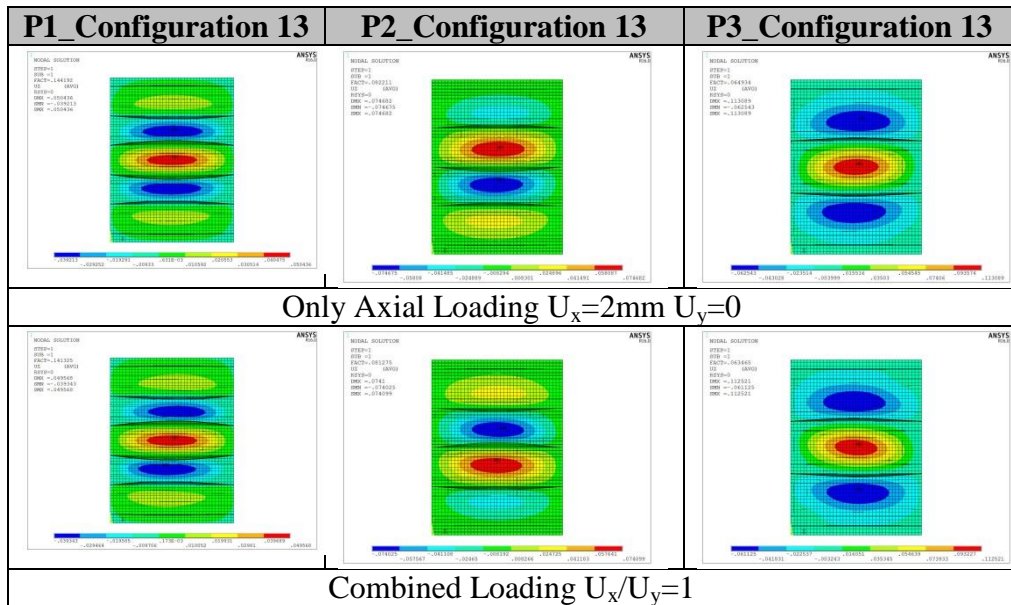


Figure 6.6 The 1st mode shape of the Configuration 13 for P1, P2 and P3

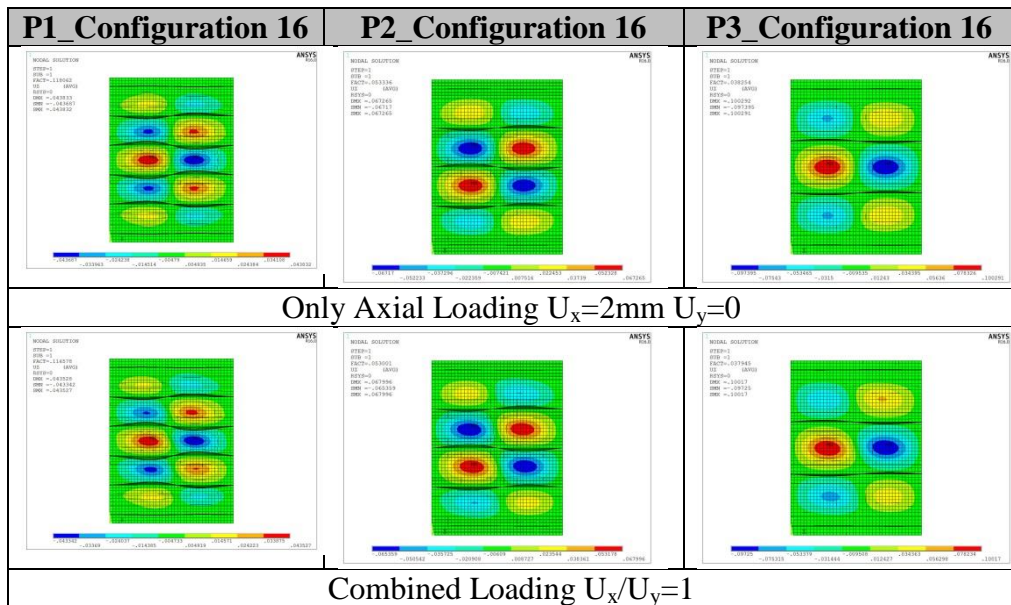


Figure 6.7 The 1st mode shape of the Configuration 16 for P1, P2 and P3

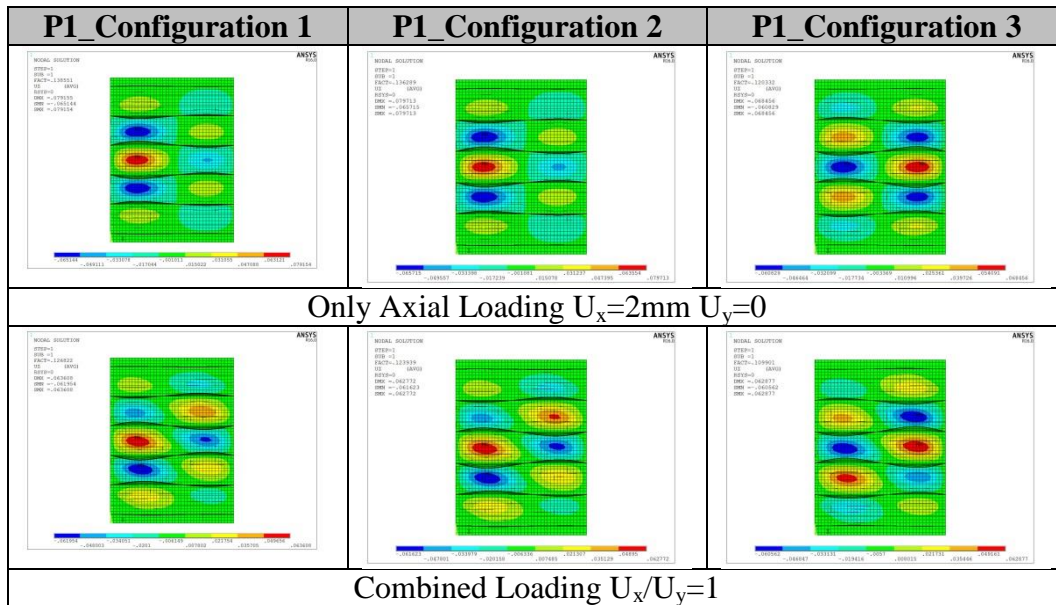


Figure 6.8 The 1st mode shape of the Configuration 1 for P1, P2 and P3

The following consequences from the mode shape investigation are reached:

- α is nearly 90^0 for pure axial loading cases as observed in the first row of the Figure 6.4 to Figure 6.8.
- After shear loading application(second row of the figures) beside the axial loading, α starts to be inclined according to the amount of the Shear Effect Ratio.
- When the shear effect ratio is small then α is very close to 90^0 as in Configuration 4, Configuration 13 after shear load application.
- When the shear effect ratio is big like Configuration 1 and Configuration 7, the angle is explicitly inclined and close to 45^0 . These outputs are also direct related with the ply orientation of the skin whether it include 90^0 or not.

After the investigation of the change on the α , it is examined the effect of the shear load on the number of half waves. It is observed that the number is not changed with shear loading application. However, it is worth mentioning that the number of half waves is only changed with increased pitch distance observed in Configuration 7. For the other remaining configurations, this phenomenon is not visualised. So it can

be concluded that the number of half waves is not effected by additional shear loading beside the axial loading but pitch distance and skin lay-up.

6.1.2 Nonlinear Post Buckling Analysis and Results

The numerical results provided by the non-linear analysis are allowed to better individuate the onset of buckling and to investigate the post-buckling behavior of the panels in the assumption of accounting only for the geometrical non-linearity, without considering eventual progressive failure of the material and separation phenomena. Since one cannot readily determine the stress and strain values in linear analysis; a nonlinear approach is sought. This is achieved by plotting the x-direction stresses on the path which is defined is 15 mm inside of the loading upper edge shown in Figure 6.9. In that way, it is able to see the effect of the shear loading on the structure with gradually increased load.

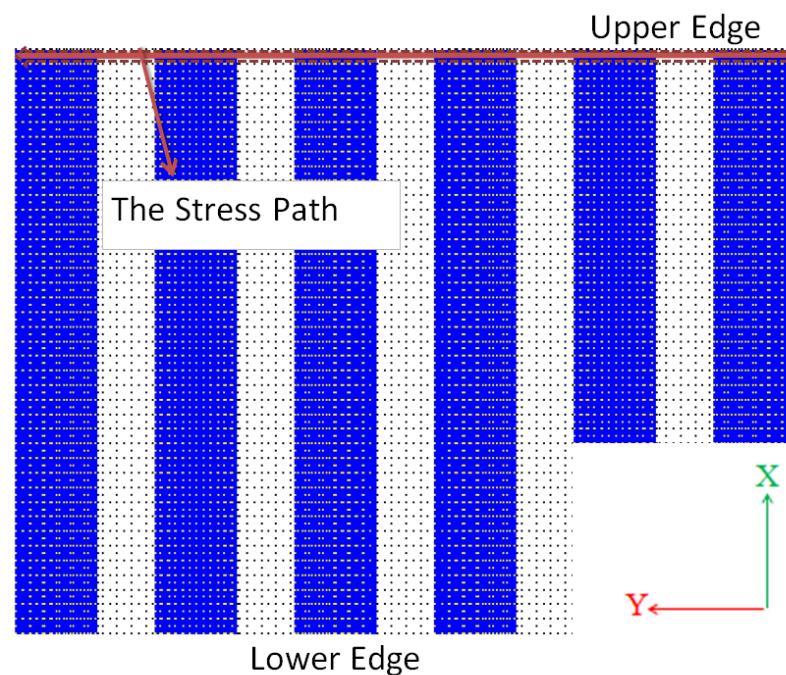


Figure 6.9 Stress Path on the panel

There are three phases investigated during the nonlinear buckling analysis. These are pre-buckling, buckling (critical) and post-buckling phases respectively.

Buckling(Critical) phase is the first buckling mode of the panel encountered during the analysis. The post-buckling phase is observed after one step forward from buckling phase. Pre-buckling phase is considered as one step before the buckling phase.

Nonlinear analyses are performed only for configuration 7 for three panels P1, P2 and P3 due to high computation time demand.

6.1.2.1 Stress State Investigation for P1

The stress distribution during the pre-buckling and buckling phases for P1 some selected curves among the all load cases are given in Figure 6.10 for each loading ratios. The dashed and solid black lines indicate the only axial loading situation during buckling and pre buckling cases respectively. The remaining curves can be evaluated with respect to these two black curves to see the effect of the shear loading. The blue area indicates the skin between the stringer called “unstiffened area”, the white area indicate the skin under the stringers called “stiffened area”.

In Figure 6.10, at first glance, it can be explicitly said that the stress for the both area (stiffened and unstiffened) increases with the application of the shear loading during the buckling phase.

Before buckling phase, even though the stresses distribution curves of the combined loading are almost similar to the pure axial compression curve (dashed black one) especially in the middle of the panel, stresses are randomly distributed on the left and right portion of the panel.

As a result, the symmetry of the stress distribution according to the mid-plane of the plate even for these two phases is distorted rather than expected for P1 under the combined loading. This is most probably because of shorter pitch distance than the other two panels.

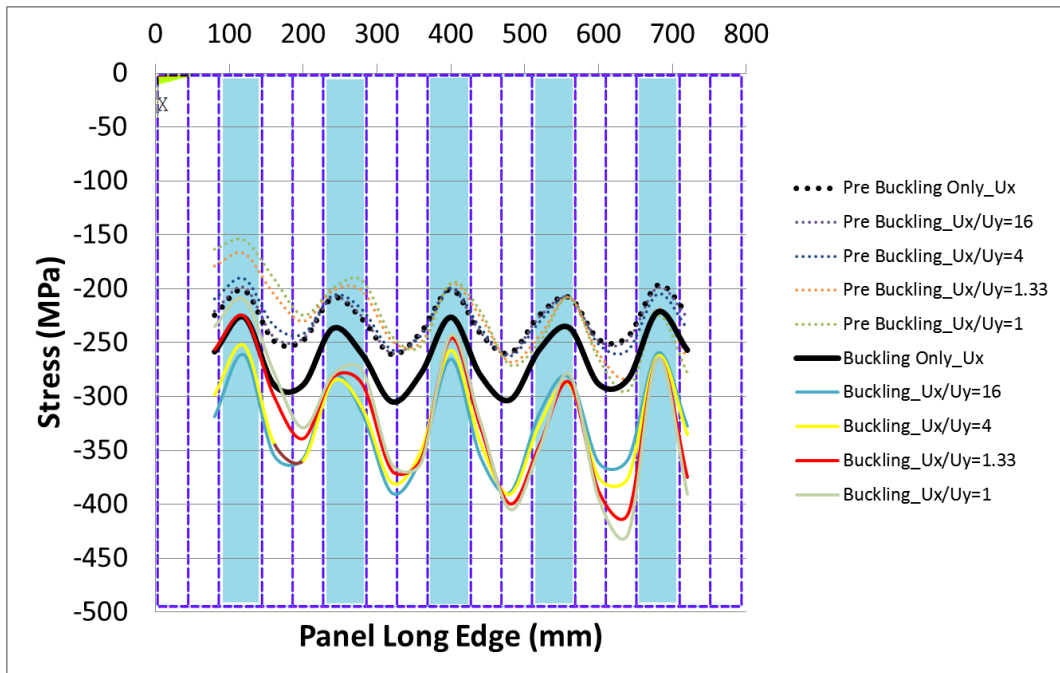


Figure 6.10 Stress Distribution on the Path for Pre Buckling and Buckling Stage for-P1_Configuration 7 with various loading ratios

To deeply investigate Figure 6.10, two load cases are differently plotted for three buckling phases (including post-buckling) as shown in Figure 6.11. The stress on the Path of the P1 is symmetrically distributed for pre-buckling, buckling and post buckling phases for pure-axial loading case. However, with shear loading application, symmetry is broken down as shown in Figure 6.11. On the skin, in some region, stress is increased but in some region stress is decreased for all three phases randomly.

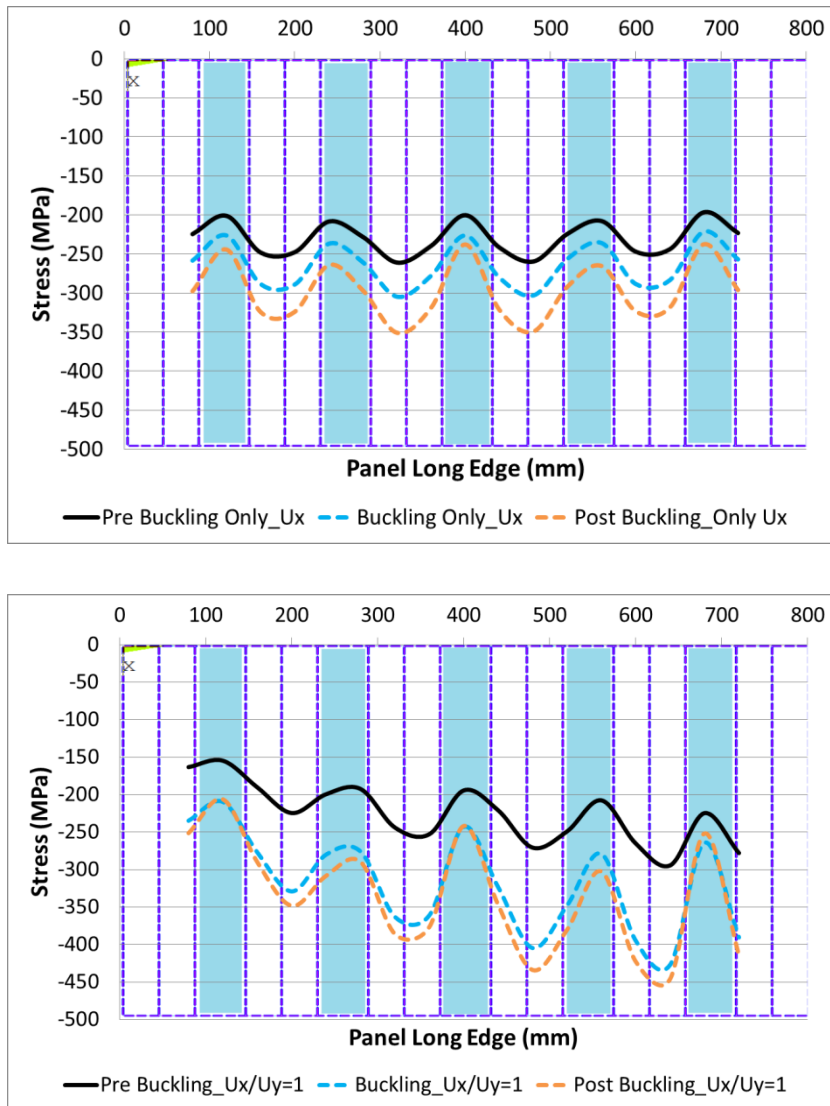


Figure 6.11 Stress Distribution Comparison between the only axial loading (U_x) and combined loading ($U_x/U_y=1$) for P1_Configuration 7

Based on the Figure 6.11, the change on the minimum (compression) stress for pre-buckling, buckling and post buckling stage is tabulated in Table 6.17 to see the effect of the shear loads evidently. After the application of the shear on the structure, it is seen that the stress change on the stiffened area is minimum two times higher than the unstiffened area during buckling and post buckling phases. This implies that the shear stress is mainly carried by the skin/stiffener flange region (stiffened area) for the P2having short pitch distance.

Table 6.17 Stress Change on the Path for only axial loading (U_x) and Combined Loading ($U_x/U_y=1$)

Unstiffened Area (Blue Region)			
Stage	Ony U_x	$U_x/U_y=1$	Change (%)
Skin_Stress_Pre Buckling (MPa)	-201	-224	11.44
Skin_Stress_Buckling(Mpa)	-236	-278	17.80
Skin_Stress_Post Bcukling (Mpa)	-264	-302	14.39

Stiffened Area (White Region)			
Stage	Ony U_x	$U_x/U_y=1$	Change (%)
Skin_Stress_Pre Buckling (MPa)	-261	-294	12.64
Skin_Stress_Buckling(Mpa)	-304	-427	40.46
Skin_Stress_Post Bcukling (Mpa)	-349	-446	27.79

6.1.2.2 Stress State Investigation for P2

The stress distribution on the path of P2 for some selected curves among the all load cases can be seen in Figure 6.12. During pre-buckling and buckling stage, nearly symmetric behaviours are observed according to mid-plane under the combined loadings around the middle area of the panel. However, at the right and left part of the panel, the symmetry of the stress distribution according to the mid-plane is slightly disturbed after shear application in addition to the axial loading.

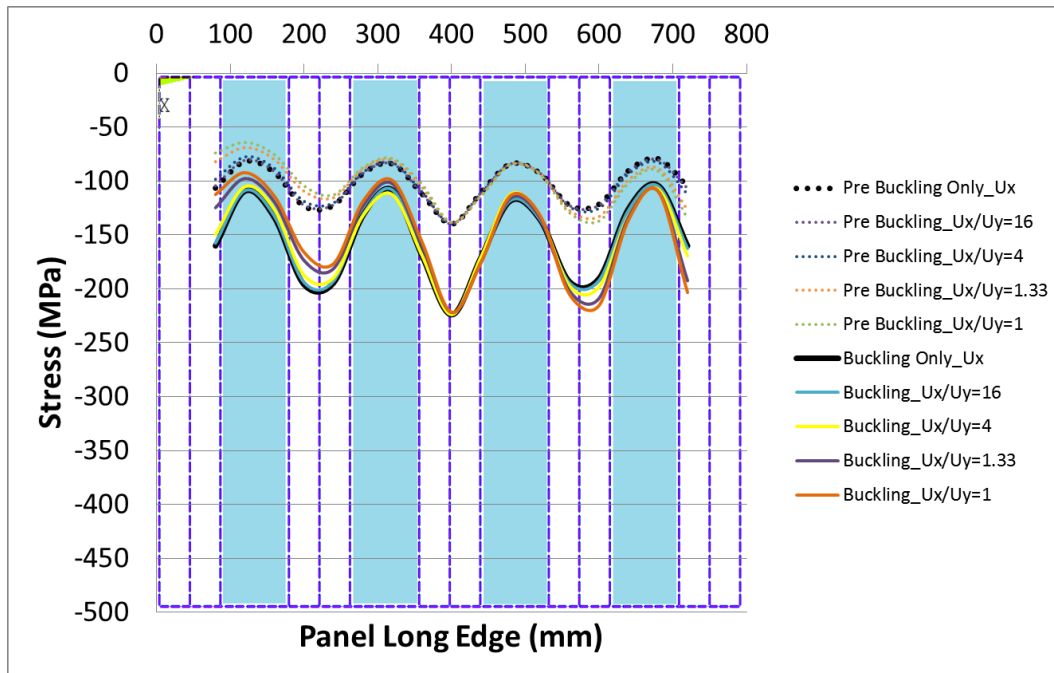


Figure 6.12 Stress Distribution on the Path for Pre Buckling and Buckling Stage for P2_Configuration 7 with various loading ratios

To also deeply investigate Figure 6.12, two load cases are differently plotted for three buckling phases as shown in Figure 6.13. The stress on the path of the P2 is symmetrically distributed for pre-buckling, buckling and post buckling phases with respect to mid-plane of the P2 under pure axial loading situation. However, after shear load application, symmetry is slightly broken down as shown in Figure 6.13. The stress distributions are observed to be very close to each other for pre-buckling and buckling phases when the pure axial loading case U_x and combined loading case $U_x/U_y = 1$ are compared. However, for the post buckling case, the stress distribution become more complex than the two other phases .

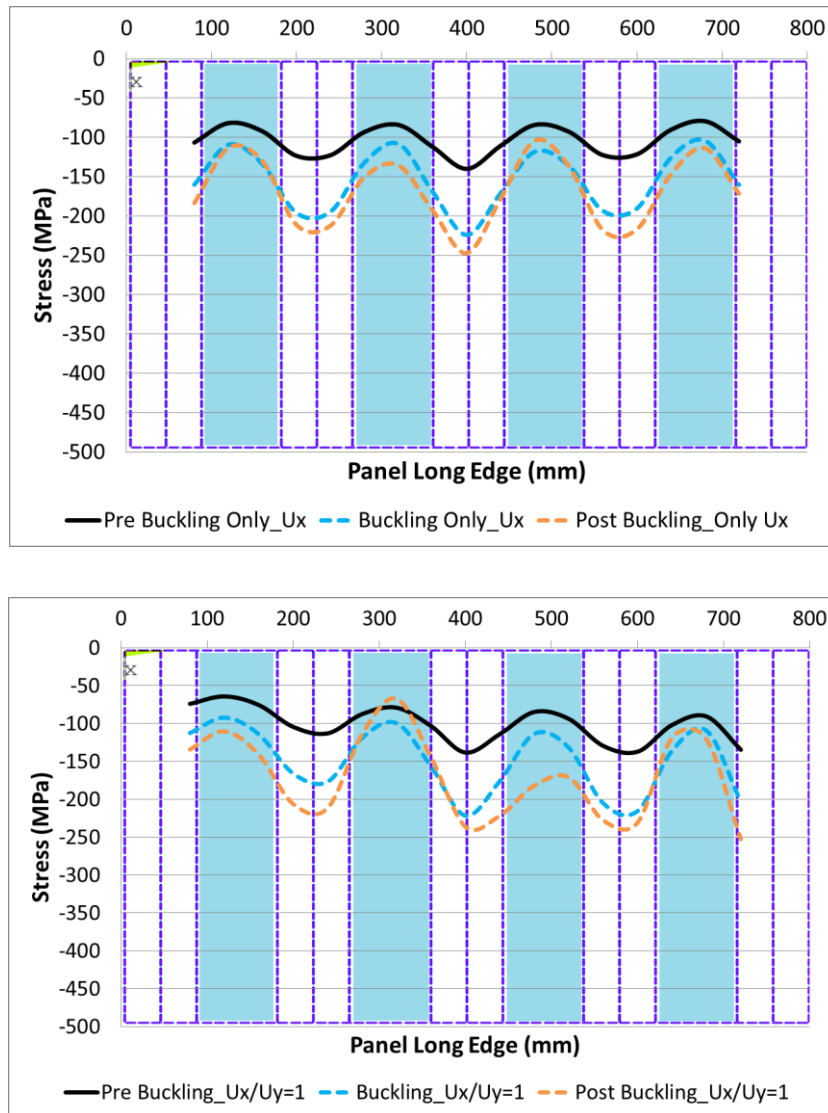


Figure 6.13 Stress Distribution Comparison between the only axial loading (U_x) and combined loading ($U_x/U_y=1$) for P2_Configuration 7

Based on the Figure 6.13, the change on the minimum (compression) stress for pre-buckling, buckling and post buckling stages for P2 is tabulated in Table 6.18. In this table, it can be seen that the stress change obtained in post-buckling phase are unexpectedly high in unstiffened area. This indicates the complexity of the stability calculation in the post-buckling phases.

Table 6.18 Stress Change on the Path of P2 for pure axial loading (U_x) and Combined Loading ($U_x/U_y=1$)

Unstiffened Area (Blue Region)			
Stage	Ony U_x	$U_x/U_y=1$	Change (%)
Skin_Stress_Pre Buckling (MPa)	-84	-90	7.14
Skin_Stress_Buckling(Mpa)	-118	-112	-5.08
Skin_Stress_Post Bcukling (Mpa)	-135	-197	45.93

Stiffened Area (White Region)			
Stage	Ony U_x	$U_x/U_y=1$	Change (%)
Skin_Stress_Pre Buckling (MPa)	-139	-138	-0.72
Skin_Stress_Buckling(Mpa)	-223	-236	5.83
Skin_Stress_Post Bcukling (Mpa)	-247	-236	-4.45

6.1.2.3 Stress State Investigation for P3

The stress distribution on the path of P3 some selected curves among the all load cases can be seen in Figure 6.14. During pre-buckling and buckling stage, nearly same behaviors are observed with the implementation of the shear load at different loading rates at the middle area of the panel. However, at the right and left part of the panel, the stress is unsymmetrically distributed according to the mid-plane after shear application in addition to the axial loading. P2 and P3 shows the similar behaviour at the stage of the pre-buckling and buckling phases.

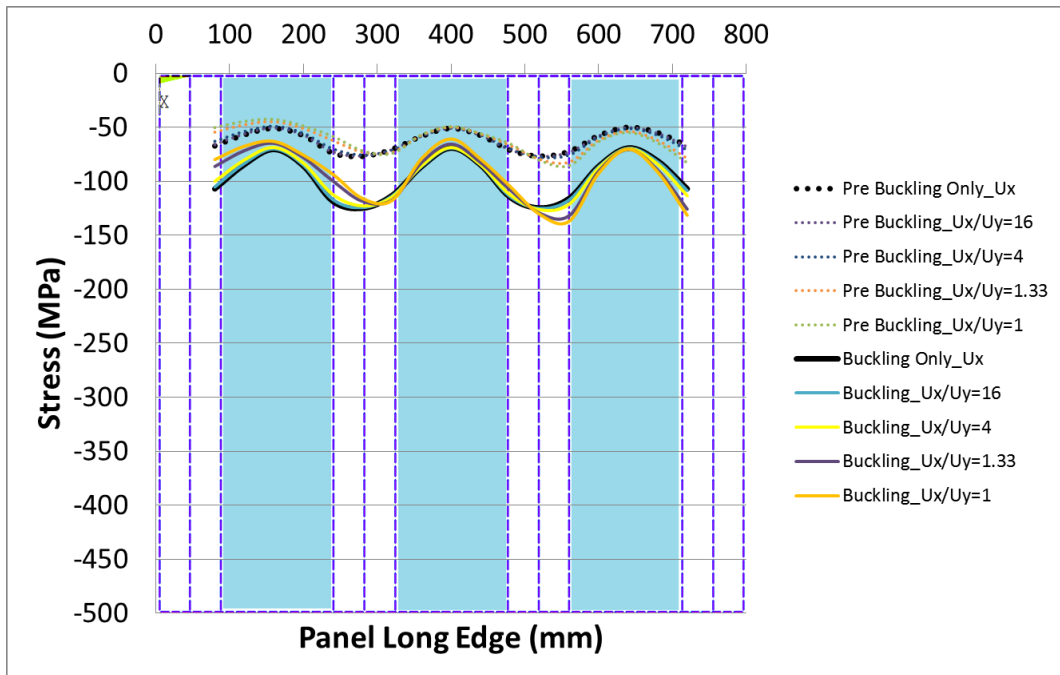


Figure 6.14 Stress Distribution on the Path for Pre Buckling and Buckling Stage for P3_Configuration 7 with various loading ratios

To also deeply investigate Figure 6.14, two load cases are differently plotted for three buckling phases as shown in Figure 6.15. The stress on the path of the P3 is linearly distributed for pre-buckling, buckling and post buckling phases for purely axial loading U_x . However, with shear load application, symmetricity is slightly broken down for pre-buckling and buckling stages as shown in Figure 6.13. The stress distribution are seen to be very similar for pre-buckling and buckling phases during the comparison of the both situations which are pure axial loading U_x and combined loading $U_x/U_y = 1$. However, for the post-buckling phase, the stress change on the path for both situation comparison is moderately high especially in stiffened area but in same manner along the curve.

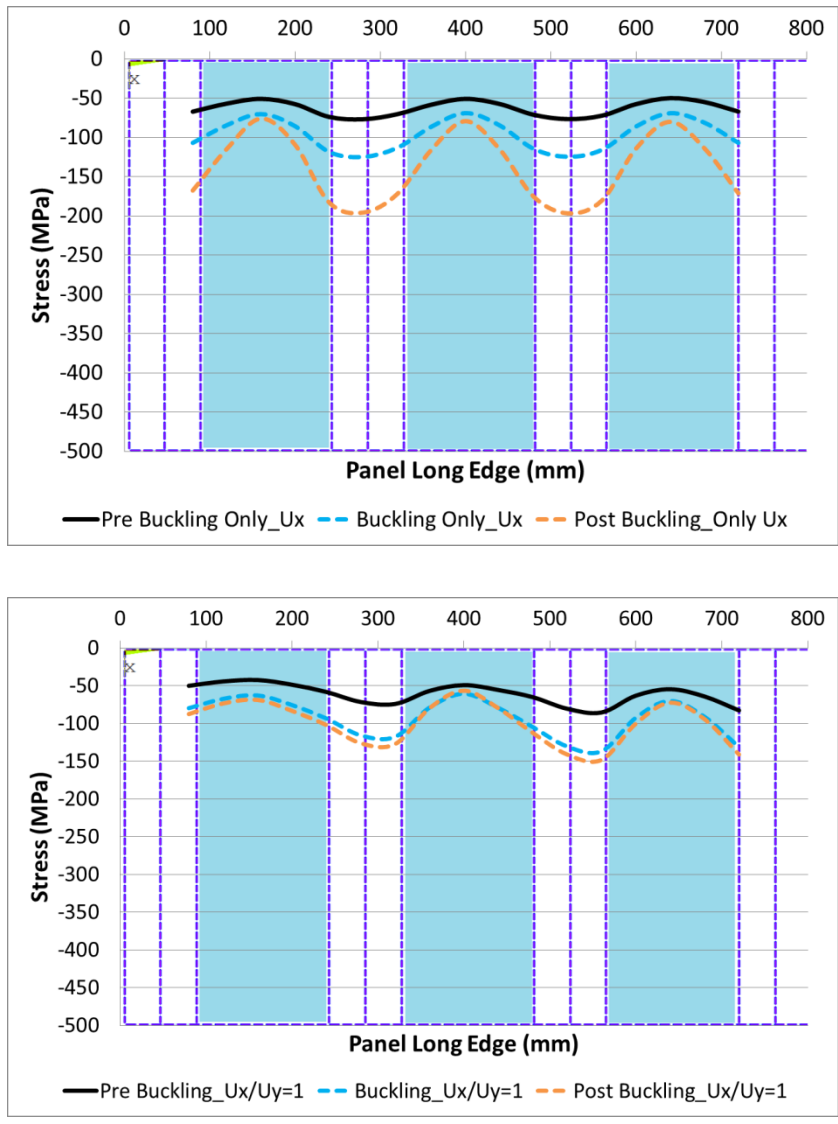


Figure 6.15 Stress Distribution Comparison between the only axial loading (U_x) and combined loading ($U_x/U_y=1$) for P3_ Configuration 7

Based on the Figure 6.15, the change on the minimum (compression) stress for pre-buckling, buckling and post buckling stages for P3 is tabulated in Table 6.18. It can be concluded that the shear effect on the P3 are positive effect during post buckling stage.

Table 6.19 Stress Change on the Path of P3 for pure axial loading (U_x) and Combined Loading ($U_x/U_y=1$)

Unstiffened Area (Blue Region)			
Stage	Ony U_x	$U_x/U_y=1$	Change (%)
Skin_Stress_Pre Buckling (MPa)	-50	-54	8.00
Skin_Stress_Buckling(Mpa)	-69	-72	4.35
Skin_Stress_Post Bcukling (Mpa)	-79	-72	-8.86

Stiffened Area (White Region)			
Stage	Ony U_x	$U_x/U_y=1$	Change (%)
Skin_Stress_Pre Buckling (MPa)	-76	-85	11.84
Skin_Stress_Buckling(Mpa)	-124	-137	10.48
Skin_Stress_Post Bcukling (Mpa)	-200	-148	-26.00

6.2 Conclusion

The conclusions drawn in this chapter are summarized as follows:

From the linear eigenvalue analysis :

- The negative Shear Effect Ratios in different level of load ratios is recognized in Table 6.1 to Table 6.6. It was concluded that the application of the shear load on the structure can have a positive effect on the axial buckling capacity of the structure for the higher load ratio relatively.
- The change occurred on critical axial buckling load due to additional shear load is not sensitive to the bending or axial stiffness of the stiffener .
- The shear effect ratio is observed small for the Configuration 10b to 12b for three panels as shown in Table 6.8 to Table 6.10 due to missing 90^0 ply oriented in perpendicular to the axial loading direction. On the other hand, for Configuration 10a to 12a, the shear effect ratio are higher value bigger than 5 due to inclusion of 90^0 ply.
- From the Figure 6.1, it is clearly seen that the effect of the shear load on the axial critical buckling capability of the structure is increased very fast for the

value of P_x/P_y lower than nearly 10. Therefore, the stiffened P2 design exposed to the low P_x/P_y ratio should be given more attention than high P_x/P_y ratio due to high gradient of degradation on the axial buckling capability of the structure.

- The interaction equation 5.3 can be used for combined in-plane axial and shear loading situation for stiffened composites plates. At least it is verified under the scope of this thesis .

From the nonlienaar analysis:

For P1:

It was observed that the stress for the both area (stiffened and unstiffened) increases with the application of the shear loading during the buckling phase in Figure 6.10. Before buckling phase, even though the stresses distribution curves of the combined loading are almost close to the pure axial compression curve (dashed black one) especially in the middle of the panel, stresses are randomly distributed on the left and right portion of the panel.

As a result, the symmetry of the stress distribution according to the mid-plane of the plate even for these two phases is distorted rather than expected for P1 under the combined loading. This is most probably because of shorter pitch distance than the other two panels.

After the application of the shear load on the structure, it is observed that the stress change on the stiffened area is minimum two times higher than the unstiffened area during buckling and post buckling phases. This implies that the shear stress is mainly carried by the skin/stiffener flange region (stiffened area) for the panel having short pitch distance.

For P2:

The stress distribution on the path of P2 can be seen in Figure 6.12. During pre-buckling and buckling stage, nearly symmetric behaviours are observed according to mid-plane under the combined loadings around the middle area of the plate. However, at the right and left part of the panel, the symmetry of the stress distribution according to the mid-plane is slightly disturbed after shear application in addition to the axial loading for these two phases.

It is also observed that the stress change obtained in post-buckling phase are unexpectedly high in unstiffened area. This indicates the complexity of the stability calculation in the post-buckling phases.

For P3:

The stress distribution on the path of P3 can be seen in Figure 6.14. During pre-buckling and buckling stage, nearly same behaviours are observed with the implementation of the shear load at different loading rates at the middle area of the plate. However, at the right and left part of the panel, the stress is unsymmetrically distributed according to the mid-plane after shear application in addition to the axial loading. P2 and P3 shows the similar behaviour at the stage of the pre-buckling and buckling phases.

It is found that the shear effect on the P3 are positive effect during post buckling stage.

CHAPTER 7

CONCLUSIONS

7.1 General Conclusion

In this study, the buckling and post buckling behavior of the stiffened P2 under combined axial and shear loading is investigated. The linear eigenvalue and geometrically nonlinear buckling analysis have been performed respectively by using the commercial finite element package program ANSYS V16. Before creating the finite element model of the stiffened P2 which is used for the analysis, the validation and sensitivity studies have been carried out.

Although the configurations are mainly chosen arbitrarily, it is generally preferred to create symmetrically balanced orthotropic composites due to their wide preference in aircraft structures.

Linear eigenvalue analyses are first performed for all the configurations of the panels. Then, a single case which further highlights the shear load effect is selected and a nonlinear analysis has also been performed. After linear eigenvalue analysis, the following results are obtained when the shear load is applied together with the axial compression load to the stiffened panel:

- The gradient of critical axial buckling load for linear balanced orthotropic plates including 90^0 plies is increased asymptotically after $P_x/P_y = 10$ due to shear load application. Before this value is reached the shear load effect can be regarded as negligible.

- The change on the critical axial buckling load for linear balanced orthotropic plates without 90^0 plies is considered small or in positive manner due to shear load regardless of the load ratio P_x/P_y . It means that the critical axial buckling force can be even increased in a small amount depending on the P_x/P_y ratios
- The number of half waves occurred during the first buckling mode shape does not change with the application of the shear load. The inclination angle α with respect to the stringer of the panels are close to 45^0 when the Shear Effect Ratio is lower than 10, but it is close to 90^0 when the Shear Effect Ratio is higher than 10.
- The Shear Effect Ratio is barely affected with the number of 45^0 ply. It means that the change on the critical axial buckling load of the stiffened panels due to variable combined loading ratio can be regarded as constant irrespective of the increased or decreased number of 45^0 plies in the laminate.

After Eigen value analysis, to see the stress distribution behavior on the panels, nonlinear post buckling analysis have been performed. After getting results on the panels via linear analysis, one configuration (Configuration 7) for three panels is selected in a criteria that the Shear Effect Ratio are relatively higher than the others. The following conclusions have been derived after nonlinear buckling analysis:

- For all panels, the symmetric stress distribution with respect to mid-plane of the P2 occurred during purely axial loading is broken down for pre and post buckling stage after application of shear forces beside the axial load. This unsymmetrical stress distribution on the P2 means various loads carried by stiffened and unstiffened parts of the panels at the same time.
- It is also generally observed that the stress carried by the stiffened area is becoming higher than the stress carried by the unstiffened part of the area after the buckling occurs. This future of post-buckling phenomenon is similar to the conventional stiffened panels made by aluminum. So, it is observed that the “effective width” calculation should also be applicable for the composite stiffened panels.

- For the smallest pitch distance panel, P1, the shear load effect on the stress distribution is felt much more than the other panels in case of both level of stress and its non-symmetrical distribution. For this panel, the stress on the P2 is mainly carried by the stiffened area/stringers after skin buckles during combined loading case like (like $U_x/U_y=1$).
- Generally with application of the shear force on the structure, the post-buckling stress distribution curves tend to converge the buckling stress curve for P1 and P3.
- For high and middle pitch distance panels, P2 and P3, the shear load effect on the stress distribution is felt less than the P1 in case of both level of stress and its non-symmetrical distribution.
- Especially for the post-buckling phase, the amount of stress change caused by the shear load is decreased when pitch distance between the stringer is increased. It is observed in the P3 that shear load have even a positive impact on the stresses occurred in the defined path of the P2

7.2 Future Work Recommendations

The following recommendations can be made in order to increase the effectiveness of the current thesis.

- The results obtained from linear and nonlinear analysis can be verified with experimental studies.
- More configurations can be taken into account by using ANSYS parametric language.
- Progressive failure analysis can be performed to see the shear loading effect on the post buckling phase.

- The buckling characteristic of different panels having variable aspect ratio under combined loading can also be investigated.

The study can be extended to include the various other stiffeners like L , Hat-type and I type.

REFERENCES

- [1] San Diego Composites, “SDC to Fabricate Stiffened Fuselage Test Panels for Sandia National Labs' FAA and EASA Effort”, 2011, Available at: <http://www.sdcomposites.com/Media/newsarticle4.html> [Accessed 30 July 2015]
- [2] S. Belesis, G. Labeas, “Development of an efficient engineering methodology for non-linear damage and post-buckling analysis of large-scale structures”, *International Journal of Structural Integrity*, Volume 1 (2), pp 126-139, 2010
- [3] L. Boni, D. Fanteria, A. Lanciotti, “Post-buckling behaviour of flat stiffened composite panels: Experiments vs. analysis”, *Composite Structures*, 94(12), pp. 3421–3433, 2012
- [4] S. Oh, K. Kim, C. Kim, “An efficient post-buckling analysis technique for composite stiffened curved panels”, *Composite Structures*, 74, pp. 361–369, 2006
- [5] W.J. Stroud, WH. Greene, MS. Anderson, “Buckling loads of stiffened panels subjected to combined longitudinal compression and shear: results obtained with PASCO, EAL, and STAGS computer programs”, TP 2215, NASA; 1984.
- [6] J. Loughlan, “Finite strip analysis of the buckling characteristics of some composite stiffened shear panels”, *Composite Structure*, 27(3), pp. 283–94, 1994

- [7] J. Loughlan, "The influence of bend-twist coupling on the shear buckling response of thin laminated composite plates", *Thin Wall Structure*, 34, pp 97–114, 1999
- [8] J. Loughlan, "The Influence of Mechanical Couplings on the Compressive Stability of Anti-symmetric Angle-ply Laminates," *Composite Structures*, vol. 57, pp. 473-482, 2002.
- [9] M.P. Nemeth, "Buckling behaviour of long symmetrically laminated plates subjected to combined loadings", TP 3195, NASA; 1992.
- [10] N-Z. Chen, GC. Soares, "Progressive failure analysis for prediction of post-buckling compressive strength of laminated composite plates and stiffened panels", *Journal of Reinforced Plastics and Composites*, 26(10), pp. 1021–1042, 2007
- [11] H.K. Jain, A. Upadhyay, "Buckling behavior of blade-, angle-, T-, and hat-stiffened FRP panels subjected to in-plane shear", *Journal of Reinforced Plastics and Composites*, 29(24), pp. 3614–3623, 2010
- [12] P. Pevzner, H. Abramovich, T. Weller, "Calculation of the collapse load of an axially compressed laminated composite stringer-stiffened curved panel – An engineering approach", *Composite Structure*, 83(4), pp. 341–353, 2008
- [13] C. Kassapoglou, "Composite Plates with Two Concentric Layups under Compression," *Composites*, vol. 39, pp. 104-112, 2008.
- [14] C. Kassapoglou, "Simultaneous cost and weight minimization of composite-stiffened panels under compression and shear", *Composite Part A*, 28A, pp. 419- 435, 1997

- [15] A.T. Sarawit, Y. Kim, M.C.M Bakker, T. Pekoz, "The finite element method for thin-walled members-applications", *Thin Walled Structures*, 41, pp. 191–206, 2003
- [16] M.W. Guo, IE. Harik, W.X. Ren, "Buckling behaviour of stiffened plates" *International Journal of Solids Structure*, 39,pp. 3039–3055, 2002
- [17] C. Bisgani, "Numerical analysis of experimental correlation of composite shell buckling and post-buckling" *Composites Part B*,31, pp. 655–667, 2000
- [18] C. Bisgani, L.Lanzi, "Post-buckling optimization of composite stiffened panels using neural networks" *Composites Structures*, 58, pp. 237–247, 2002
- [19] G.H. Rahimi, M. Zandi, S.F. Rasouli, "Analysis of the effect of stiffener profile on buckling strength in composite iso-grid stiffened shell under axial loading", *Aerospace Science and Technology*, 24(1), pp. 198–203, 2013
- [20] Y.B. SudhirSastry , P. R. Budarapu, N. Madhavi, Y. Krishna, "Buckling analysis of thin wall stiffened composite panels", *Computational Materials Science*, 2014
- [21] C. Bisagni and P. Cordisco, "An Experimental Investigation into the Buckling and Post-buckling of CFRP Shells under Combined Axial and Torsion Loading," *Composite Structures*, vol. 60, pp. 391-402, 2003.
- [22] B. G. Falzon and D. Hitchings, "Capturing Mode-switching in Postbuckling Composite Panels using A Modified Explicit Procedure," *Composite Structures*, vol. 60, pp. 447-453, 2003.
- [23] M. W. Hilburger and J. H. Starnes Jr., "Effects of Imperfections of the Buckling Response of Composite Shells," *Thin-Walled Structures*, vol. 42, p. 2004, 369- 397.

- [24] S. Zhu, J. Yan, Z. Chen, M. Tong, Y. Wang, “Effect of the stiffener stiffness on the buckling and post-buckling behavior of stiffened composite panels – Experimental investigation”, *Composite Structures*, 120, pp. 334-345, 2015
- [25] L. P. Kollár , G. S. Springer, “Mechanics of Composite Structures”, 1st Ed., Cambridge University Press, 2003 (New York)
- [26] R. Degenhardt, A. Kling, K. Rohwer, A.C. Orifici, R.S. Thomson, “Design and analysis of stiffened composite panels including post-buckling and collapse”, *Computers and Structures*, 86, pp. 919-929, 2008
- [27] C. Kassapoglou, “Design and Analysis of Composite Structures: With Applications to Aerospace Structures, 1st Ed., John Wiley & Sons Ltd, 2013
- [28] M.W.Hilburger, J.H. Starnes Jr., “Effects of imperfections on the buckling response of compression loaded composite shells”, *International Journal of Non-Linear Mechanics*, 37(4–5), pp. 623–643, 2002
- [29] G.J. Simites, “Buckling and postbuckling of imperfect cylindrical shells, a review”, *Applied Mechanics*, 39(10), 1517–1524, 1986
- [30] M.K. Chryssanthopoulos, C. Poggi, “Stochastic imperfection modeling in shell buckling studies”, *Thin- Walled Structure*, 23, 179–200, 1995
- [31] L. Lanzi, “Anumerical and experimental investigation on composite stiffened panels into post-buckling”, *Thin-Walled Structures*, 42, 1645–1664, 2004
- [32] B.G. Falzon, D. Hitchhings, “ An introduction to Modelling Buckling and Collapse”, NAFEMS Ltd., 2006

- [33] C. Meeks, E. Greenhalgh, B. G. Falzon, “Stiffener debonding mechanisms in post-buckled CFRP aerospace panels”, *Composites, Part A* 36, pp. 934–946, 2005
- [34] K. A. Stevens, R. Ricci and G. A. O. Davies, “Buckling and post-buckling of composite structures”, *Composites, Volume 26(3)*, pp. 189-199, 1995
- [35] E.J.Barbero, “Finite Element Analysis of Composite Materials”, CRC Press, 2008
- [36] ANSYS V16 Help Manual
- [37] S. Zhu, J. Yan, Z. Chen, M. Tong, Y. Wang, “Effect of the stiffener stiffness on the buckling and post-buckling behaviour of stiffened composite panels – Experimental investigation”, *Composite Structures*, 120, pp. 334-345, 2015
- [38] L.Lanzi, V. Giavotto, “Post-buckling optimization of composite stiffened panels: Computations and experiments”, *Composite Structures*, 73, pp. 208-220, 2006
- [39] R. Zimmermann, R., Klein, H., Kling, A., “Buckling and post-buckling of stringer stiffened fibre composite curved panels – Tests and computations”, *Composite Structures* 73, pp. 150–161, 2006
- [40] T. Taki, T. Kitagawa, “ Post-buckling strength of composite stiffened panel under shear load”, 1st AIAA Aircraft Engineering, Technology, and Operations Congress, AIAA, pp 3995-3934, 1995
- [41] A. Riccio, A. Raimondo, S. Fragale, F. Camerlingo, B. Gambino, C. Toscano and D. Tescione, “Delamination buckling and growth phenomena in stiffened composite panels under compression”, *Journal of Composite Materials*, Vol. 48(23), pp. 2843–2855, 2013

- [42] M.M. Alinia, “A study into optimization of stiffeners in plates subjected to shear loading”, *Thin-Walled Structures*, 43, pp. 845–860, 2005

- [43] A. Aalberg, M. Langseth, P.K. Larsen, “Stiffened aluminium panels subjected to axial compression”, *Thin-Walled Structures*, 39, pp. 861–885, 2001

- [44] E.F. Bruhn, “Analysis and Design of Flight Vehicle Structures”, Tri-State Offset Company, pp. C5-11, 1973

APPENDIX A

STIFFNESS MATRICES

For the configurations mentioned on the thesis, A,B and D matrices which constitute the stiffness matrix of the laminate are given in this appendix.

Table A1: Stiffness Matrix A,B and D Values with layup information for the configuration

Configuration Number	Type of element	Lay-up sequence	Number of Layer	Thickness s (mm)	A11	A12	A16	A22	A26	A66	D11	D12	D16	D22	D26	D66
Configuration 1	skin_1	(0 90 45 -45) _s	8	0.936	58035	17919	0	58035	0	20058	6413	466	222	3746	222	622
	flange_1	(0 90 45 0 -45) _s	10	1.17	92623	18554	0	60152	0	21228	12063	1064	667	7470	667	1369
	web_1	(0 90 45 0 -45 45 0 0) _s	20	2.34	185247	37109	0	120305	0	42456	87522	14828	1333	56111	1333	17267
Configuration 2	skin_1	(0 90 45 -45) _s	8	0.936	58035	17919	0	58035	0	20058	6413	466	222	3746	222	622
	flange_1	(0 90 45 0 -45) _s	10	1.17	92623	18554	0	60152	0	21228	12063	1064	667	7470	667	1369
	web_1	(45 0 -45 45 0 -45 90 0) _s	16	1.872	148540	35838	0	83599	0	40116	42654	13413	1333	19244	1333	14662
Configuration 3	skin_1	(0 90 45 -45) _s	8	0.936	58035	17919	0	58035	0	20058	6413	466	222	3746	222	622
	flange_1	(0 90 45 0 -45) _s	10	1.17	92623	18554	0	60152	0	21228	12063	1064	667	7470	667	1369
	web_1	(0 90 45 0 -45 90) _s	10	1.17	92623	18554	0	60152	0	21228	14777	1906	-1111	3072	-1111	2211
Configuration 4	skin_2	(0 45 0 -45 45 -45) _s	12	1.404	111834	34568	0	46892	0	37776	24484	3714	1778	5519	1778	4241
	flange_2	(0 90 0 45 -45) _s	12	1.404	127212	19190	0	62270	0	22398	27723	897	213	7869	213	1424
	web_1	(0 90 45 0 -45 45 0 0) _s	20	2.34	185247	37109	0	120305	0	42456	87522	14828	4445	56111	4445	17267
Configuration 5	skin_2	(0 45 0 -45 45 -45) _s	12	1.404	111834	34568	0	46892	0	37776	24484	3714	1778	5519	1778	4241
	flange_2	(0 90 0 45 -45) _s	12	1.404	127212	19190	0	62270	0	22398	27723	897	213	7869	213	1424
	web_2	(45 0 -45 45 0 -45 90 0) _s	16	1.872	148540	35838	0	83599	0	40116	42654	13413	1333	19244	1333	14662
Configuration 6	skin_2	(0 45 0 -45 45 -45) _s	12	1.404	111834	34568	0	46892	0	37776	24484	3714	1778	5519	1778	4241
	flange_2	(0 90 0 45 -45) _s	12	1.404	127212	19190	0	62270	0	22398	27723	897	213	7869	213	1424
	web_3	(0 -45 0 45 90) _s	10	1.17	92623	18554	0	60152	0	21228	14777	1906	-1111	3072	-1111	2211
Configuration 7	skin_3	(0 90 45 -45 0 45 -45) _s	14	1.638	113952	35203	0	81481	0	38946	29080	4713	1111	20931	1111	5550
	flange_3	(0 90 0 45 0 -45) _s	14	1.638	161800	19825	0	64388	0	23568	38456	1687	657	17565	657	2523
	web_1	(0 90 45 0 -45 45 0 0) _s	20	2.34	185247	37109	0	120305	0	42456	87522	14828	4445	56111	4445	17267
Configuration 8	skin_3	(0 90 45 -45 0 45 -45) _s	14	1.638	113952	35203	0	81481	0	38946	29080	4713	1111	20931	1111	5550
	flange_3	(0 90 0 45 0 -45) _s	14	1.638	161800	19825	0	64388	0	23568	38456	1687	657	17565	657	2523
	web_2	(45 0 -45 45 0 -45 90 0) _s	16	1.872	148540	35838	0	83599	0	40116	42654	13413	1333	19244	1333	14662
Configuration 9	skin_3	(0 90 45 -45 0 45 -45) _s	14	1.638	113952	35203	0	81481	0	38946	29080	4713	1111	20931	1111	5550
	flange_3	(0 90 0 45 0 -45) _s	14	1.638	161800	19825	0	64388	0	23568	38456	1687	657	17565	657	2523
	web_3	(0 -45 0 45 90) _s	10	1.17	92623	18554	0	60152	0	21228	14777	1906	1111	3072	1111	2211
Configuration 10	skin_4	(0 90 0 -45 45 0 -45 90 0 0) _s	22	2.574	243760	30055	-8118	113876	-8118	35937	147264	12805	-2704	57773	-2704	16052
	flange_4	(0 90 0 0 0 90 0 45 0 -45 0) _s	22	2.574	267684	22366	0	105329	0	28248	151578	5392	1121	68198	1121	8638
	web_1	(0 90 45 0 -45 45 0 -45 90 0) _s	20	2.34	185247	37109	0	120305	0	42456	87522	14828	4445	56111	4445	17267
Configuration 11	skin_4	(0 90 0 -45 45 0 -45 90 0 0) _s	22	2.574	243760	30055	-8118	113876	-8118	35937	147264	12805	-2704	57773	-2704	16052
	flange_4	(0 90 0 0 0 90 0 45 0 -45 0) _s	22	2.574	267684	22366	0	105329	0	28248	151578	5392	1121	68198	1121	8638
	web_4	(0 90 0 45 0 -45 -45 0 45 90 0) _s	24	2.808	254424	38379	0	124540	0	44796	185530	16938	4445	80037	4445	21154
Configuration 12	skin_4	(0 90 0 -45 45 0 -45 90 0 0) _s	22	2.574	243760	30055	-8118	113876	-8118	35937	147264	12805	-2704	57773	-2704	16052
	flange_4	(0 90 0 0 0 90 0 45 0 -45 0) _s	22	2.574	267684	22366	0	105329	0	28248	151578	5392	1121	68198	1121	8638
	web_5	(0 90 0 0 0 90 0 0 0 -45 0 45 90 0) _s	28	3.276	338979	24272	0	144153	0	31758	321668	10761	-1556	132313	-1556	17456

